A Unified Framework for Trajectory Planning, Threat Assessment, and Semi-Autonomous Control of Passenger Vehicles

by

Sterling J Anderson

Bachelor of Science in Mechanical Engineering
Brigham Young University (2007)

Submitted to the
Department of Mechanical Engineering
in partial fulfillment of the requirements for the degree of

Master of Science in Mechanical Engineering

at the

Massachusetts Institute of Technology

June, 2009

Signature of Author

Department of Mechanical Engineering
May 18, 2009

Certified By

Karl Iagnemma
Principal Research Scientist
Thesis Supervisor

Accepted By

Professor David E. Hardt
Chairman, Committee on Graduate Studies

A Unified Framework for Trajectory Planning, Threat Assessment, and Semi-Autonomous Control of Passenger Vehicles

by

Sterling J Anderson

Submitted to the Department of Mechanical Engineering
on May 18, 2009, in partial fulfillment of the requirements for the degree of
Master of Science in Mechanical Engineering

ABSTRACT

This thesis describes the design of an active safety framework that performs trajectory planning, threat assessment, and semi-autonomous control of passenger vehicles in hazard avoidance scenarios. The vehicle navigation task is formulated as a constrained optimal control problem with the constraints bounding a navigable region of the environment derived from forward-looking sensors. First, a constrained model predictive controller is designed to iteratively plan an optimal or "best-case" vehicle trajectory through the constrained corridor. This "best-case" scenario is then used to establish the minimum threat posed to the vehicle given its current state and driver inputs. Based on this threat assessment, the level of controller intervention required to prevent departure from the navigable corridor is calculated and driver/controller inputs are scaled accordingly. This approach minimizes controller intervention while ensuring that the vehicle does not depart from a navigable corridor. It also provides a unified architecture into which various vehicle models, actuation modes, trajectory-planning objectives, driver preferences, and levels of autonomy can be seamlessly integrated without changing the underlying controller structure.

Simulated and experimental results are presented to demonstrate the framework's ability to incorporate multiple threat metrics and configurable intervention laws while sharing control with a human driver. Various maneuvers are tested, including lane-keeping, hazard avoidance, and multiple hazard avoidance and show that this framework capable of maintaining vehicle stability while semi-autonomously avoiding road hazards and conceding significant control to the human driver.

Thesis Supervisor: Karl Iagnemma
Title: Principal Research Scientist

ACKNOWLEDGEMENTS

I would like to thank Dr. Karl Iagnemma for his guidance and advice throughout this research and the writing of this thesis. I would also like to thank Steven Peters for introducing me to many of the software tools used in this work and for his help during experimental testing. Thanks also to Tom Pilutti and the guys at Ford Motor Company for supporting these experiments and to the United States Department of Defense and Ford Motor Company for providing financial support for this research.

Finally, I would like to thank my wonderful wife and beautiful daughter, whose selfless sacrifice and enduring support have both inspired and enabled much of my work.

TABLE OF CONTENTS

LIST OF FIGURES

LIST OF TABLES

1

CHAPTER 1: INTRODUCTION

1.1 Problem Statement and Motivation

Recent traffic safety reports from the National Highway Traffic Safety Administration (NHTSA) show that in 2007 alone, over 41,000 people were killed and another 2.5 million injured in motor vehicle accidents in the United States [1]. The longstanding presence of passive safety systems in motor vehicles, combined with the ever-increasing influence of active systems, has contributed to a decline in these numbers from previous years. Still, the need for improved collision avoidance technologies remains significant.

Passenger safety in human-controlled motor vehicles has historically focused on *passive* safety systems. Such systems, which include seat belts, air bags, and crumple zones, concentrate primarily on mitigating the effects of collisions on passengers. In recent years, the focus of motor vehicle safety has shifted from simply minimizing the damage caused by collisions to actively preparing for and avoiding accidents altogether. With the advent of anti-lock brakes, yaw stability control, roll stability control, and traction control, such *active* safety systems have begun to play a major role in collision mitigation [2].

While effective at reducing accident frequency, current active safety systems are still limited in one respect: their accident avoidance methods are fundamentally "reactive" in nature. In each of these systems, intervention is based on current vehicle (and possibly road surface) conditions. Because they do not utilize 1) sensory information related to the vehicle surroundings or 2) a prediction of the vehicle's path through its

surroundings, they are limited in their ability to assess the threat of impending accidents, and thus cannot exert corrective actions to avoid them.

Recent developments in onboard sensing and drive-by-wire technology have facilitated the development of active safety systems that consider the vehicle's surroundings and share steering and/or braking control with the driver. These "predictive" systems generally attempt to honor driver intentions, opposing them only when doing otherwise would lead to a collision or loss of control. This differs from the abovementioned reactive systems which seek to match the driver's desired (steering-braking- or acceleration-implied) trajectory by minimizing longitudinal and/or lateral wheel slip. For example, anti-lock braking systems react to excessive longitudinal slip and a driver's forceful braking inputs by controlling wheel slip. Similarly, excessive longitudinal or lateral wheel slip makes traction- or stability-control systems a sensible form of interaction which presumably does not alter the driver's intended trajectory.

For predictive safety systems that alter the vehicle trajectory, however, controller intervention more significantly affects the driver's desired vehicle trajectory. In order to determine when, how, and how strongly to intervene, predictive systems must first assess the threat posed to the vehicle by a given scenario and its associated environmental constraints, vehicle states, and driver inputs/performance level. Such systems should honor safe driver inputs and maneuvers while intervening when necessary to correct or override those deemed unsafe or insufficient given the current (and/or predicted) threat scenario. This intervention should strike a necessary balance between the level and frequency of intervention: not altering the driver's steering and braking inputs "too much", "too soon", or "too often" while still guaranteeing that the vehicle avoid hazards independent of that driver input.

1.2 Background and Literature Review

In recent years, extensive research has focused on intelligent vehicle navigation. Many warning, intervention (i.e. driver-assistance or semi-autonomous control), and autonomous control schemes have been developed to perform lateral and longitudinal vehicle guidance [2-5]. Supporting technologies such as onboard sensing, lane detection

techniques, and obstacle recognition algorithms have also been proposed and implemented in test vehicles [6-9].

1.2.1 Autonomous Vehicle Navigation and Control

As described in [21,23-25], the autonomous vehicle guidance system may be broken down into three main tasks: trajectory generation, trajectory re-planning, and low-level control. The trajectory generation task pre-computes the vehicle trajectory. This may be performed online or offline. In ground vehicle applications, the desired trajectory may be selected either by driving a vehicle along a desired trajectory and recording GPS waypoints to use as a subsequent reference path as in [14-18], or by predefining a navigable corridor that circumnavigates road hazards as in [19]. When the former planning approach is used, a trajectory re-planner may modify the desired trajectory based on current measurements or in response to disturbances. For the latter, however, an original vehicle trajectory through the constrained environment must be computed by a trajectory re-planner. The task of a trajectory re-planner is thus to compute (or re-compute) online the desired vehicle trajectory based on current measurements and the occurrence of disturbances such as wind gusts, road elevation changes, or obstacles. This requires information from onboard sensing to perceive and plan for such occurrences.

The low-level control system may use any of a multitude of vehicle actuation modes (e.g. front and rear wheel steering, differential braking, active suspension, velocity control etc.) to track reference commands generated by the trajectory re-planner. While the low-level controller is not required to share the same vehicle or environmental model as the trajectory re-planner [12,20], recent work in autonomous vehicle control using Model Predictive Control (MPC) has shown that using similar models for trajectory re-planning and low-level control can improve the guidance, navigation, and control system's path-tracking performance [15,21,22].

In [23], a corridor – as opposed to a specific path – is preselected and a Finite Horizon Constrained Optimal Controller (FHCOC) is used perform both the re-planning and low-level control tasks required to keep the vehicle within the navigable corridor while satisfying input constraints, safety constraints, and ride comfort preferences. This approach reduces the path planning task to the simpler task of corridor selection and

merges the path re-planning and low level control tasks into the same MPC calculation. Furthermore, because the corridor selection in this approach does not plan a specific vehicle trajectory, the "re-planning" task performed online by the model predictive controller may be more clearly described as an online trajectory "plan" (rather than a "re-plan"). Having noted the distinction between a pre-computed path/trajectory plan and the iterative, online path/trajectory re-plan that is calculated via MPC within a constrained corridor, the remainder of this thesis will refer to the MPC trajectory prediction as a path/trajectory plan.

Fully-autonomous vehicle navigation techniques have been developed to track pre-defined trajectories [14,24], travel within lane markings [6,23,25,26], or avoid obstacles [27] via front wheel steering [15,28,29], rear wheel steering [30], four-wheel-steering [31], and differential brake steering [3,32]. Control laws employed in these systems include PID schemes [12], linear-quadratic regulators [33], non-linear fuzzy controllers [34], and finite-horizon constrained optimal controllers [23].

1.2.2 Semi-Autonomous Vehicle Navigation and Control

Among existing proposals for semi-autonomous vehicle navigation, lane-keeping systems using audible warnings [27,35], haptic alerts [4,36], steering torque overlays [23,37], and various combinations of these have been developed with mixed results [4]. In a recent subproject of the European PReVENT consortium, a lane-keeping system was designed to prevent lane departure by perceiving the environment, making heuristic-based trajectory planning decisions based on perceived threat, and implementing warning mechanisms or slight steering torque overlay when the vehicle drifts from the desired trajectory [38].

Many of the semi-autonomous systems developed in previous work address only one piece of the active safety problem. While some use planning algorithms such as rapidly-exploring random trees [7,39,40], evolutionary programming [41,42] or potential fields [43-45] to plan a safe vehicle path, others simply begin with such a path presumed [3,16,31]. The threat posed by a particular path is seldom assessed by the controller itself and is often only estimated by a simple threat metric based on, for example, the constant deceleration required to stop before or constant lateral acceleration required to steer

around a static or dynamic road hazard [46-51]. Finally, hazard avoidance is commonly performed using one or more actuation methods (e.g. steering, differential braking, etc.) without explicitly accounting for the effect of driver inputs on the vehicle trajectory [38]. Such controllers selectively replace (rather than assist) the driver in performing the driving task.

Yu addressed shared control problem in mobility aids for the elderly by designing an adaptive shared controller which allocates control authority between the human user and a controller in proportion to the user's performance [52]. Measures of user performance in this controller include deviation from a pre-defined trajectory, tip over margins, and distance to obstacles. These metrics and the associated intervention are designed to act on current and past user performance, however, and do not anticipate future deviations, tip over margins, or distances to obstacles. This reactive approach to semi-autonomy, while sufficient to control low speed mobility aids, is not well suited for high speed applications with significant inertia effects and no pre-planned trajectory.

1.3 Purpose and Outline of this Thesis

In this thesis, a framework for passenger vehicle active safety is developed that performs vehicle trajectory planning, threat assessment, and hazard avoidance in a unified manner. This framework leverages the predictive and constraint-handling capabilities of MPC to plan trajectories through a pre-selected corridor, assess the threat this path poses to the vehicle, and regulate driver and controller inputs to maintain this threat below a given threshold.

First, an objective function is established to capture desirable performance characteristics of a safe or "optimal" vehicle path through a bounded corridor. The boundaries of this corridor trace the edges of the navigable road surface and are assumed to have been derived from forward-looking sensor data and a higher-level corridor planner. A model predictive controller then calculates the "best case" vehicle trajectory through this bounded corridor using a model of the vehicle and environmental disturbances. This predicted trajectory and its associated control inputs are assumed to provide a "best case" or minimum-threat avoidance maneuver given the vehicle's current state. Key stability metrics from this prediction are then used to calculate the intervention

required to prevent departure from the safe region of travel and driver/controller inputs are scaled accordingly. Figure 1.1 shows a block diagram of this system.

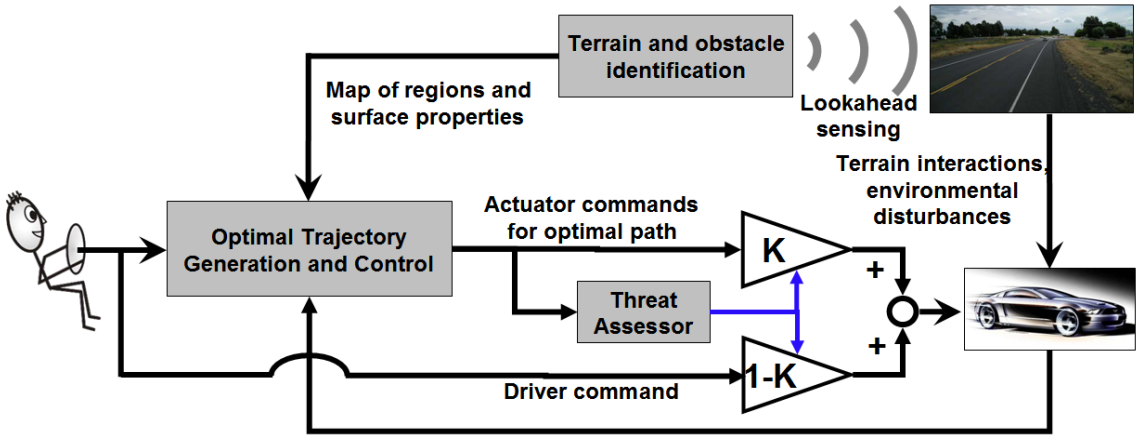

Figure 1.1: Diagram of an active safety system

This thesis is organized as follows. Chapter 2 describes the constrained MPC problem setup, establishes its utility in trajectory planning, and demonstrates its effectiveness in autonomous lane/corridor tracking. Methods for assessing the threat implicit to a given maneuver are then presented in Chapter 3, followed by a semi-autonomous control framework and intervention law in Chapter 4.

2

CHAPTER 2: PATH PLANNING

In this proposed semi-autonomous framework, the best case (or baseline) vehicle path through a given region of the state space is established by a model predictive controller. Metrics from this predicted path will be used to assess the threat presented to the vehicle and steering/braking inputs calculated by the controller will be used to track the path. This chapter describes the model predictive controller setup and demonstrates – via simulation and experiment – its ability to plan optimal trajectories through static and time-varying constrained roadway corridors.

2.1 Problem Statement

Previous research from as early as 1938 has shown that human drivers tend to operate vehicles within a field of safe travel [53] rather than along a specific path. Effective semi-autonomous controllers should account for and allow this freedom of motion within a navigable corridor to avoid unnecessarily constraining human driver. Additionally, a semi-autonomous controller should accurately predict departure from the navigable corridor early enough to keep the vehicle from leaving it. In high-threat situations, this may require the controller to assume full control of the vehicle in order to guide it to safety autonomously (or until control can safely be returned to the driver).

Model Predictive or "receding horizon" Control (MPC) can be configured to meet each of these needs [54-56]. By constraining the vehicle position to remain within the navigable corridor, this optimal control method may be designed to assert little or no control when the driver keeps the vehicle within that corridor. The predictive nature of the algorithm allows it to anticipate and avoid imminent corridor departure by considering both current and predicted vehicle states and environmental conditions.

Finally, a semi-autonomous controller based on the foundation of constrained MPC may be configured to appropriate full control authority to the controller in high-threat situations with confidence that, acting autonomously, the controller can guide the vehicle to safety. Further advantages offered by this control method are discussed in 2.1.3.

This chapter begins with a description of the MPC problem setup and a definition of key terms. The remainder of the chapter then explores the relationship between critical controller parameters, including objective function setup, constraint enforcement, and prediction/control horizons on MPC-based vehicle navigation within constrained corridors. Key metrics of this relationship include corridor-keeping performance (defined proximately), vehicle stability, and controller robustness to unmeasured disturbances. The MPC controller that emerges from this chapter will serve as the foundation to the semi-autonomous navigation framework developed in Chapter 3.

2.1.1 Model Predictive Control

Model Predictive (or "receding horizon") Control is a family of finite-horizon optimal control schemes that iteratively minimizes a performance objective defined for a forward-simulated plant model subject to performance and input constraints [33,57,58]. Stated another way, MPC uses a model of the plant to predict future vehicle state evolution and optimize a set of inputs such that this prediction satisfies constraints and minimizes a user-defined objective function. When it was originally developed in the petrochemical process control industry in the late 1970's, MPC's intensive computational requirements restricted its application to processes with low control update rates. Subsequent improvements in the speed of computing hardware and the efficiency of optimization algorithms have significantly expanded its range of opportunity to include diverse applications ranging from robot manipulators [59,60] to vehicle navigation systems [14,15,21,61], inventory management [62], and clinical anesthesia [63].

The algorithm sequence is as follows. At each time step, t, the current plant state is sampled and a cost-minimizing control sequence spanning from time t to the end of a control horizon of n sampling intervals, $t+n\Delta t$, is computed subject to inequality constraints. The first element in this input sequence is implemented at the current time

and the process is repeated at subsequent time steps. The basic MPC problem setup as implemented in the current work is described here.

For a discrete plant model described by

$$\mathbf{x}_{k+1} = \mathbf{A}\mathbf{x}_k + \mathbf{B}_u\mathbf{u}_k + \mathbf{B}_v\mathbf{v}_k \tag{2.1}$$

$$y_k = \mathbf{C}\mathbf{x}_k + \mathbf{D}_v\mathbf{v}_k \tag{2.2}$$

with **x**, **y**, **u**, and **v** representing states, outputs, inputs, and disturbances of the system respectively, a quadratic objective function over a prediction horizon of p sampling intervals is defined as

$$J_k = \sum_{i=k+1}^{k+p} \frac{1}{2}\left(\mathbf{y}_i - \mathbf{r}_i\right)^{\mathrm{T}} \mathbf{R}_y \left(\mathbf{y}_i - \mathbf{r}_i\right) + \sum_{i=k}^{k+p-1} \frac{1}{2}\mathbf{u}_i{}^{\mathrm{T}}\mathbf{R}_u\mathbf{u}_i + \sum_{i=k}^{k+p-1} \frac{1}{2}\Delta\mathbf{u}_i{}^{\mathrm{T}}\mathbf{R}_{\Delta u}\Delta\mathbf{u}_i + \frac{1}{2}\rho_\varepsilon\varepsilon^2 \tag{2.3}$$

where $\mathbf{R_y}$, $\mathbf{R_u}$, and $\mathbf{R_{\Delta u}}$ represent diagonal weighting matrices penalizing deviations from $\mathbf{y_i} = \mathbf{r_i}$, and $\mathbf{u_i} = \mathbf{0}$, ρ_ε represents the penalty on constraint violations and ε represents the maximum constraint violation over the prediction horizon p. Inequality constraints are defined as:

$$\begin{aligned}
&\mathbf{y}^{j}{}_{\min}(i) - \varepsilon\mathbf{V}^{j}{}_{\min}(i) \le \mathbf{y}^{j}(k+i+1\,|\,k) \le \mathbf{y}^{j}{}_{\max}(i) + \varepsilon\mathbf{V}^{j}{}_{\max}(i)\\
&\mathbf{u}^{j}{}_{\min}(i) \le \mathbf{u}^{j}(k+i+1\,|\,k) \le \mathbf{u}^{j}{}_{\max}(i)\\
&\Delta\mathbf{u}^{j}{}_{\min}(i) \le \Delta\mathbf{u}^{j}(k+i+1\,|\,k) \le \Delta\mathbf{u}^{j}{}_{\max}(i)\\
&i = 0,\ldots,\ p-1\\
&\varepsilon \ge 0
\end{aligned} \tag{2.4}$$

where the vector $\Delta\mathbf{u}$ represents the change in input from one sampling instant to the next, the superscript "$(\bullet)^{\mathrm{j}}$" represents the j^{th} component of a vector, k represents the current time, and the notation $(\bullet)^{j}(k+i|k)$ denotes the value predicted for time $k+i$ based on the information available at time k. The vector **V** allows for variable constraint softening over the prediction horizon, p, when ε is included in the objective function. With n representing the number of free control moves, $\Delta\mathbf{U_k}$ and $\mathbf{U_k}$ are calculated by choosing a blocking vector $\mathbf{J_m}$ such that

$$\Delta \mathbf{U}_k = \begin{bmatrix} \Delta u(k) \\ \vdots \\ \Delta u(k+p-1) \end{bmatrix} = \mathbf{J}_m \begin{bmatrix} z_0 \\ \vdots \\ z_{n-1} \end{bmatrix} \tag{2.5}$$

and

$$\mathbf{U}_k = \begin{bmatrix} \mathbf{I} & 0 & \cdots & 0 \\ \mathbf{I} & \mathbf{I} & \cdots & 0 \\ \vdots & \vdots & \ddots & \vdots \\ \mathbf{I} & \mathbf{I} & \mathbf{I} & \mathbf{I} \end{bmatrix} \Delta \mathbf{U}_k + \begin{bmatrix} \mathbf{I} \\ \mathbf{I} \\ \vdots \\ \mathbf{I} \end{bmatrix} \mathbf{u}_{k-1} \tag{2.6}$$

where $\mathbf{z} = [z_0, \ldots, z_{n-1}]^T$ represents the free optimization variables of the optimization problem. By augmenting the vectors **y**, **U**, Δ**U**, and **V** over the prediction horizon as

$$\mathbf{Y}_{k+1} = \begin{bmatrix} y_{k+1} \\ y_{k+2} \\ \vdots \\ y_{k+p} \end{bmatrix}, \mathbf{U}_k = \begin{bmatrix} u_k \\ u_{k+1} \\ \vdots \\ u_{k+p-1} \end{bmatrix}, \Delta \mathbf{U}_k = \begin{bmatrix} \Delta u_k \\ \Delta u_{k+1} \\ \vdots \\ \Delta u_{k+p-1} \end{bmatrix}, \mathbf{V}_k = \begin{bmatrix} v_k \\ v_{k+1} \\ \vdots \\ v_{k+p-1} \end{bmatrix}, \tag{2.7}$$

the weighting matrices $\mathbf{S_u}$, $\mathbf{S_{u1}}$, $\mathbf{S_x}$, and $\mathbf{H_x}$ can be calculated to express the augmented plant outputs over *p* by

$$\begin{bmatrix} y_{k+1} \\ \vdots \\ y_{k+p} \end{bmatrix} = \mathbf{S}_x \mathbf{x}_k + \mathbf{S}_{u1} \mathbf{u}_{k-1} + \mathbf{S}_u \begin{bmatrix} \Delta \mathbf{u}_k \\ \vdots \\ \Delta \mathbf{u}_{k+p-1} \end{bmatrix} + \mathbf{H}_v \begin{bmatrix} \mathbf{v}_k \\ \vdots \\ \mathbf{v}_{k+p-1} \end{bmatrix}. \tag{2.8}$$

The objective function can also be expressed in terms of the augmented outputs, inputs, and disturbances by calculating $\mathbf{K_x}$, $\mathbf{K_u}$, $\mathbf{K_{ut}}$, $\mathbf{K_v}$, and $\mathbf{K_{\Delta u}}$ such that

$$J = \left(x_k{}^{\mathrm{T}} \mathbf{K}_x + u_{k-1}{}^{\mathrm{T}} \mathbf{K}_u + \mathbf{U}_{k-1}{}^{\mathrm{T}} \mathbf{K}_{ut} + \mathbf{V}_k{}^{\mathrm{T}} \mathbf{K}_v \right) \Delta \mathbf{U}_k + \frac{1}{2} \Delta \mathbf{U}_k{}^{\mathrm{T}} \mathbf{H} \Delta \mathbf{U}_k + \rho_\varepsilon \varepsilon^2 \tag{2.9}$$

and expressing the constraints as

$$\mathbf{A}_c \Delta \mathbf{U}_k \leq \mathbf{b}_c . \qquad (\mathbf{2.10})$$

Having thus expressed the control problem as a quadratic program, it can then be solved using conventional optimization routines [33,57].

2.1.2 Notes on Stability

Previous work in robust MPC methods has shown that in finite-horizon control problems, stability can be guaranteed by forcing predicted behavior to reach steady state within a finite number of sampling intervals. This stability condition has inspired the use of end-point constraints [64-67], min-max feedback formulations [68], and stabilizing feedback loops which replace transfer functions with finite impulse responses while using future values of the reference signal (rather than future values of the control inputs) as degrees of freedom in the optimization routine [69]. Each of these approaches effectively seeks to retain a margin for future feedback action, making it available to the MPC optimization only as prediction time passes. This guarantees that the optimization will remain feasible even when disturbances and/or model mismatch create discrepancy between predicted and true state evolution.

When applied to transient control problems, stabilizing MPC imposes significant restrictions on the target set/cost function combination. In vehicle control problems, mission requirements dictate the target set, which is rarely invariant as stabilizing MPC requires. In [70], a variable horizon is used in combination with the constraint tightening approach in order to enable robust entry into an arbitrary (and not necessarily invariant) target set. This approach includes the horizon as a decision variable in the optimization and tightens target constraints as a function of this horizon. Further, by determining an appropriate objective function cost on time, this approach guarantees finite-time entry into the target set despite disturbances. In this work, input and input rates were constrained to remain within feasible limits while terminal constraints on vehicle position were tightened to ensure a feasible end-state within the navigable corridor.

2.1.3 Advantages of Model Predictive Control in Vehicle Navigation

Model predictive control offers a number of significant advantages that make it particularly well-suited to autonomous and semi-autonomous vehicle navigation problems. Its ability to explicitly consider environmental, performance and actuator constraints enables corridor-based navigation and allows it to operate near the limits imposed by those constraints. This environmentally-aware prediction, coupled with an objective-function-optimal control law, has been shown to closely mimic the performance of a human driver [54]. Its finite prediction horizon fits naturally with and may be based on the information provided by finite-horizon, forward-looking sensors. Additionally, the model-based nature and multivariable-compatibility of the control calculation allows MPC to account for and easily adapt to structural changes and actuator availability from one vehicle model and/or loading configuration to the next. This adaptability may allow for reduced-cost controller implementation across product families and through ever-shifting safety requirements.

Finally, MPC's predictive nature allows certain constrained configurations to effectively plan their own path within a partitioned environment without requiring any pre-defined vehicle trajectories. That is, where other control methods require a specific pre-planned path through the environment (which is often planned by a separate and suboptimal system), MPC can plan its own (optimal) path given a set of situational position constraints. The path thus planned through the (pre-delineated) safe operating environment potentially offers a number of advantages over alternative trajectory planning methods; not only is it explicitly aware of vehicle dynamics, measured disturbances, and actuator limitations, but the constraint-satisfying trajectory plan it generates is both feasible (since it is obtained from an already-calculated set of control inputs) and optimal (with respect to some performance metric such as minimum lateral acceleration over a future time horizon, minimum wheel slip, etc). In the semi-autonomous framework described below, this optimal prediction can serve not only as a best case trajectory plan, but also as an effective threat assessor. The remainder of this chapter develops and demonstrates an MPC-based autonomous controller in corridor-based active hazard avoidance.

2.2 Assumptions

In this thesis it is assumed that the position of road lanes is available with no noise or uncertainty and that road hazards have been detected, located, and mapped into a 2-dimensional navigable corridor. Existing systems and previous work in onboard sensing and sensor fusion justify this as a reasonable assumption [8,71]. Radar, LIDAR, and vision-based lane-recognition systems [2,7,9], along with various sensor fusion approaches [72,73] have been proposed to provide the lane, position, and environmental information needed by this framework.

Additionally, where multiple corridor options exist (such as cases where the roadway branches or the vehicle must navigate around an obstacle in the center of the lane), it is assumed that a high-level path planner has selected a single corridor through which the vehicle should travel.

2.3 Simulation Studies

Simulations were conducted to explore the effect of various MPC configurations on its utility and suitability as a path planner. Setup and results from these simulations are discussed below.

2.3.1 Simulation Setup

Autonomous control maneuvers were simulated using two different vehicle plant models. The first plant ("Plant A") was represented by a nonlinear ADAMS® model* of a generic truck featuring a double wishbone suspension, passive roll stabilizers, and rack and pinion steering. Tire forces were approximated via a Pacejka tire model. An isometric view of this model is shown in Figure 2.1 and its parameters are defined in Appendix A.

* Steven Peters wrote and generously lent an ADAMS-Matlab interface to couple this model with the Simulink-based controller.

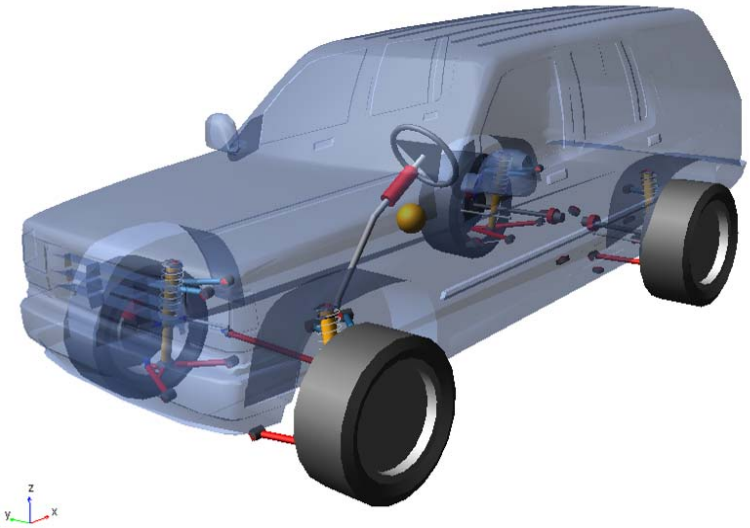

Figure 2.1. ADAMS plant model

The second vehicle plant model ("Plant B") is similar to the one presented in [17]. This model describes longitudinal and lateral tire forces with the semi-empirical Pacejka tire model, where the longitudinal and cornering forces are assumed to depend on the normal force, tire slip angle, surface friction, and longitudinal slip.

I) Vehicle Model

Two different vehicle models were used in this study's control calculations. The first ("Model A") accounts for the kinematics of a 4-wheeled vehicle, along with its lateral, yaw, and roll dynamics. This controller model was used for simulations conducted with Plant A (for which roll dynamics are appreciable).

The second model ("Model B") does not consider suspension compliance, making it better suited for passenger vehicles with low centers of gravity and little appreciable roll dynamics. This more computationally efficient model was used to control Plant B in simulation and the test vehicle in experiment. Vehicle states for Model A include the position of its center of gravity [x, y], the vehicle yaw angle ψ, yaw rate $\dot{\psi}$, sideslip angle β, roll angle φ, and roll rate $\dot{\varphi}$ as illustrated in Figure 2.2 (a and b). Model B is described by the same set of states less the roll angle φ, and roll rate $\dot{\varphi}$. This model is illustrated by Figure 2.2 (a) alone.

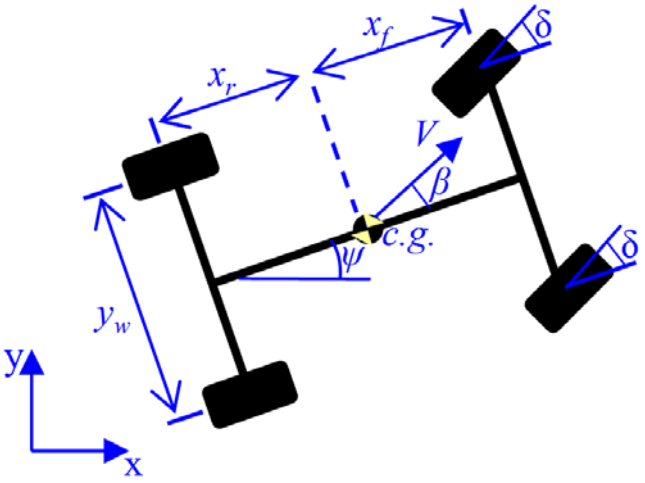

(a)

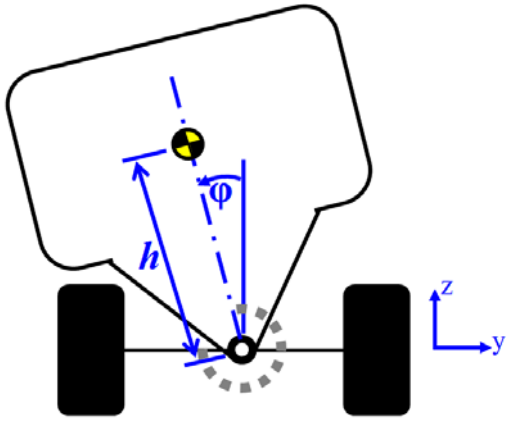

(b)

Figure 2.2: Vehicle roll (a and b) and slip (a only) models used in MPC controller

Tire compliance is included in the model by approximating lateral tire force (F_y) as the product of each tire's cornering stiffness (C) and sideslip angle (α) as shown in (2.11) and illustrated in Figure 2.3.

$$F_y = C\alpha \tag{2.11}$$

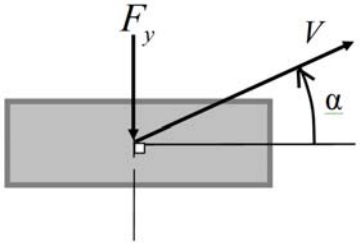

Figure 2.3: Linearized tire compliance model used in equations of motion

Table 2.1 defines and quantifies each model's parameters. These parameters were chosen to best match the vehicle plant being tested: roll model parameters were chosen to emulate those of the ADAMS plant while the slip model parameters were matched to the low-roll-center simulation model and experimental plant.

Table 2.1: Vehicle model parameters

Symbol	Description [units]	Value	
		Roll Model	**Slip Model**
m	Total vehicle mass [kg]	2450	2050
I_{zz}	Yaw moment of inertia [kg·m^2]	3053	3344
x_f	C.g. distance to front wheels [m]	1.13	1.43
x_r	C.g. distance to rear wheels [m]	1.43	1.47
y_w	Track width [m]	1.56	1.44
C_f	Front cornering stiffness [N/deg]	1640	1433
C_r	Rear cornering stiffness [N/deg]	1140	1433
μ	Surface friction coefficient	{0.25, 0.5, 1}	1
m_s	Chassis sprung mass [kg]	1880	--
I_{xx}	Roll moment of inertia [kg·m^2]	834	--
h	Sprung c.g. height [m]	0.34	--
k_f	Front axle roll stiffness [N·m/rad]	30 x 10^3	--
k_r	Rear axle roll stiffness [N·m/rad]	30 x 10^3	--
b_f	Front axle roll damping [N·m·s/rad]	1600	--
b_r	Rear axle roll damping [N·m·s/rad]	1600	--

Equations of motion for the roll model are

$$\dot{x} = V\cos(\psi + \beta) \tag{2.12}$$

$$\dot{y} = V\sin(\psi + \beta) \tag{2.13}$$

$$\sum F_y = m\left[\dot{V}\sin(\psi+\beta) + V\left(\dot{\psi}+\dot{\beta}\right)\cos(\psi+\beta)\right] - m_x h\ddot{\varphi}\sin\varphi \tag{2.14}$$

$$\sum M_z = I_{zz}\ddot{\psi} \tag{2.15}$$

$$\sum M_x = I_{xx}\ddot{\varphi} \tag{2.16}$$

Linearized about a constant speed and assuming small slip angles, these become

$$\dot{x} = V \tag{2.17}$$

$$\dot{y} = V(\psi + \beta) \tag{2.18}$$

$$\dot{\beta} = \frac{-D(C_f + C_r)}{mV}\beta + \left(\frac{D(C_r x_r - C_f x_f)}{mV^2} - 1\right)\dot{\psi} + \frac{m_s g h^2 - h(k_f + k_r)}{VI_{xx}}\varphi - \frac{h(b_f + b_r)}{VI_{xx}}\dot{\varphi} + \frac{DC_f}{mV}\delta \tag{2.19}$$

$$\ddot{\psi} = \frac{(C_r x_r - C_f x_f)}{I_{zz}}\beta - \frac{(C_r x_r^{\,2} + C_f x_f^{\,2})}{I_{zz}V}\dot{\psi} + \frac{C_f x_f}{I_{zz}}\delta \tag{2.20}$$

$$\ddot{\varphi} = \frac{-(C_f + C_r)h}{I_{xx}}\beta + \frac{(C_r x_r - C_f x_f)h}{VI_{xx}}\dot{\psi} + \frac{(m_s g h - k_f - k_r)}{I_{xx}}\varphi + \frac{C_f h}{I_{xx}}\delta \tag{2.21}$$

where C_f and C_r represent the cornering stiffness of the lumped front wheels and the lumped rear wheels, $D = 1 + \frac{m_s h^2}{I_{xx}}$, and x_f and x_r denote the longitudinal distances from the c.g. of the front and rear wheels, respectively.

Equations of motion for the slip model include

$$\dot{x} = V\cos(\psi + \beta) \tag{2.22}$$

$$\dot{y} = V\sin(\psi + \beta) \tag{2.23}$$

$$\sum F_y = m\left[\dot{V}\sin(\psi + \beta) + V(\dot{\psi} + \dot{\beta})\cos(\psi + \beta)\right] \tag{2.24}$$

$$\sum M_z = I_{zz}\ddot{\psi} \tag{2.25}$$

Similarly linearized about a constant speed and assuming small slip angles, these become

$$\dot{x} = V \tag{2.26}$$

$$\dot{y} = V(\psi + \beta) \tag{2.27}$$

$$\dot{\beta} = \frac{-(C_r + C_f)}{mV}\beta + \left(\frac{(C_r x_r - C_f x_f)}{mV^2} - 1\right)\dot{\psi} + \frac{C_f}{mV}\delta \tag{2.28}$$

$$\ddot{\psi} = \frac{(C_r x_r - C_f x_f)}{I_{zz}}\beta - \frac{(C_r {x_r}^2 + C_f {x_f}^2)}{I_{zz}V}\dot{\psi} + \frac{C_f x_f}{I_{zz}}\delta \tag{2.29}$$

II) Objective Function and Constraint Handling

The controller's projected path along a predefined trajectory or through a constraint-imposed corridor is shaped by the performance objectives implicit in the MPC cost function. Many options exist for characterizing desirable vehicle trajectories [54]. In this chapter, various vehicle states and trajectory characteristics, including vehicle sideslip β, yaw rate $\dot{\psi}$, roll angle φ, and lateral acceleration $\ddot{y}$ are penalized in the objective function to understand how minimizing each affects the controller's ability to 1) track a predefined reference trajectory and 2) navigate within a constrained corridor.

For reference trajectory tracking, lateral deviation of the vehicle's center of gravity (y_y) from the corridor centerline (r_y) is penalized by including $R_{yy} > 0$ in an objective function of the form

$$J_k = \sum_{i=k+1}^{k+p} \frac{1}{2}(y_i - r_i)^{\mathrm{T}} \mathbf{R}_y (y_i - r_i) + \sum_{i=k}^{k+p-1} \frac{1}{2} {u_i}^{\mathrm{T}} \mathbf{R}_u u_i + \sum_{i=k}^{k+p-1} \frac{1}{2} \Delta {u_i}^{\mathrm{T}} \mathbf{R}_{\Delta u} \Delta u_i \tag{2.30}$$

where

$$\mathbf{R}_y = diag(R_{\beta\beta} \quad R_{\dot{\psi}\dot{\psi}} \quad R_{\psi\psi} \quad R_{\ddot{y}\ddot{y}} \quad R_{\dot{\varphi}\dot{\varphi}} \quad R_{\varphi\varphi}). \tag{2.31}$$

The resulting trajectory-tracking setup through a hazard-containing environment may then be illustrated by Figure 2.4.

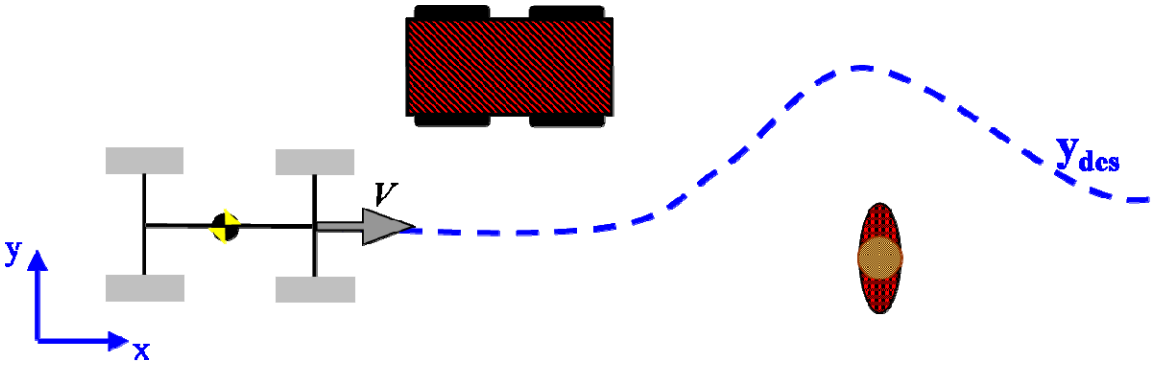

Figure 2.4: Illustration of a trajectory-tracking control setup

For corridor-keeping, penalties on deviation from a desired trajectory (R_y) are replaced with lateral position constraints. As explained in 2.2, this form of corridor-based navigation assumes that the environment has been delineated previously, with the boundaries of the navigable road surface at each time step described by the constraint vectors

$$\mathbf{y}^{y}{}_{\max}(k)=\begin{bmatrix} y^{y}{}_{\max}(k+1) \\ \vdots \\ y^{y}{}_{\max}(k+p) \end{bmatrix}, \quad \mathbf{y}^{y}{}_{\min}(k)=\begin{bmatrix} y^{y}{}_{\min}(k+1) \\ \vdots \\ y^{y}{}_{\min}(k+p) \end{bmatrix}. \tag{2.32}$$

In (2.32), $\mathbf{y}^{y}{}_{\max}$ and $\mathbf{y}^{y}{}_{\min}$ represent the upper and lower limits on the vehicle lateral position (y) as illustrated in Figure 2.5. These limits exclude more than simply off-road/out-of-lane regions from the navigable corridor – they also extend to stationary and/or moving hazards in the roadway such as debris, pedestrians or other vehicles. Thus, a hazard in the roadway looks to the controller like a constriction in the corridor as illustrated in Figure 2.5.

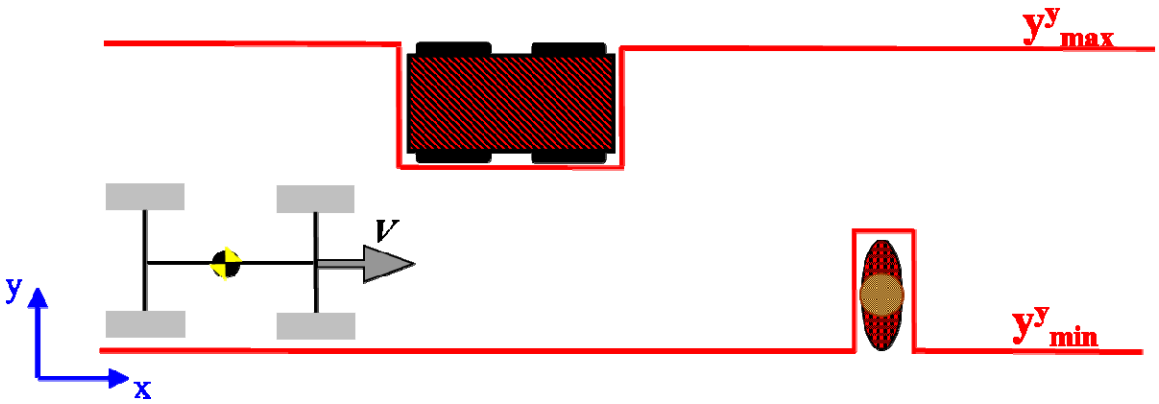

Figure 2.5: Illustration of constraint placement (y^{y}_{max} , y^{y}_{min}) for static hazards

In order for the constraint space to remain feasible,

$$y^{y}_{max} - y^{y}_{min} > 0. \qquad \textbf{(2.33)}$$

Constraints were softened as described in (2.4) by including the magnitude of their violation (ε) in the objective function, which takes the form

$$J_k = \sum_{i=k+1}^{k+p} \frac{1}{2} y_i^{\mathrm{T}} \mathbf{R}_y y_i + \sum_{i=k}^{k+p-1} \frac{1}{2} u_i^{\mathrm{T}} \mathbf{R}_u u_i + \sum_{i=k}^{k+p-1} \frac{1}{2} \Delta u_i^{\mathrm{T}} \mathbf{R}_{\Delta u} \Delta u_i + \frac{1}{2} \rho_y \varepsilon_y^{\,2}, \quad \mathbf{R}_{yy} = 0 \qquad \textbf{(2.34)}$$

A spatial interpretation of the constrained and unconstrained approaches is illustrated in Figure 2.6.

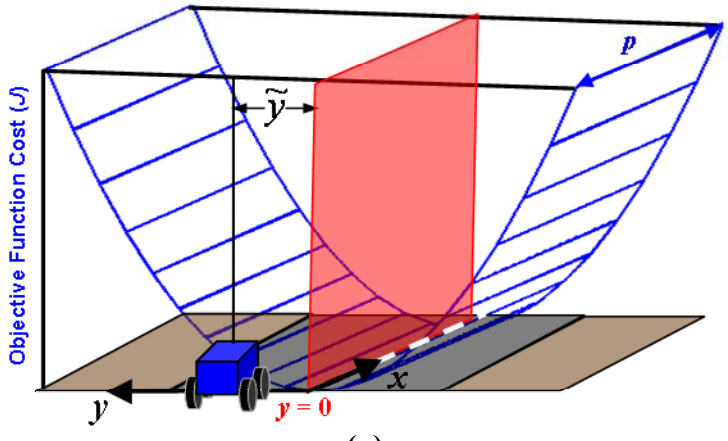

(a)

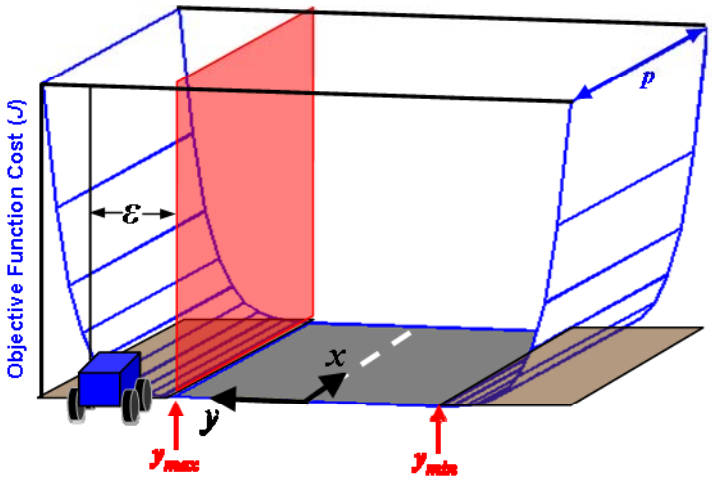

(b)

Figure 2.6. Spatial interpretation for autonomous vehicle navigation using (a) penalties on lateral position deviation from a specific trajectory ($R_{yy} > 0$ and $\rho_y = 0$) vs. (b) penalties on departure from a constrained corridor ($R_{yy} = 0$ and $\rho_y > 0$)

In summary, the constrained MPC controller was configured to use vehicle position, input magnitude, and input rate constraints to avoid hazards while minimizing one of many possible performance measures to maximize vehicle stability. By enforcing vehicle position constraints at the boundaries of the navigable region of the road surface (i.e. the lane edges on an unobstructed road), the controller forces the MPC-generated path to remain within the constraint-bounded corridor whenever dynamically feasible. Coupling this lateral position constraint with input constraints, input rate constraints, and vehicle dynamic considerations, the corridor delineated by $\mathbf{y}^{y}_{\max}$ and $\mathbf{y}^{y}_{\min}$ translates to a safe operating "tube" within the state space [19,74].

III) Prediction and Control Horizons

Few studies have investigated the influence of prediction (p) and control horizon (n) on MPC performance. Those that have [75,76] studied horizon length have shown that, in general, longer prediction horizons lead to more stable controllers, with stability in the limiting case (as Hp $\rightarrow \infty$) approaching that of infinite horizon linear quadratic regulators. In the autonomous simulations presented here, p was varied to assess its effect on control performance. In experiments, p was fixed at 35 or 40 samples, with $n = p/2$.

Chapter 3 explores how varying prediction and control horizon length affects threat assessment and vehicle trajectory in various hazard scenarios.

IV) Maneuvers through Static Corridors

Lane keeping, hazard avoidance, and double lane change maneuvers were simulated to test this controller's ability to keep the vehicle within a navigable corridor bounding static hazards. Qualitatively, each of these maneuvers requires varying degrees of constraint-handling and trajectory optimization. Lane-keeping tests gauge the controller's ability to keep the vehicle – initially headed out of the corridor – inside it. Hazard avoidance tests require that the controller keep the vehicle inside a constricting corridor by navigating around a roadway obstacle, and double lane change maneuvers measure the controller's ability to handle maneuvers with significant load transfer.

V) Maneuvers through Time-Varying Corridors

Moving hazards were factored into the autonomous control problem by estimating their future position based on their current position, velocity, and (optionally) acceleration. In the simulation results shown below, unnavigable regions representing obstacles moving in one dimension (results may be generalized to 2-dimensional motion) were factored into the placement of time-varying corridors as follows:

Given a (constant) host velocity $\dot{x}_{host}$ and obtaining the current velocity of roadway hazards $\dot{x}_{haz}$ from tracking sensors or vehicle-to-vehicle communication, where $x_{host}(t)$ and $x_{haz}(t)$ represent the current position of the host and hazard, respectively at time t, the estimated time to collision Δt_c evaluated at time t_0 is given by

$$\Delta t_c\big|_{t_0} = t_c - t_0 = \begin{cases} \dfrac{\tilde{x}(t_0)}{\dot{\tilde{x}}(t_0)} & \begin{cases} \text{for } \dot{\tilde{x}}(t_0) < 0, \quad \tilde{x}(t_0) > 0 \\ \text{or } \dot{\tilde{x}}(t_0) > 0, \quad \tilde{x}(t_0) < 0 \end{cases} \\ \infty & \begin{cases} \text{for } \dot{\tilde{x}}(t_0) < 0, \quad \tilde{x}(t_0) < 0 \\ \text{or } \dot{\tilde{x}}(t_0) < 0, \quad \tilde{x}(t_0) < 0 \end{cases} \end{cases} \tag{2.35}$$

to first order where $\dot{\tilde{x}}(t) = \dot{x}_{haz}(t) - \dot{x}_{host}$, $\tilde{x}(t) = x_{haz}(t) - x_{host}(t)$, or

$$\Delta t_c\big|_{t_0} = t_c - t_0 = \begin{cases} \dfrac{-\dot{\tilde{x}}(t_0) - \sqrt{\dot{\tilde{x}}^2(t_0) - 2\ddot{x}_{haz}(t_0)\cdot\tilde{x}(t_0)}}{\ddot{x}_{haz}} & \begin{cases}\text{for } \ddot{x}_{haz}(t_0) \neq 0,\ \dot{\tilde{x}}(t_0) < 0 \\ \text{or } \ddot{x}_{haz}(t_0) < 0,\ \dot{\tilde{x}}(t_0) \geq 0\end{cases} \\ \dfrac{\tilde{x}(t_0)}{\dot{\tilde{x}}(t_0)} & \text{for } \ddot{x}_{haz}(t_0) = 0,\ \dot{\tilde{x}}(t_0) < 0 \\ \infty & \begin{cases}\text{for } \ddot{x}_{haz}(t_0) > 0,\ \dot{\tilde{x}}(t_0) \geq 0 \\ \text{or } \ddot{x}_{haz}(t_0) = 0,\ \dot{\tilde{x}}(t_0) \geq 0\end{cases} \end{cases} \quad \textbf{(2.36)}$$

to second-order (requiring that $\tilde{x}(t_0) \leq 0$ in (2.36)).

Given $\Delta t_c\big|_{t_0}$, the x position of each road hazard at t_c is then estimated as

$$x_{haz}\left(t_c\big|_{t_0}\right) = x_{haz}(t_0) + \dot{x}_{haz}(t_0)\cdot\Delta t_c\big|_{t_0} \quad \textbf{(2.37)}$$

or

$$x_{haz}\left(t_c\big|_{t_0}\right) = x_{haz}(t_0) + \dot{x}_{haz}(t_0)\cdot\Delta t_c\big|_{t_0} + \frac{1}{2}\ddot{x}_{haz}(t_0)\cdot\Delta t_c\big|_{t_0}^{\,2} \quad \textbf{(2.38)}$$

to first- and second-order, respectively. Hazard depth from the host vehicle's perspective is then estimated by

$$\Delta x_{haz}\left(t_c\big|_{t_0}\right) \approx \Delta x_{haz}(t_0) - \dot{x}_{haz}(t_0)\cdot\left(\Delta x_{haz}(t_0)/\dot{\tilde{x}}(t_0)\right). \quad \textbf{(2.39)}$$

Constraints on vehicle position are drawn at each sampling instant to form a convex (in y) corridor from the outline of each hazard's anticipated position and depth at time t_c. Figure 2.7 illustrates what a snapshot of this time-varying constraint placement might look like to the controller.

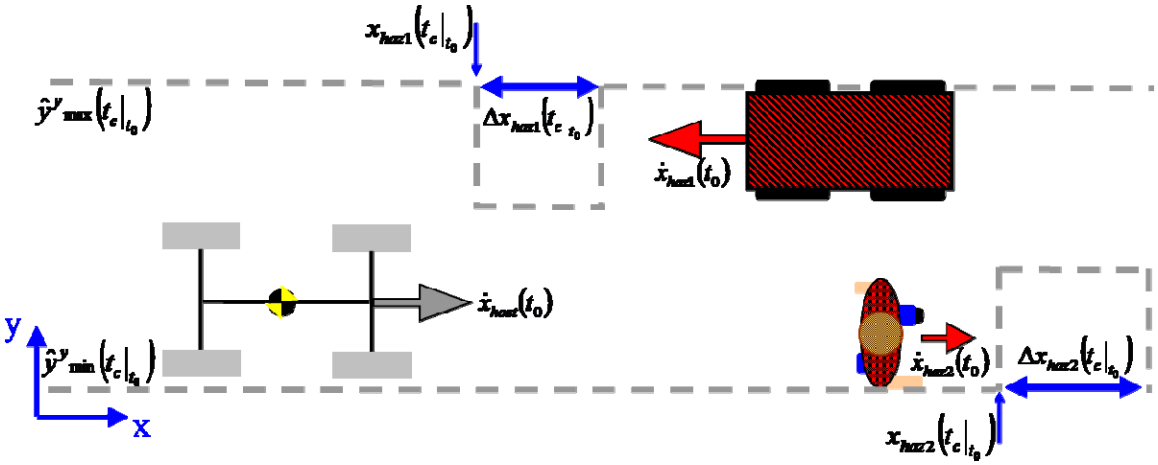

Figure 2.7: Illustration of constraint placement (y^y_{max} , y^y_{min}) for moving hazards

Notice that the constraint "shadow" cast by a hazard moving in the opposite direction as the host vehicle appears shallower than the hazard's true depth. Similarly, the shadow cast by a hazard moving in the same direction as the host vehicle is effectively deepened.

VI) Actuator Configuration

In previous studies, autonomous path-tracking control has been performed via front wheel steering [15,28], rear wheel steering [30], four-wheel-steering [31], differential brake (i.e. front and/or rear wheel skid-) steering [3,32], and combinations of braking and steering [16,22,77,78]. In [29], an LQ controller used each of these input strategies to track a modified step trajectory similar to a single lane change. Comparing each strategy, this study found that front wheel steering provided the greatest efficiency in terms of the ratio of peak tire force used to total available tire force. Four wheel steering showed similar efficiency to front wheel steering, followed by front- and four-wheel braking input schemes. Due to load transfer experienced during braking maneuvers, along with low efficiency in general for differential brake steering, rear wheel steering is ill-suited as a standalone actuation method for autonomous hazard avoidance applications.

In the simulations shown below, front wheel steering was used predominantly, though to demonstrate this control framework's applicability to multiple actuator configurations, one result is shown that uses a combination of front wheel steer with four

wheel differential braking. Yaw moment actuation is added to the control calculation by including $(1/I_{zz})M_z$ in equation (2.20) for the roll model and (2.29) for the slip model. The moment command M_z may then be distributed across the four wheels using various braking allocation schemes. In the simulation shown below, it was distributed evenly across all four wheels.

2.3.2 Simulation Results

Autonomous MPC-based control was successfully simulated using both static and moving hazards. The results below demonstrate the controller's suitability for both sets of conditions.

I) Static Hazards

Static hazards such as lane/road edges and stationary obstacles can be avoided by planning a specific path around them or by excluding them from a bounded corridor via position constraints. The simulation results below note the differences between these two approaches, demonstrate the advantages provided by "corridor-keeping" over "trajectory tracking", and illustrate the effect of prediction horizon length on corridor-tracking performance.

a) Trajectory Tracking vs. Corridor-Keeping

Figure 2.8 shows simulation results for double lane change maneuvers performed using a) a reference trajectory with lateral deviation from that trajectory penalized ($R_{yy} > 0$ and $\rho_y = 0$) and b) a constrained corridor with $R_{yy} = 0$ and lateral position constrained to remain within the corridor ($\rho_y > 0$). In both simulations, vehicle sideslip β was also penalized by setting $R_{\beta\beta} > 0$.

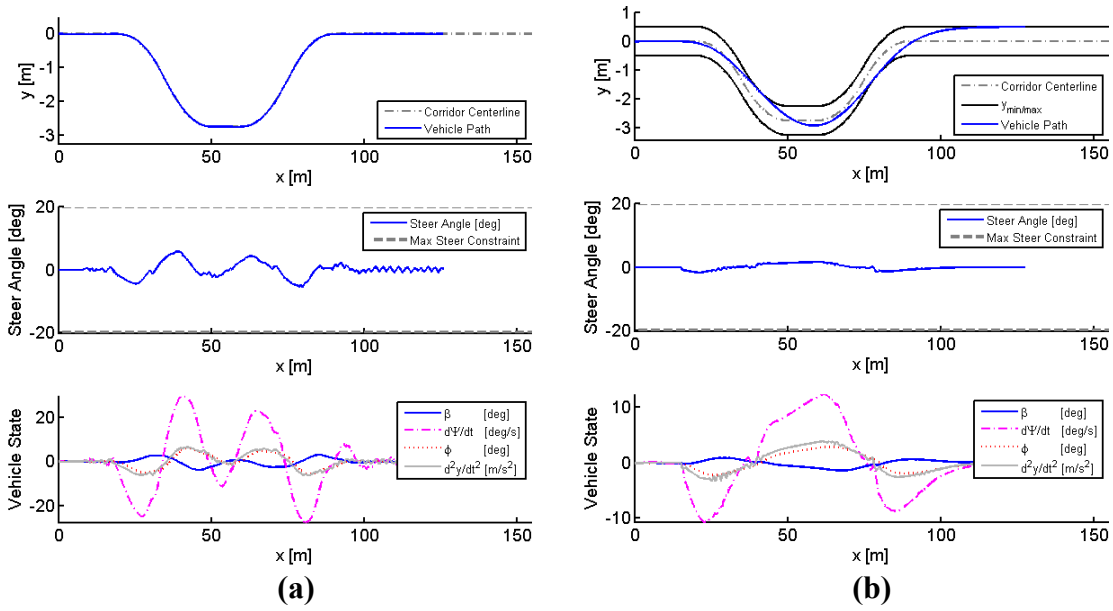

Figure 2.8: Simulation results for a double lane change path-tracking (a) and corridor-keeping (b) maneuver

As Figure 2.8 (a) and (b) illustrate, constraint-based navigation allows the controller greater freedom to minimize sideslip and stability/comfort-related performance metrics (such as steer angle, yaw rate, roll angle, and lateral acceleration) while still ensuring that the vehicle does not leave the navigable roadway. In contrast, trajectory-following does not consider an available corridor of travel, requiring instead that the controller sacrifice other performance metrics to ensure as little deviation from the path centerline as possible.

Figure 2.9 (a) – (c) show the RMS lateral position (y) and sideslip (β) experienced by an autonomously-controlled vehicle as it navigates a 1-m wide lane during a double lane change maneuver. Figure 2.9 (a) and (b) plot the maximum and root mean square (RMS) lateral deviation (y) and vehicle sideslip (β) against the ratio of the objective function weights R_{yy} / R_{XX}, where R_{XX} penalizes one of several possible nonzero vehicle states such as sideslip β ($R_{XX} = R_{\beta\beta}$), yaw rate $\dot{\psi}$ ($R_{XX} = R_{\dot{\psi}\dot{\psi}}$), roll angle φ ($R_{XX} = R_{\varphi\varphi}$), lateral acceleration a_{lat} ($R_{XX} = R_{\ddot{y}\ddot{y}}$), and lateral load transfer LTF ($R_{XX} = R_{LTF,LTF}$). Figure 2.9 (c) shows simulation results for the weighting ratios labeled *i*), *ii*), and *iii*) in (a) and (b).

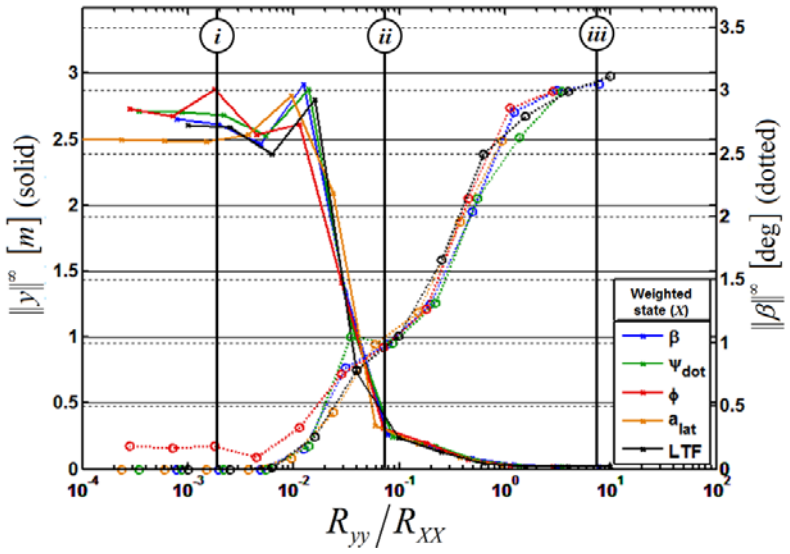
i
ii
iii
Weighted state (X)
β
Ψdot
ϕ
alat
LTF
$\|y\|^{\infty}$ [m] (solid)
$\|\beta\|^{\infty}$ [deg] (dotted)
R_{yy}/R_{XX}

(a)

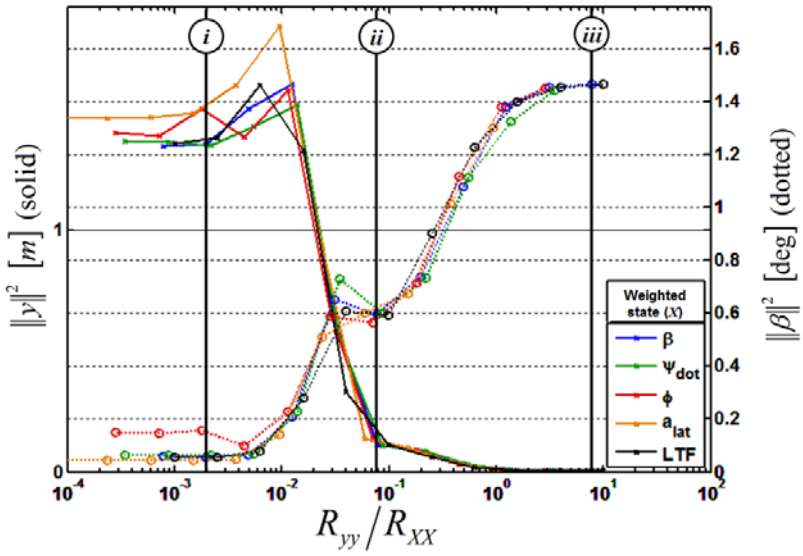
i
ii
iii
Weighted state (X)
β
Ψdot
ϕ
alat
LTF
$\|y\|^{2}$ [m] (solid)
$\|\beta\|^{2}$ [deg] (dotted)
R_{yy}/R_{XX}

(b)

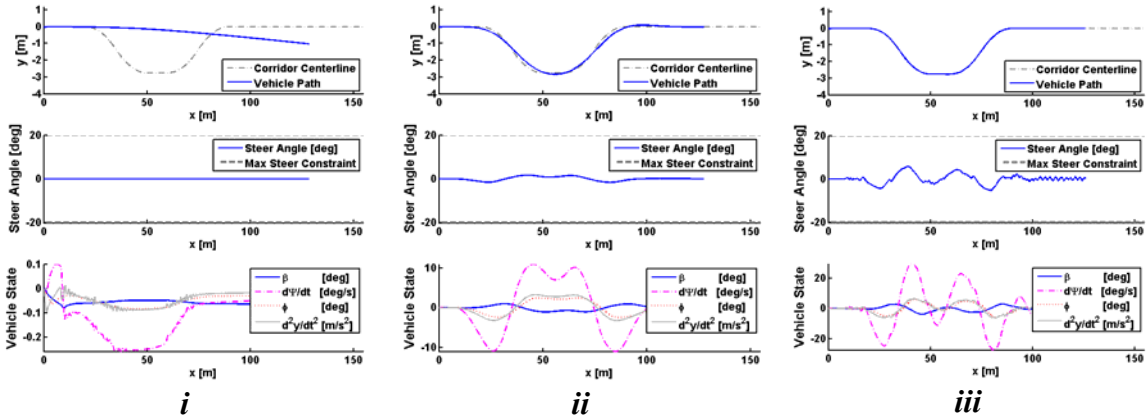
Corridor Centerline
Vehicle Path
x [m]
y [m]
Steer Angle [deg]
Max Steer Constraint
Vehicle State
β [deg]
dΨ/dt [deg/s]
ϕ [deg]
d²y/dt² [m/s²]

i ***ii*** ***iii***

(c)

Figure 2.9. Tradeoffs between maximum (a) and RMS (b) lateral vehicle position (dotted) and other vehicle states (solid) observed for various relative weightings R_{yy}/R_{XX} in a path-tracking scenario.

As expected, Figure 2.9 shows that as R_{yy} / R_{XX} increases, the vehicle trajectory more closely matches the desired trajectory at the expense of more control effort and greater sideslip, lateral acceleration, and related vehicle states. Also note that similar results are obtained for various choices of R_{XX} due to dynamic coupling of sideslip, yaw rate, roll, lateral acceleration, and load transfer. This result suggests that MPC-based trajectory tracking control of ground vehicles may penalize any of these in combination with lateral position error with similar results and controller tuning tradeoffs.

Figure 2.10 shows how these tradeoffs differ in a constrained corridor-keeping framework when the penalty on lateral deviation from the centerline (R_{yy}) is replaced with a soft constraint on lateral deviation from the navigable corridor via **(**2**.**4**)**.

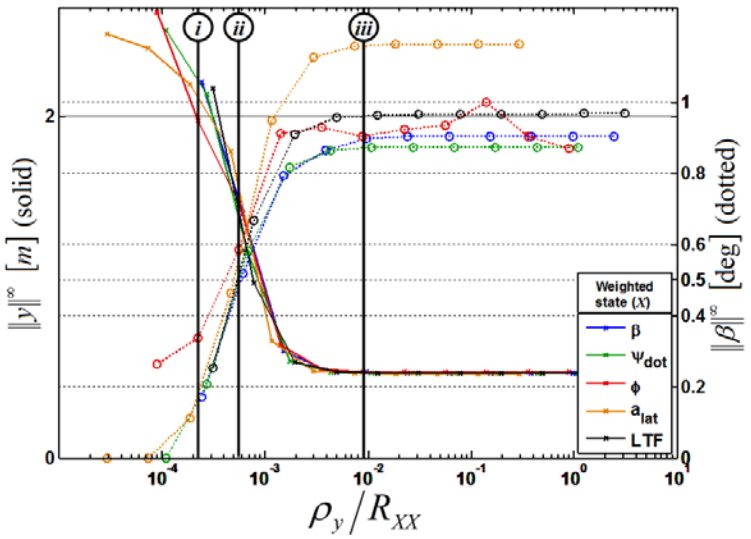

(a)

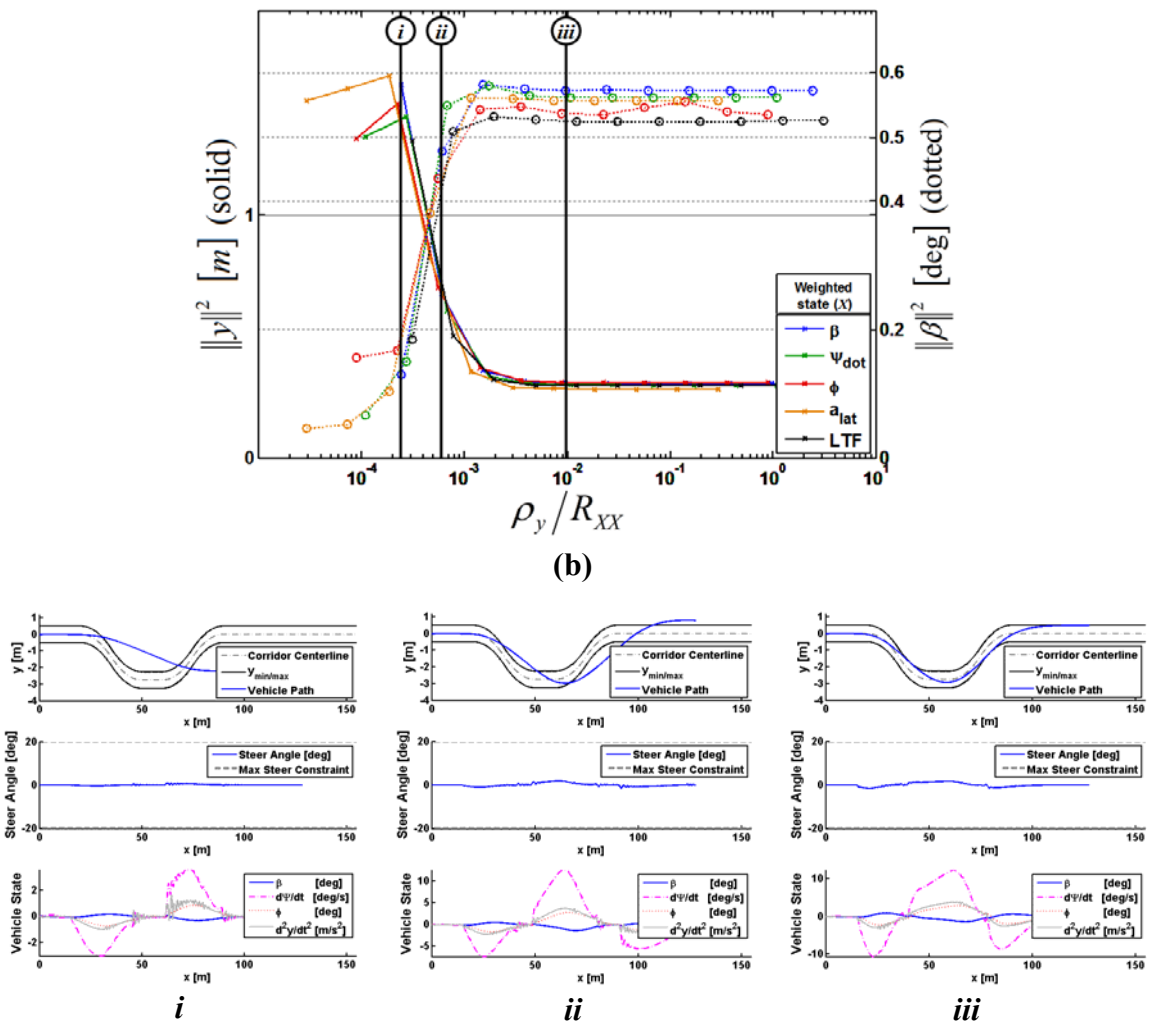

Figure 2.10. Corridor-keeping performance tradeoffs between maximum (a) and RMS (b) vehicle states observed for various position-constraint-to-vehicle state penalties (ρ_y/R_{XX})

Comparing Figure 2.10 with Figure 2.9 shows that by constraining lateral vehicle position (rather than weighting its deviation from the lane centerline) and penalizing stability-critical performance criteria, the vehicle trajectory can be tuned to satisfy roadway-imposed constraints while simultaneously reducing vehicle sideslip, lateral acceleration, and other stability-critical states. Notice that instead of leveling off at the 3.25º (max) and 1.5º (RMS) sideslip required by the trajectory-tracking controller, the corridor-keeping alternative remains within the navigable roadway while requiring only ~0.9º (max) and ~0.55º (RMS) sideslip. Figure 2.11 shows a set of corridor-keeping

maneuvers performed with different vehicle states penalized and $\rho_y / R_{XX} \approx 0.01$ (corresponding to position *iii* in Figure 2.10).

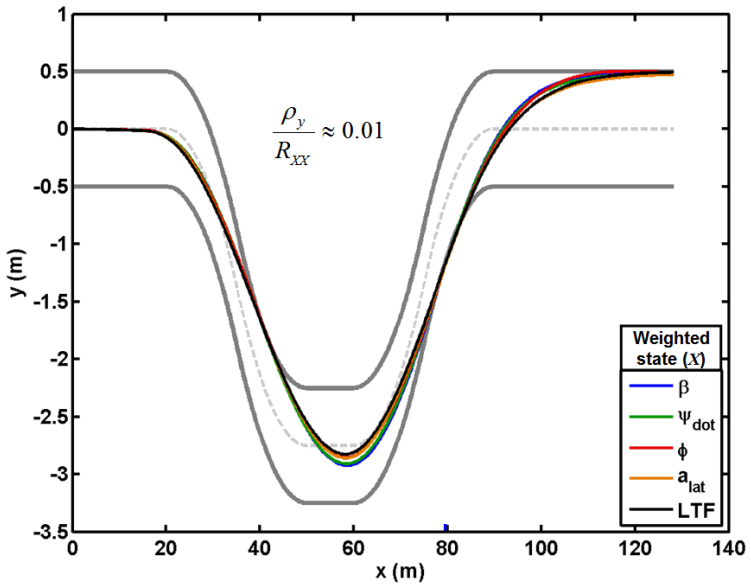

Figure 2.11. Autonomous corridor-keeping controller with various states *X* weighted in the objective function

As Figures 2.9—2.11 illustrate, various vehicle states can be penalized in the objective function with relatively similar path- or corridor tracking results due to dynamic coupling of these states in the vehicle model. Having noted this similarity, front wheel sideslip ($\alpha = (x_f / V)\dot{\psi} + \beta - \delta$) was chosen as the trajectory characteristic to minimize in the corridor-based MPC framework for the remainder of the tests presented in this thesis. This choice was motivated by a number of observations. In addition to offering similar performance to that obtained by minimizing other trajectory characteristics in the objective function, front wheel sideslip strongly influences the controllability of front-wheel-steered vehicles since cornering friction begins to decrease above critical slip angles. These critical angles are well-known and provide a direct mapping from environmental conditions to vehicle handling limitations. The linearized tire compliance model's failure to account for this decrease further motivates the suppression of front wheel slip angles to reduce controller-plant model mismatch. In [30] it is shown that limiting tire slip angle to avoid this strongly nonlinear (and possibly unstable) region of the tire force curve can significantly enhance vehicle stability and performance. Finally,

trajectories that minimize wheel slip also tend to minimize lateral acceleration and yaw rates, leading to a safer and more comfortable ride.

b) Prediction Horizon

Figure 2.12 illustrates tradeoffs between lateral vehicle position and vehicle sideslip for various relative objective function weightings and prediction horizons. Notice that for short prediction horizons $(n = 15)$, small changes in objective function weightings leads to large variation in sideslip and lateral vehicle position. Similarly, longer prediction horizons ($n \geq 25$) lead to more uniform state tradeoffs as they allow the controller to anticipate roadway hazards earlier.

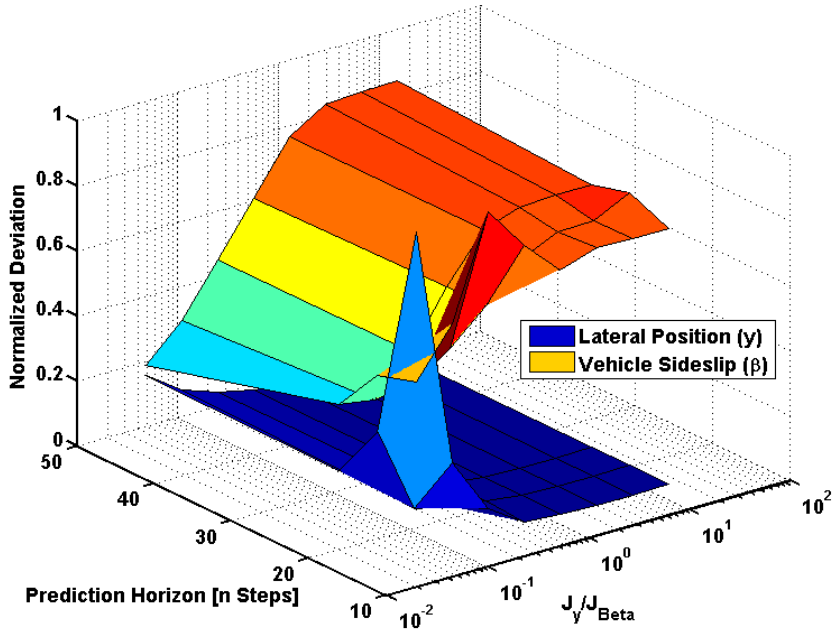

Figure 2.12. Response surface illustrating the relationship between lateral vehicle position, sideslip, and prediction horizon length (with control horizon = 12)

Figure 2.13 shows the effect of combining steering and differential braking (i.e. four wheel skid steering) in the MPC control calculation to navigate autonomously within a constrained corridor. Notice that compared to controlling only steering angles, using both actuation modes allows the controller to reduce vehicle sideslip with a brake-imposed moment while controlling lateral vehicle position via an applied steer angle. These differences, along with the larger steer command required in the combined input

case to compensate for the yaw-correcting moment applied by the brakes, are apparent in a comparison of Figure 2.13 to Figure 2.10(c)*iii*.

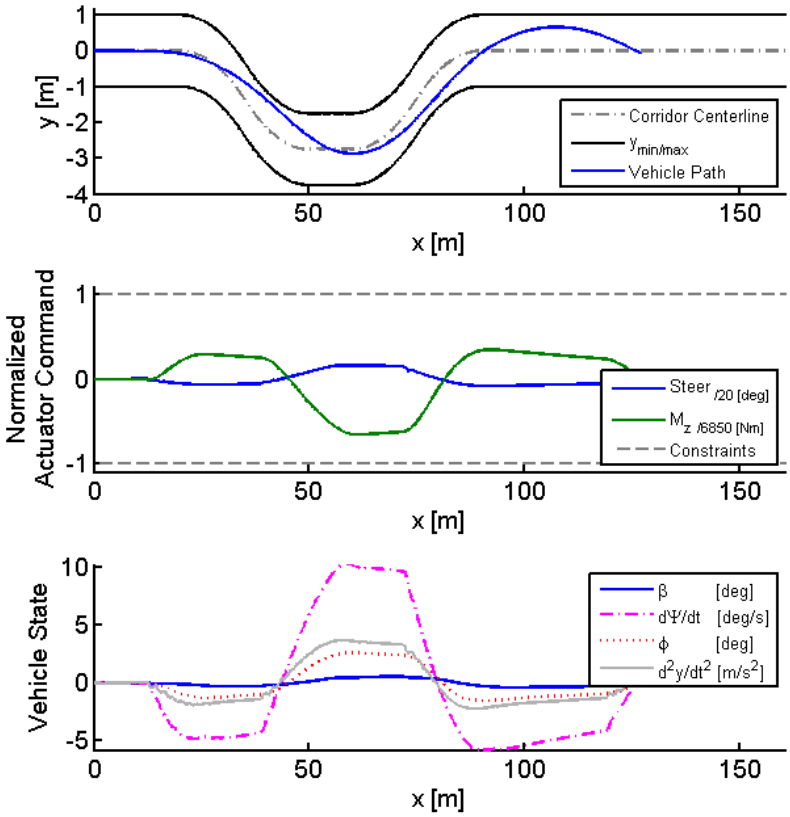

Figure 2.13: Simulation showing the combined effect of steering and braking actuation on autonomous corridor-keeping

II) Moving Hazards

Figure 2.14 shows the result of autonomous vehicle navigation through a moving corridor in which the velocity of hazards 1 and 2 varied as shown in the final subplot. Note that in these plots, the host vehicle is located at the leftmost edge of the predicted trajectory. The trajectory prediction is color-coded according to the front wheel sideslip predicted at each sample, with the step predicting the largest sideslip marked by a circle.

T1 = 1.05 sec

T2 = 4.25 sec

T3 = 5.95 sec

T4 = 6.15 sec

T5 = 7.80 sec

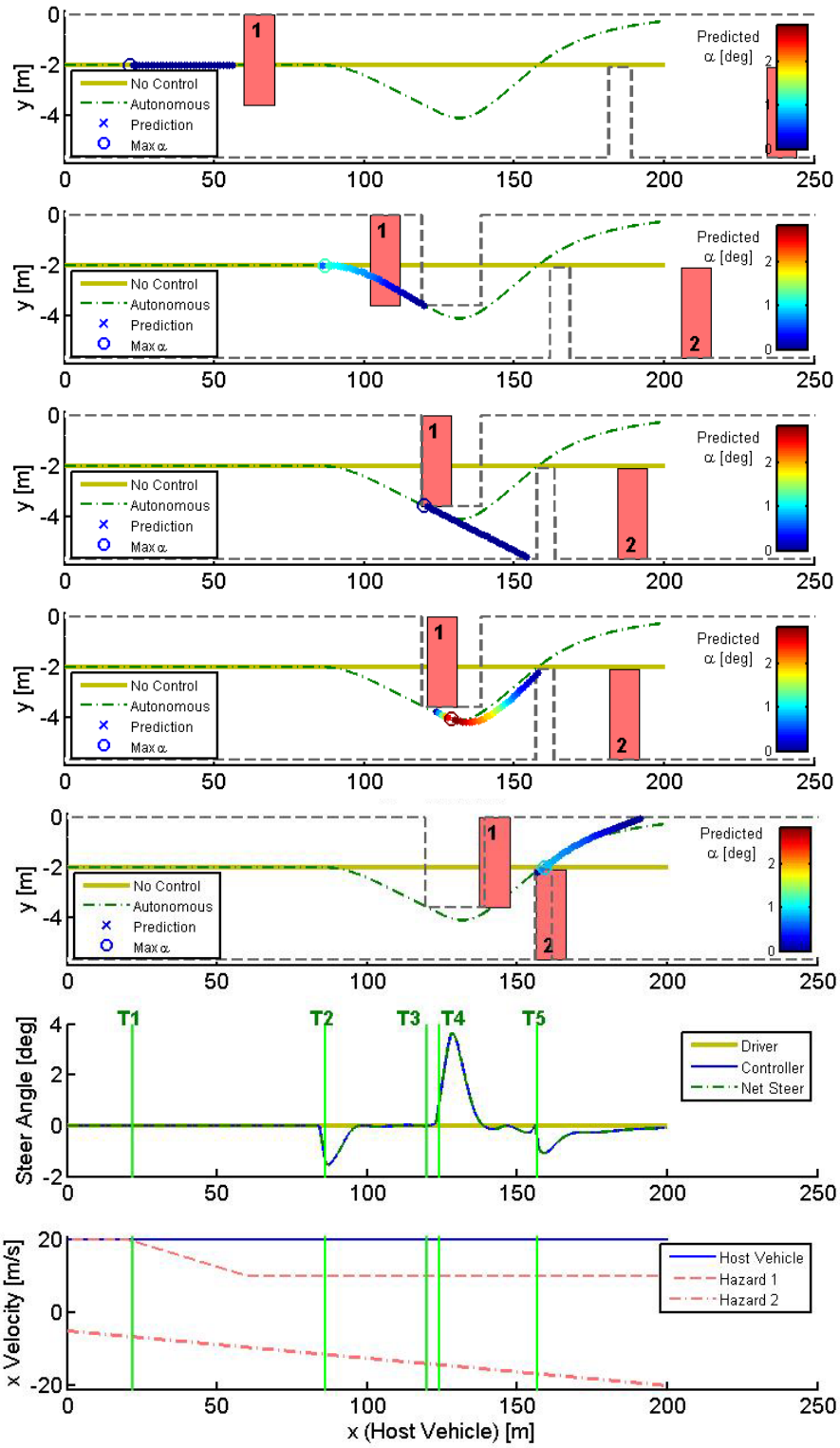

Figure 2.14: Autonomous vehicle navigation through moving hazards using a first-order estimation of future hazard position

At T1, hazard 1 is moving with the same velocity as the host vehicle ($\tilde{x}_1 = 0$) and thus poses no threat. By T2, hazard 1 has decelerated to a constant velocity of 10 m/s ($\tilde{x}_1 = -10$), leading to a finite time to collision as given by (2.35) and a corresponding placement of the lateral position constraint (2.37). At T3, the host vehicle successfully clears the corner of hazard 1 and by T4, the prediction has "seen" hazard 2 (which is gaining speed in the opposite/negative direction). By T5, the host vehicle successfully clears the second hazard and proceeds toward the outside edge of the navigable corridor.

Note that by using the first-order-hold described by (2.35) and (2.37), the predicted collision time and location does not account for the acceleration of each hazard. This is corrected to a small degree by updating hazard position and velocity at every sampling instant (20 hz). For larger hazard accelerations, the second-order prediction described by **(**2**.**36**)** and (2.38) is better suited to forecast future hazard position.

2.4 Experimental Studies

2.4.1 Experimental Setup

Experimental testing was performed using a human-driver-operated test vehicle at Ford's Dearborn Development Center on dry asphault ($\mu \approx 1$). As current law requires a mechanical linkage between the driver and the wheels, an Active Front Steer (AFS) setup was used to couple driver and actuator inputs via a planetary gear. For autonomous control tests, the driver input was removed from the control problem by asking the driver to hold the steering wheel at $\delta_{driver} = 0$. An inertial and GPS navigation system was used to measure vehicle position, sideslip, yaw angle, and yaw rate while a 1 GHz dSPACE processor ran controller code and interfaced with steering actuators. As in simulations, lane data was assumed to have been derived from forward-looking sensors and was therefore predefined virtually.

Table 2.2 shows the controller parameters used in autonomous experiments.

Table 2.2: Controller parameters

Symbol	Description	Value [units]
p	Prediction horizon	{35, 40} [steps]
n	Control horizon	{18, 20} [steps]
Δt_{MPC}	Prediction time step	0.05 [s]
$R_{\alpha\alpha}$	Weight on front wheel slip	0.2657 [1/rad^2]
R_u	Weight on steering input	0.01 [1/rad^2]
$R_{\Delta u}$	Weight on steering input rate (Δ per Δt)	0.01 [1/rad^2]
$u_{\min/\max}$	Steering input constraints	± 10 [deg]
$\Delta u_{\min/\max}$	steering input rate (per Δt) constraints	± .75 [deg] (15 deg/s)
$y^y{}_{\min/\max}$	Lateral position constraints	Scenario-dependent
ρ_ε	Weight on constraint violation	1 x 10^5
V	Variable constraint relaxation on vehicle position	[1.25, ···, 1.25, 0.01]

Two common scenarios were used to analyze the performance of the autonomous system. In both, obstacles and hazards were represented to the driver by cones and lane markings and to the controller by a constrained corridor (with constraint mapping performed by "virtual sensors" and *a priori* high-level planning). Single hazard avoidance tests required that the vehicle avoid a roadway-restricting hazard on a straight roadway. Multiple hazard avoidance tests required that the vehicle navigate around two hazards with a double lane change maneuver. These scenarios are described below.

Hazard avoidance tests required that the vehicle avoid an obstacle in the current lane of travel. In these tests, the vehicle was driven at a constant velocity in the center of a lane with the driver holding the steering wheel at $\delta = 0$, as if asleep or inattentive. A row of cones blocked the vehicle's lane of travel, requiring the controller to: 1) plan a safe lane change maneuver around them, 2) assess the threat posed by that maneuver, and 3) intervene as necessary to avoid the hazard. Figure 2.15 illustrates this test setup.

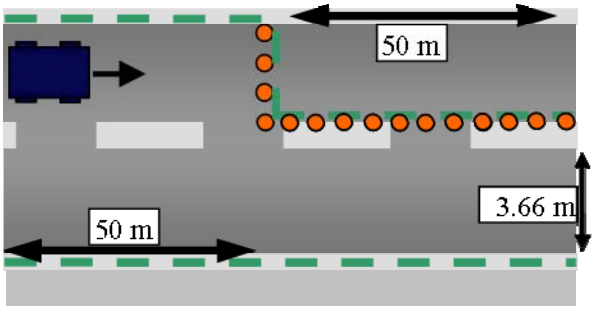

Figure 2.15: Hazard avoidance test setup showing hazard cone placement (large circles) and lane boundaries (dashed) enforced by the controller

Multiple hazard avoidance experiments tested the controller's ability to navigate more complex road/hazard setups that required maneuvers with appreciable load transfer. In these tests (illustrated in Figure 2.16), both lanes of travel were blocked at different locations, forcing the vehicle to change lanes to avoid the first hazard, then change lanes again to avoid the second, as in a double lane change maneuver.

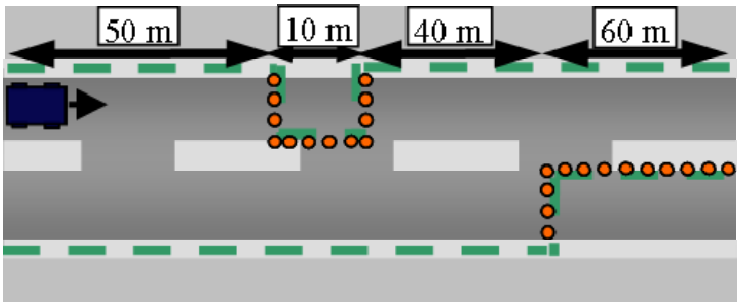

Figure 2.16: Multiple hazard avoidance test setup showing hazard cone placement (circles) and lane boundaries (dashed)

2.4.2 Experimental Results

Experimental results closely matched those achieved in simulation. In each experiment, the control system successfully maneuvered the vehicle through a constrained corridor (i.e. around hazards) while minimizing front wheel sideslip. Figure 2.17 shows the results of autonomous hazard avoidance experiments conducted at $V = 14$ and 10 m/s.

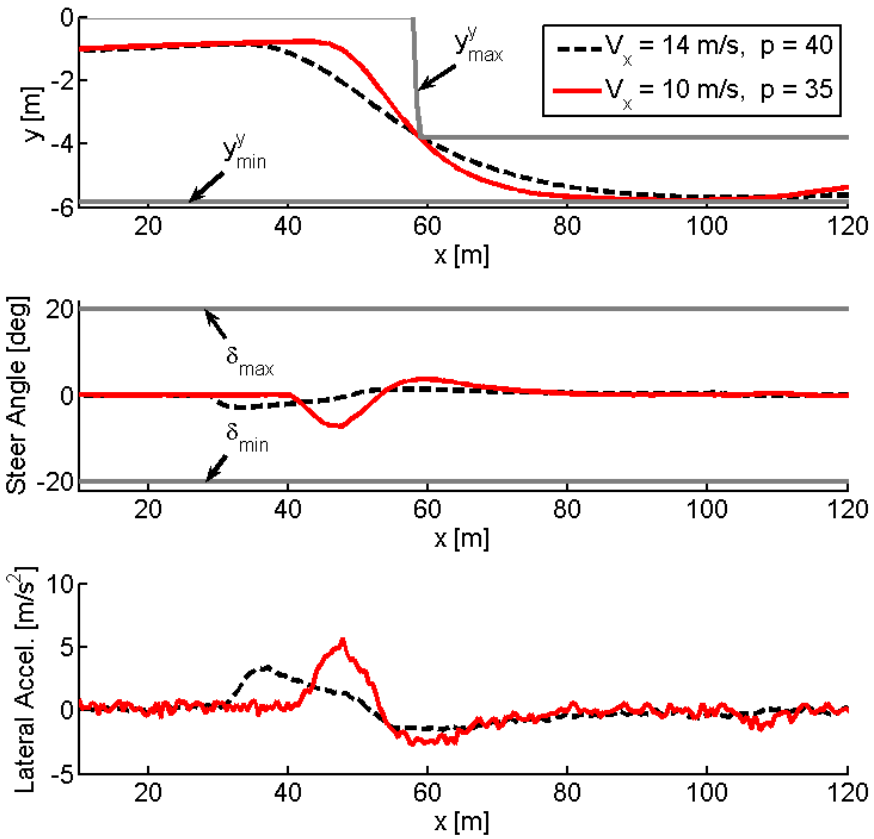

Figure 2.17: Autonomous hazard avoidance experiments at 10 and 14 m/s

Notice that both experiments successfully avoided the corner of the hazard while smoothing the avoidance maneuver (to reduce front wheel sideslip). Also note that the prediction horizon distance scales with velocity (p samples spaced by Δt_{MPC} span $x_{pred} = V_{host} \cdot \Delta t_{MPC} \cdot p$). This velocity scaling allows the controller to effectively "see" the hazard from a greater distance when the vehicle is traveling faster, which in turn allows the controller to find and follow a smoother path around the hazard. The third subplot of Figure 2.17 shows how a 40-sample prediction horizon at 14 m/s compares to a 35-sample prediction horizon at 10 m/s. At the higher speed, lateral acceleration is reduced due to a combination of 5 additional prediction samples and an extended preview distance.

Figure 2.18 shows the results of multiple hazard avoidance experiments at varying velocities and through various corridors. In each experiment, the autonomous controller successfully kept the vehicle within the corridor. Notice that even with a shorter (less computationally-expensive) prediction horizon of 35 samples, the experiment conducted

at 10 m/s (Figure 2.18 c) foresaw and began to maneuver around the hazard while still at a distance of 17.5 meters – earlier than the 10 meters from which the 5 m/s, 40-sample horizon experiment first saw the hazard.

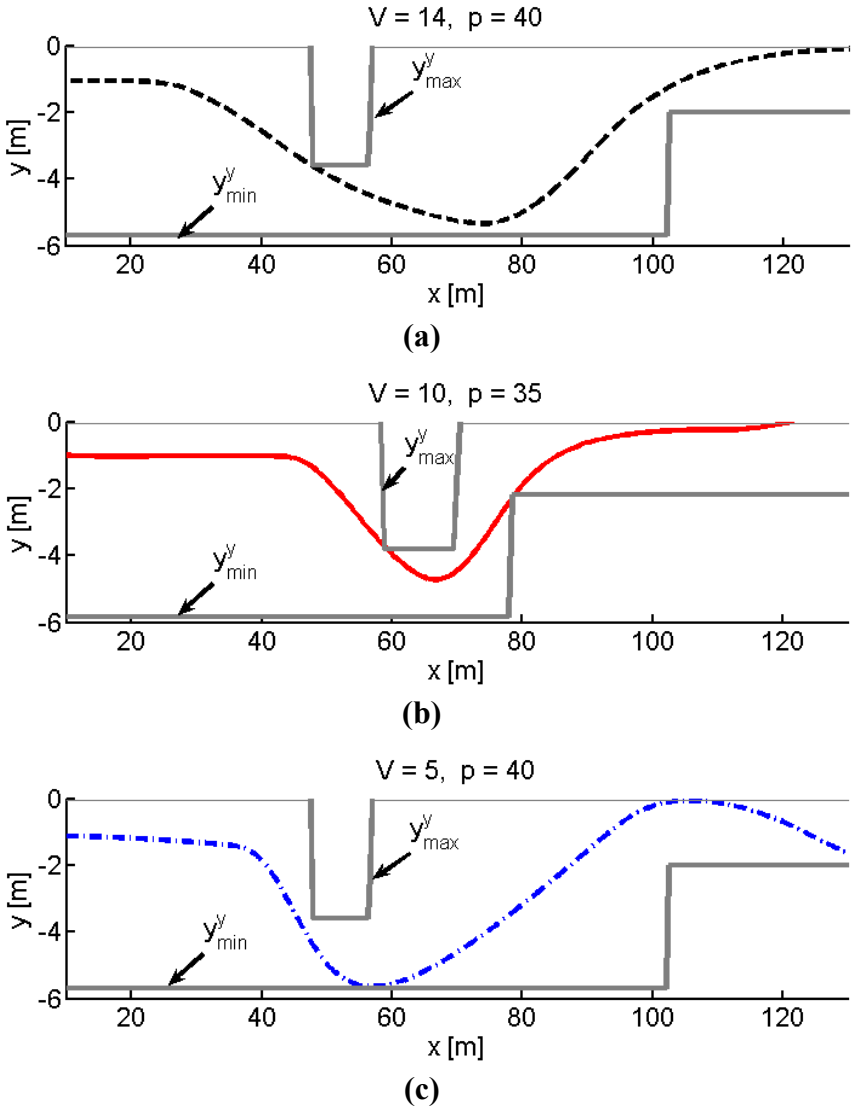

Figure 2.18: Autonomous multiple hazard avoidance experiments at $V = 14$ (a), $V = 10$ (b), and $V = 5$ (c) m/s

2.5 Summary and Conclusions

This chapter has presented a constrained optimal controller that both plans and tracks a best case (with respect to some user-defined criteria) trajectory through a constrained corridor. This corridor-keeping controller has been shown in simulation and

experiment to safely navigate around both static and moving hazards while satisfying actuator constraints and minimizing sideslip at the front wheels. Various objective function and constraint setups have been presented and their results discussed. The controller developed in this chapter now serves as a foundation for the threat assessment and semi-autonomous control presented in Chapters 3 and 4.

3

CHAPTER 3: THREAT ASSESSMENT

3.1 Introduction

The semi-autonomous vehicle navigation framework presented in this thesis was designed specifically for semi-autonomous control of passenger vehicles. The optimal-control-based method that it uses to get from sensor information (and corresponding corridor boundaries) to controller intervention, however, also provides a metric for analyzing the threat posed to the vehicle by a given scenario. This metric is comparable to and in many situations more useful/accurate than existing metrics. This chapter explains.

The basic premise of threat assessment is as follows. First, sensing systems such as radar, LIDAR, or cameras are used to detect, classify, and track objects in the host vehicle's vicinity. Once these potential hazards have been localized and their motion has been estimated, a threat metric is used to predict (or "assess") the threat they pose to the host vehicle. Many threat assessment technologies are designed to then trigger and/or implement countermeasures to reduce the threat. These countermeasures can be passive or active. Examples of passive countermeasures include driver warning [35,79] and seatbelt pretensioning [80]. Active countermeasures include braking [27], steering [30,31], and other forms of actuation that seek to reduce the threat by altering the host vehicle's trajectory. The effectiveness of both passive and active threat assessment and countermeasures depends on their ability to correctly identify hazards and accurately assess the threat those hazards pose to the host vehicle.

Threat metrics described in the literature predominantly use time-based, distance-based, and deceleration-based measures to characterize the threat level of a given

scenario. Time-based threat measures project time to collision (TTC) based on current speeds, positions, trajectories, and (in some formulations) other vehicle states [47,48,81]. Distance-based metrics are generally calculated using prevailing range and vehicle speeds and require constant velocity/acceleration assumptions and simple hazard geometry [50,51]. Finally, acceleration-based metrics assess the threat of a given maneuver based on the minimum (and often assumed constant) lateral or longitudinal acceleration that a simple avoidance maneuver would require, given the current position, velocity, and acceleration of both host and hazard [46,49]. In [46], the inventors estimate the lateral acceleration required to execute a constant radius evasive maneuver. Their implementation then compares this acceleration to a threshold value. When the required acceleration reaches this threshold, braking countermeasures are implemented to reduce the vehicle's longitudinal velocity.

While the above threat metrics have been shown to provide useful estimates of the danger posed by a given maneuver, they are not well suited to consider multiple hazards, complex vehicle dynamics, or complicated environmental geometry with its attendant constraints. The geometrically-simple (straight-line or constant-radius-curve) avoidance maneuvers assumed by these metrics may also misestimate the true threat posed by scenarios where the optimal avoidance trajectory follows a curve of varying radius or non-constant velocity/acceleration.

In contrast, calculating instantaneous threat from an MPC-derived optimal avoidance trajectory inherently considers multiple hazards, actuator limitations/effects, measured disturbances, and (using nonlinear MPC), variable vehicle velocities and accelerations. Configuring the controller to plan a (sideslip-minimizing) trajectory within a safe region of travel ensures that the MPC-based threat assessment provides a true "best case" instantaneous threat assessment. In a driver warning context, threshold threat values may trigger driver warnings at critical/desired threat thresholds. For semi-autonomous control via computer control, threat assessment may be used to determine when and how strongly to intervene. The latter application is the topic of the next chapter. This chapter focuses on the design and development of the threat assessment metric itself.

3.2 Optimal-Control-Based Threat Assessment

Chapter 2 presented the design of a corridor-based trajectory-planning method based on constrained optimal control. When the objective function and constraints are defined as described in 2.3.1, the vehicle path calculated at each time step by the MPC controller is assumed to be the best case or safest path through the environment. Key metrics from this prediction may be used to assess the instantaneous threat posed to the vehicle.

The MPC objective function can be configured to force the constrained optimal solutions to satisfy corridor constraints before minimizing front wheel sideslip. This hierarchy of objectives is achieved by setting constraint violation weights (ρ_ε) significantly higher than the competing minimization weight ($R_{\alpha\alpha}$) on front slip. Then when constraints are not active, as illustrated by the gray vehicle in Figure 3.1, front wheel sideslip – and the corresponding threat – remains low. When the solution is constrained, predicted front wheel sideslip increases with the severity of the maneuver required to remain within the navigable corridor. The dark vehicle in Figure 3.1 illustrates how the MPC-predicted optimal vehicle trajectory might appear as the lateral acceleration, tire slip angles and corresponding threat increase in the presence of an active constraint.

Physical limits on tire cornering friction dictate maximum safe angles of wheel sideslip. These angles provide an objective limit against which predicted sideslip may be normalized; when predicted threat approaches this known limit, loss of stability is imminent. This inherent limitation on stability-critical states such as front wheel slip makes them particularly well suited as objective threat assessors.

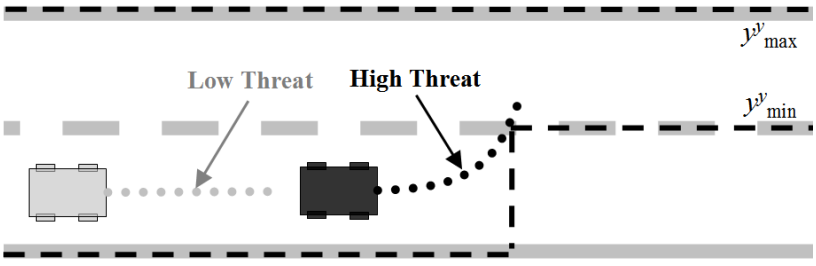

Figure 3.1: Obstacle avoidance scenario showing MPC trajectory plans with varying levels of required front wheel sideslip corresponding to varying levels of threat

3.2.1 Threat Calculation

Various norms may be used to reduce the vector of predicted vehicle states $\vec{x}$ to a scalar threat metric $\mathbf{\Phi}_{\vec{x}}(k)$ (instantaneous threat assessment at time *k*). In this work, the performance of several norms was studied. Table 3.1 describes how each was calculated.

Table 3.1. Norms used to reduce predicted states to a scalar threat metric $\mathbf{\Phi}_{\vec{x}}(k)$

Symbol	Description	Calculation
$\mathbf{\Phi}_{\vec{x}}{}^{0}(k)$	First / nearest predicted *x*	$\mathbf{\Phi}_{\vec{x}}{}^{0}(k) = \lvert x_{k+1} \rvert$
$\mathbf{\Phi}_{\vec{x}}{}^{1}(k)$	Average predicted state $\vec{x}$	$\mathbf{\Phi}_{\vec{x}}{}^{1}(k) = \left\lvert \frac{\sum_{i=1}^{p}(x_{k+i})}{p} \right\rvert$
$\mathbf{\Phi}_{\vec{x}}{}^{2}(k)$	2-Norm of predicted state $\vec{x}$	$\mathbf{\Phi}_{\vec{x}}{}^{2}(k) = \sqrt{\frac{\sum_{i=1}^{p}(x_{k+i})^2}{p^2}}$
$\mathbf{\Phi}_{\vec{x}}{}^{\infty}(k)$	Maximum predicted state $\vec{x}$	$\mathbf{\Phi}_{\vec{x}}{}^{\infty}(k) = \max\lvert \vec{x} \rvert$

3.2.2 Control Horizons

The length of the MPC prediction and control horizons (*p* and *n* respectively) influences both the size and profile of predicted vehicle states $\vec{\mathbf{x}}$. Longer horizons "see" hazards sooner and allow the controller more distance over which to plan an evasive maneuver. The number and placement of control inputs determined by *n* and J_m (2.5), respectively, also affect the evasive maneuver and its attendant threat assessment.

3.2.3 Threat Metrics

Just as various vehicle states may be penalized in the objective function without significantly changing the MPC-generated trajectory plan (as discussed in 2.3.2 I), these states may also be used interchangeably to assess threat posed by a given trajectory

prediction. In this chapter, threat assessment based on lateral acceleration ($\vec{x} = \ddot{\vec{y}} \equiv \vec{a}_y$), front wheel slip ($\vec{x} = \vec{\alpha}$), and a modified objective function cost ($\vec{x} = \vec{J}_{SI}$) are compared.

While lateral acceleration is commonly used in existing threat metrics, front wheel slip was chosen based on three observations. First, front wheel slip is directly tied to, and tends to be a good indicator of, vehicle stability and controllability by front wheel steering. Second, available surface friction places a measureable limit on how large front wheel slip angles can become before loss of control is imminent. This limit provides a useful benchmark against which threat assessments can be compared to assess maneuver stability. Finally, when the cost function's only state objective is to minimize front wheel slip (while remaining within corridor- and actuator-imposed constraints), the path prediction explicitly minimizes the very metric used to assess threat. This hierarchy of objectives – remain within the corridor while minimizing front slip as much as possible – thereby provides a "best case" or minimal-threat assessment from a dynamically-feasible maneuver.

For some scenarios, however, the controller may not completely satisfy position constraints, making α an incomplete indicator of the true anticipated threat. These scenarios may arise when complex corridors cause constraints such as maximum input value or maximum input rate to activate. In these situations, the MPC-predicted vehicle path may violate position constraints, making $\Phi_\alpha = f(\alpha_{\text{predicted}})$ an incomplete threat assessment since it does not does not capture the additional threat posed by the predicted departure from the navigable corridor. To account for such scenarios, an alternative threat metric similar to the objective function cost may be used, where $\vec{x} = \vec{J}_{SI}$, with $\vec{J}_{SI}$ defined as

$$\vec{J}_{\text{SI}}(k) = \frac{1}{2} R_\alpha \begin{bmatrix} \alpha_{k+1}{}^2 \\ \alpha_{k+2}{}^2 \\ \vdots \\ \alpha_{k+p}{}^2 \end{bmatrix} + \frac{1}{2} R_\delta \begin{bmatrix} \delta_k{}^2 \\ \delta_{k+1}{}^2 \\ \vdots \\ \delta_{k+p-1}{}^2 \end{bmatrix} + \frac{1}{2} R_{\Delta\delta} \begin{bmatrix} \Delta\delta_k{}^2 \\ \Delta\delta_{k+1}{}^2 \\ \vdots \\ \Delta\delta_{k+p-1}{}^2 \end{bmatrix} + \frac{1}{2} \rho_{\text{SI}} \begin{bmatrix} \varepsilon^2{}_{k+1} \\ \varepsilon^2{}_{k+2} \\ \vdots \\ \varepsilon^2{}_{k+p} \end{bmatrix} \tag{3.1}$$

This threat metric, while somewhat more difficult to interpret physically, accounts for the additive presence of the various objective function considerations, such as

constraints, input costs, etc, and increases rapidly when constraints are violated. This rate of intervention is tuned independent of the controller cost function by introducing a modified (and adjustable) constraint violation weight, ρ_{SI}. From (2.3), the cost-based prediction $\vec{J}_{SI}$ is related to the predicted front wheel sideslip by

$$\tilde{\vec{J}}_{\vec{\alpha}} = \left(\vec{\alpha} - \vec{r}_{\vec{\alpha}}\right)^T R_{\alpha\alpha}\left(\vec{\alpha} - \vec{r}_{\vec{\alpha}}\right). \tag{3.2}$$

With $\vec{r}_{\alpha} = 0$, this relation allows the cost-based threat assessment $\Phi_{\tilde{J}_{SI}}$ to be mapped to an equivalent (and physically-bounded) front-wheel-slip-based assessment Φ_J via

$$\Phi_J = \sqrt{\frac{\Phi_{\tilde{J}_{SI}}}{R_{\alpha\alpha}}}. \tag{3.3}$$

Simulation results below show how these prediction calculations, threat metrics, and prediction horizons affect the threat assessment.

3.3 Simulation Setup

Two hazard avoidance scenarios were simulated to compare various threat assessments to a simple metric that assumes a constant radius turn (CRT). The first was a single hazard avoidance scenario in which the vehicle drove toward and maneuvered around a single hazard represented by a corner in the constraint corridor (Figure 3.2 a). The second was a lane change maneuver in which the vehicle was required not only to avoid the first hazard, but to then perform the equivalent of a single lane change in order to remain within the constrained corridor (Figure 3.2 b).

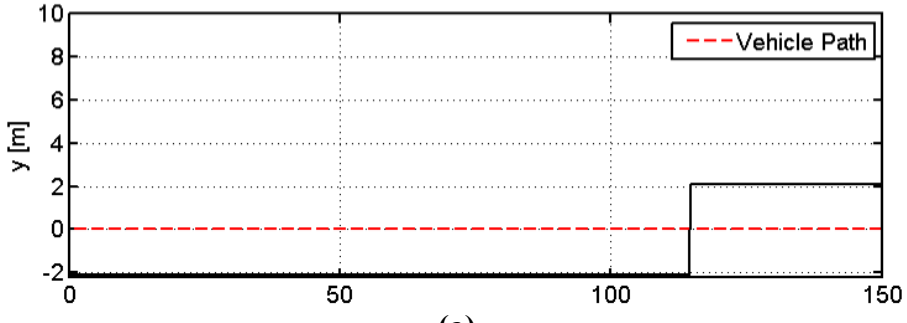

(a)

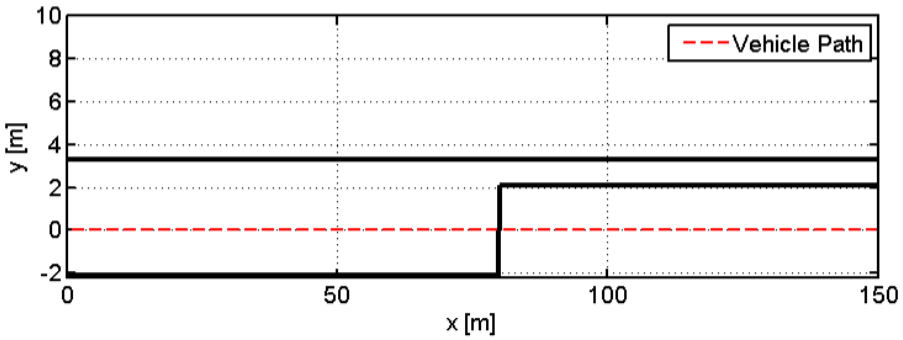

(b)

Figure 3.2: Illustration of hazard avoidance (a) and lane-change (b) maneuvers used in threat assessment simulations

Two types of simulation were conducted. In the first, threat was assessed as the vehicle traveled directly through a road hazard rather than attempting to avoid it. These "passive" tests compared the lateral acceleration calculated by the MPC-based framework to that estimated by a CRT and illustrated the effect of prediction calculations, controller horizons, and threat metric choices on this framework's threat assessment.

The second set of tests studied how closely predicted threat (which was based on the MPC controller's prediction of future vehicle states) matched true threat/states when the controller navigated the vehicle autonomously. Except for prediction horizon p, control horizon n, and constraint relaxation $\mathbf{V}$, these tests used the same controller parameters as those described in Table 2.2. Table 3.2 lists the horizon lengths and relaxation vectors used in these simulations.

Table 3.2: Controller parameters tested in threat assessment simulations

Symbol	Description	Value [units]
p	Prediction horizon	{30, 35, 40, 45, 50, 55, 60} [steps]
n	Control horizon	{2, p/2, p} [steps]
$\mathbf{V}$	Variable constraint relaxation on vehicle position	$[1 \times 10^{-20} \ldots 1 \times 10^{-20}]$ $[1 \times 10^{-5} \ldots 1 \times 10^{-5}]$

In the context of autonomous control, threat assessment evaluation criteria change slightly. Whereas passive threat assessment seeks to describe threat with respect to a "best possible" maneuver, threat assessment in the presence of active countermeasures must also consider the planned avoidance maneuver's similarity to what the controlled vehicle can actually achieve or will actually experience. For other threat assessment metrics (e.g. CRT-based prediction), this comparison of expected to actual threat becomes less useful for two reasons: first, threat assessors that assume CRTs rarely implement a control law that seeks to follow that CRT [27,46]. When they do implement active countermeasures, these systems more often seek to avoid the hazard by non-CRT-compatible means such as braking or combined braking and steering. This disconnect between what is actually predicted and what the controller seeks to achieve inherently changes the utility of a threat assessment since it no longer represents an true/achievable maneuver, but instead only some notion of how close the vehicle is to collision.

The framework developed in this thesis was designed with the intention of providing a best case – and *achievable* – threat assessment. That is, given a set of initial conditions, the threat predicted by the optimal trajectory is presumably attainable if the MPC-calculated inputs are implemented. Thus, autonomously-controlled hazard avoidance and lane change maneuvers were used in addition to similar maneuvers without active countermeasures to assess how closely this framework's predicted best case threat matched the true values of the metric on which it was based (ie. how closely true front wheel slip at a given point represents the predicted front wheel slip at the same point).

3.4 Simulation Results

Simulation results for various threat calculations, prediction/control horizons, and threat metrics are shown below. First, simulations that did not implement active countermeasures are presented to compare the proposed framework's threat assessment to that predicted by a CRT. Results from similar scenarios using an MPC-based autonomous control are then presented.

3.4.1 Threat Assessment without Active Countermeasures

The MPC-based threat assessor provided an accurate prediction of the threat posed by single hazard avoidance and lane change scenarios. The results below demonstrate its efficacy in each.

I) Single Hazard Avoidance

Figure 3.3 shows the results of a single hazard avoidance test with no active countermeasures, a prediction horizon of 40 samples, and a control horizon of the same length. Lateral vehicle acceleration ($\vec{x} = \ddot{\vec{y}} \equiv \vec{a}_y$) was used as the threat metric in order to compare this framework's assessments to those predicted by a CRT.

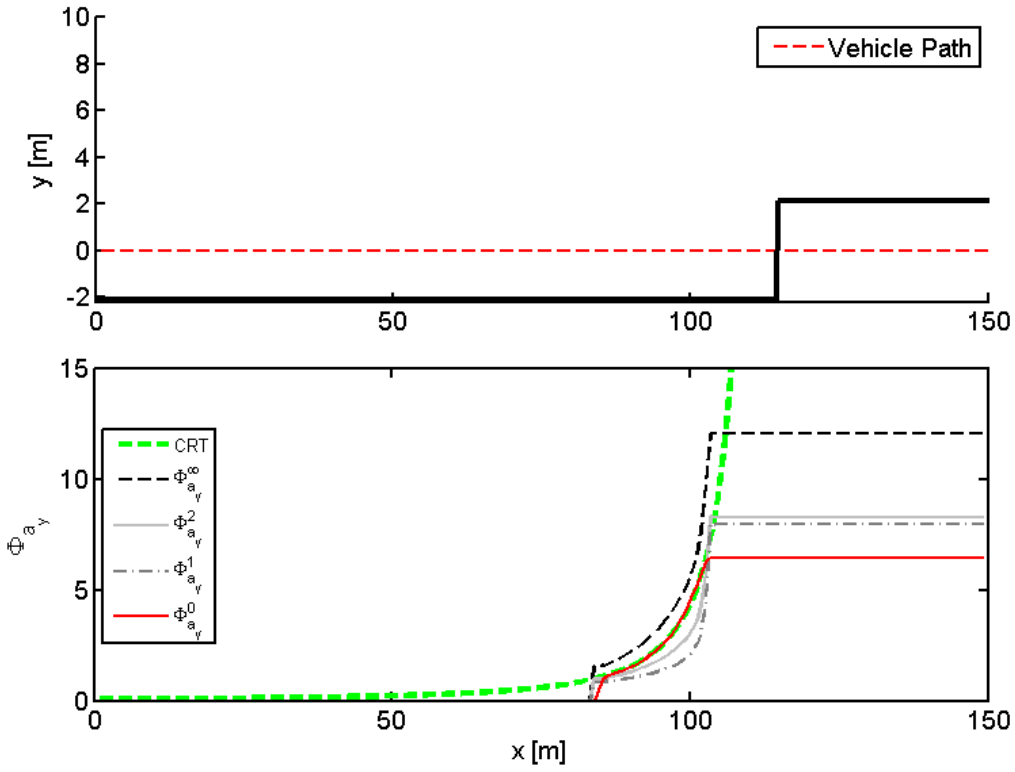

Figure 3.3: Threat assessment comparison

Notice that the "0" norm of the optimal maneuver's prediction most closely resembles the CRT assessment. This similarity arises from the MPC calculation, whose first prediction is calculated based on the current steer angle (which is constant between samples). This constant steer angle roughly translates to a short-lived (one time sample

long) CRT and thereby causes the framework's predicted lateral acceleration to closely mirror the CRT's. Also note that the ∞ norm causes this framework's threat assessment to increase at roughly the same rate, though slightly earlier than the CRT assessment.

The average and root mean square norms on predicted sideslip both match the CRT assessment when the hazard is initially detected and then again just before the steering constraints activate. This is due to the fact that when the hazard is first detected, the objective-function-minimizing avoidance maneuver exhibits a relatively-constant radius of curvature. This causes both average and root mean square values to mimic the acceleration required by a CRT. As soon as the end of the prediction passes the corner of the hazard ($x \approx 114$ m), the controller begins to relax its predicted inputs and required lateral acceleration on all positions with $x > 114$ m. This causes the threat assessment based on these norms to decrease. Just before the steering constraints activate, the predicted maneuver becomes infeasible, the steering angle reaches its limit, and predicted lateral acceleration from the resultant vehicle trajectory peaks at a constant value similar to what the CRT requires at that location.

Figure 3.4 shows the trajectories, threat assessments, and steering inputs calculated by the controller, along with each prediction's location (k) within the prediction horizon p. Notice that when the hazard was first "seen", the controller planned an avoidance trajectory of relatively constant lateral acceleration as mentioned above. From $\sim 100 \leq x_{host} \leq \sim 85$, this path plan required increasing levels of lateral acceleration initially while tapering off to low lateral acceleration past the hazard. Also notice that because the ∞ norm selects the maximum lateral acceleration resulting from any two (possibly unequal) steer commands over the prediction horizon, it provides a more conservative estimate of threat in this particular scenario than the CRT-based assessment. For generous steering rate constraints, this result is expected to be common to most other scenarios.

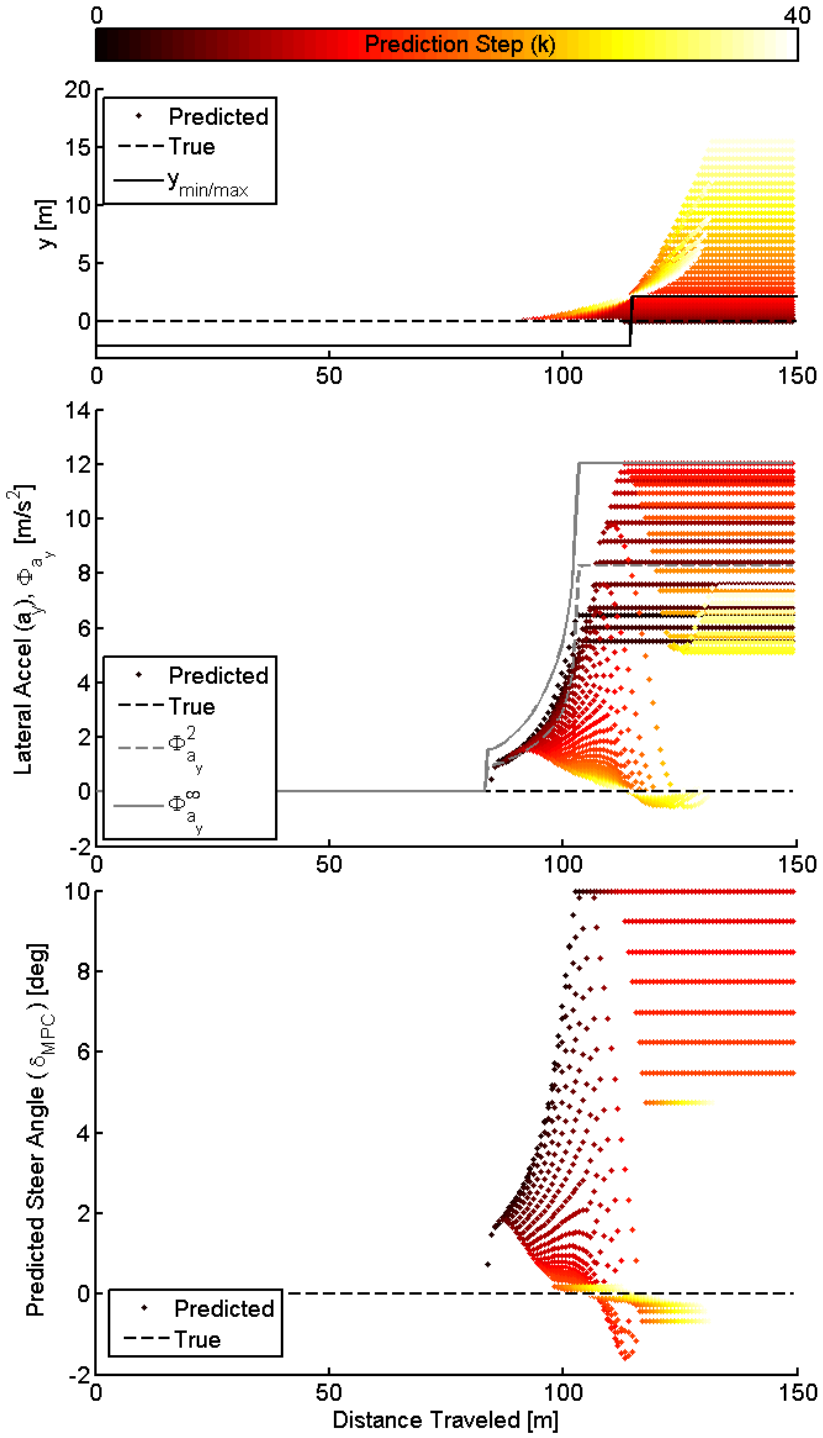

Figure 3.4: Predicted vehicle trajectories and attendant threat assessments and optimal steering inputs

Figure 3.5 shows the result of varying prediction horizon on threat assessments calculated from the lateral acceleration metric. As these plots illustrate, lengthening the

prediction horizon tends to change primarily the distance from which the hazard is first detected. As soon as the controller "sees" it, regardless of the prediction horizon length, the lateral acceleration required to avoid it jumps to a value similar to that required by a CRT. Controllers with each of these prediction horizons, metrics, and threat calculations then follow the same threat line until the steering constraints activate at $\delta = 10$ deg.

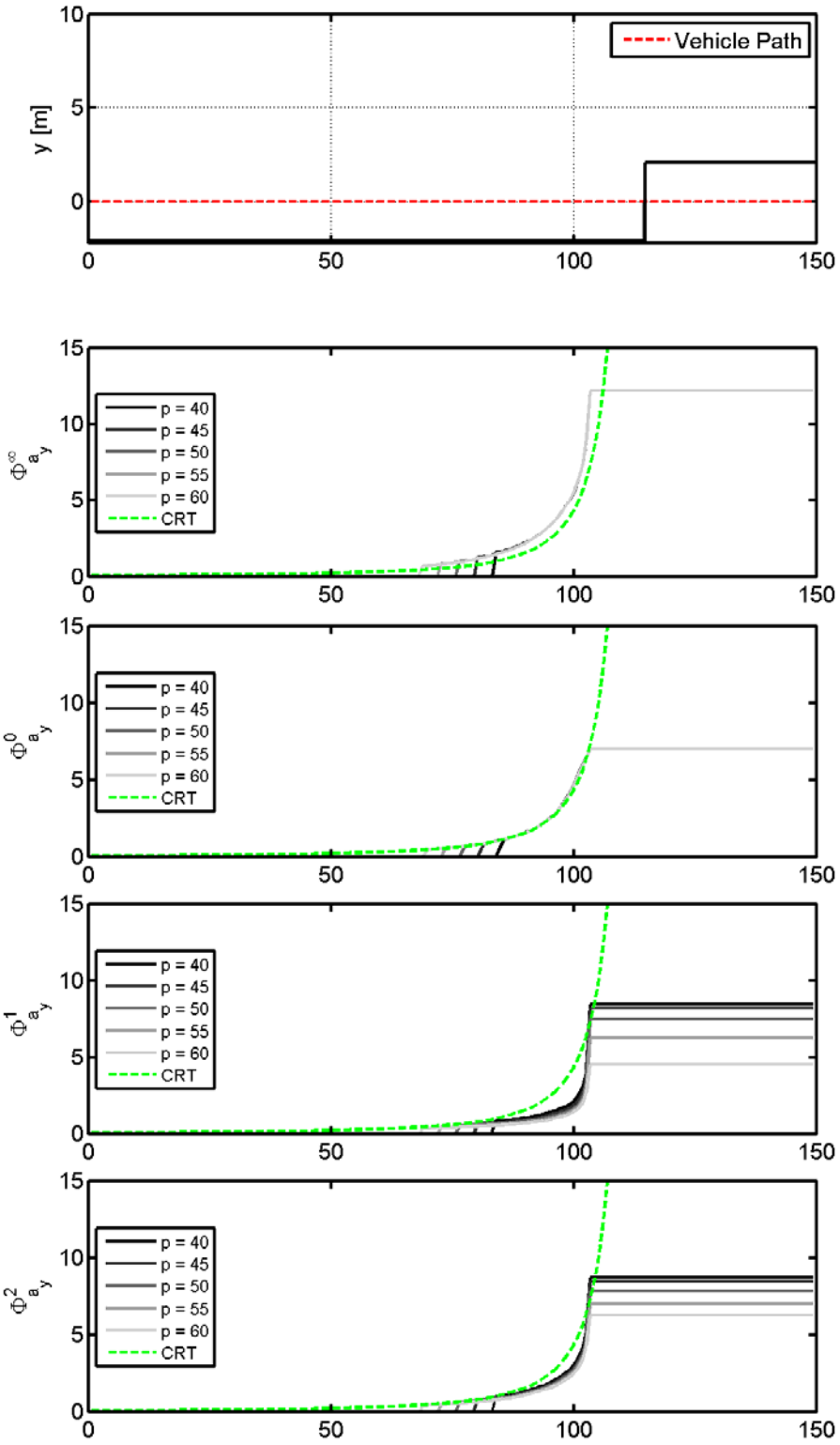

Figure 3.5: Effect of prediction horizon (*p*) on threat assessments

The length of the control horizon (*n*) was shown to exert relatively little influence on this framework's threat assessment. Only at very small values ($n = 2$), did this

parameter appreciably affect the threat assessment and then only for long (p > 45) prediction horizons. Figure 3.6 illustrates.

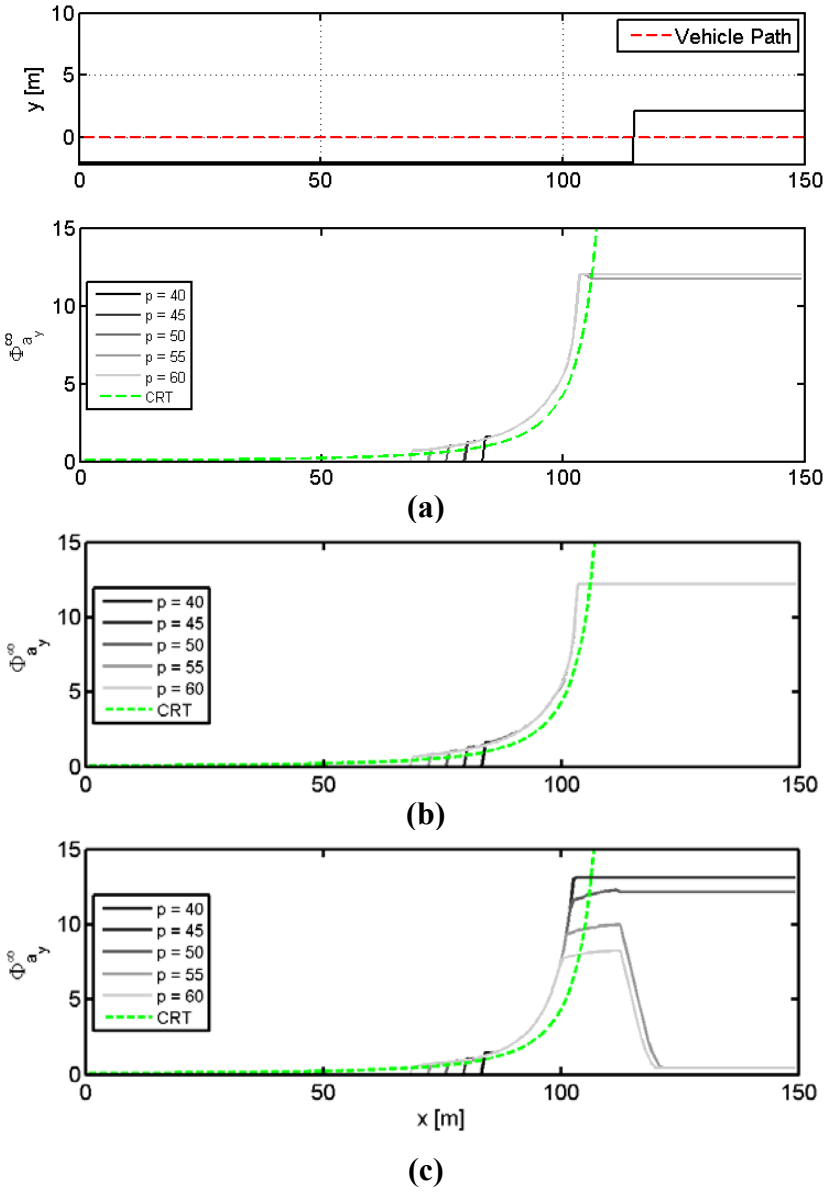

Figure 3.6: Threat assessments resulting from *n=p* (a), *n=p/2* (b), and *n=2* (c)

The drop in predicted threat observed for the third set (n=2) of prediction-control horizons is the result of the controller's attempt to plan an objective-function-optimal path around the hazard using only two control inputs. Once avoiding the hazard using two inputs becomes impossible (x≈100 m), the optimal solution seeks to minimize total constraint violation using maneuver that requires a lower lateral acceleration. Figure 3.7 shows the optimal trajectories and steering inputs calculated when p = 60 and n = 2.

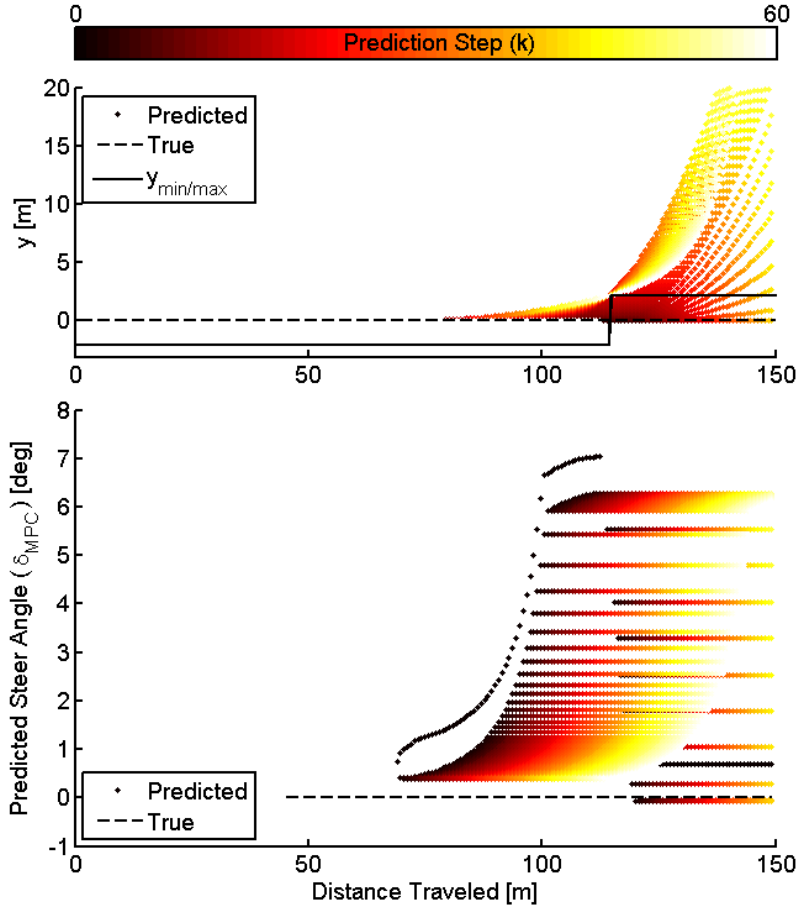

Figure 3.7: Predicted vehicle trajectories and attendant steering inputs

Notice that J_m in these simulations allocated both control inputs at the first two steps of the optimal control calculation, causing the controller to calculate a large control input for the first step, followed by a reduced input for the second. Steering rate limits constrained the step change between these two inputs and thus led to a solution requiring greater vehicle sideslip than would be required had more control inputs been allowed or the inputs been spaced differently. It is not unreasonable to expect that, with real-time adaptation of J_m, the threat assessment for n=2 could be decreased, but for threat assessment purposes, this configuration provides a conservative estimate of threat.

II) Lane Change

For lane change maneuvers, the MPC-based framework correctly assessed a slightly higher threat than the CRT prediction as the vehicle approached the road hazard. Whereas the CRT maneuver predicts only the lateral acceleration required to avoid the

corner of the first hazard, the MPC-based assessment also accounts for the lateral acceleration required to avoid leaving the road surface after the first hazard has been avoided. Figure 3.8 compares the threat calculated using various norms and prediction horizons to the CRT assessment.

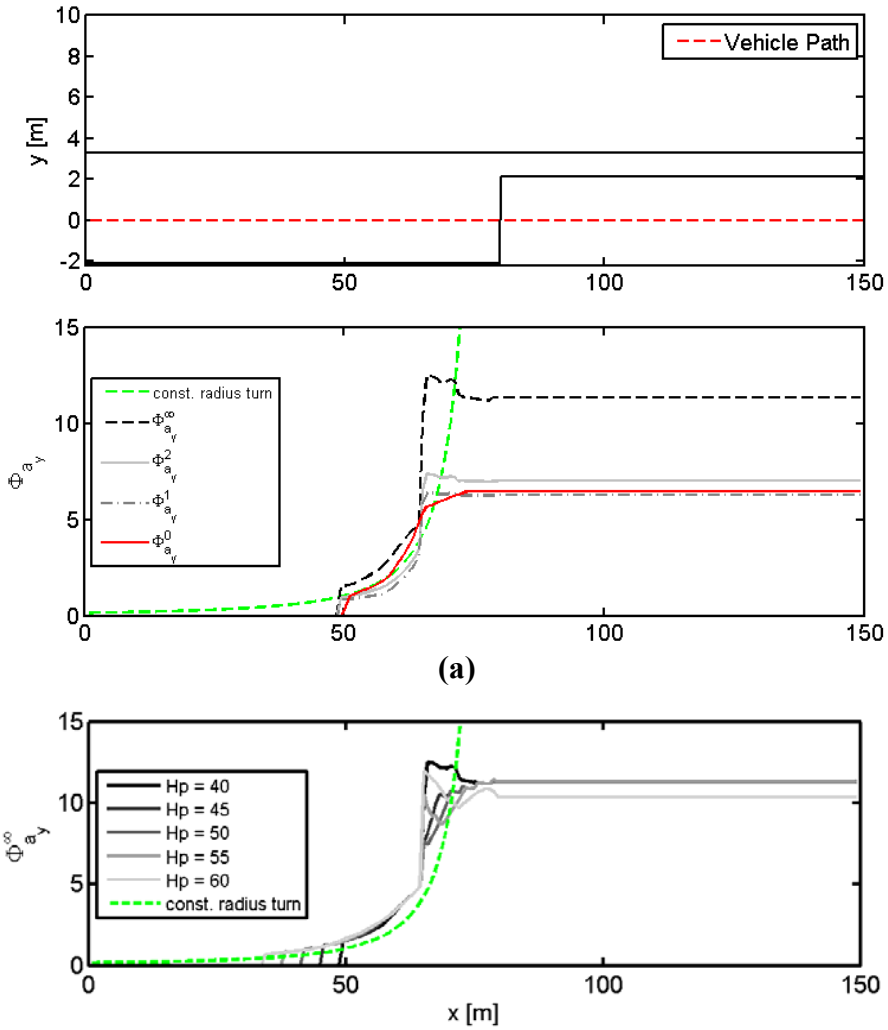

(a)

(b)

Figure 3.8: Lane change maneuvers without active intervention showing how the proposed framework's threat assessment varied by (a) threat calculation and (b) prediction horizon

As Figure 3.8 illustrates, the threat assessed by the ∞-norm in this scenario rises sharply as soon as the opposite road edge is detected. When the driver does not respond or correct course as in this simulation, predicted threat settles to a lower value for the same reasons as discussed above (trajectory cost minimization). Meanwhile, the CRT-

based threat assessment considers only the corner of the nearest hazard, causing its prediction to completely miss the additional lateral acceleration required to level off in the avoidance lane. Figure 3.9 illustrates how infeasible initial conditions caused by driver (and controller) inaction affect the control inputs and predicted trajectories computed by this MPC formulation.

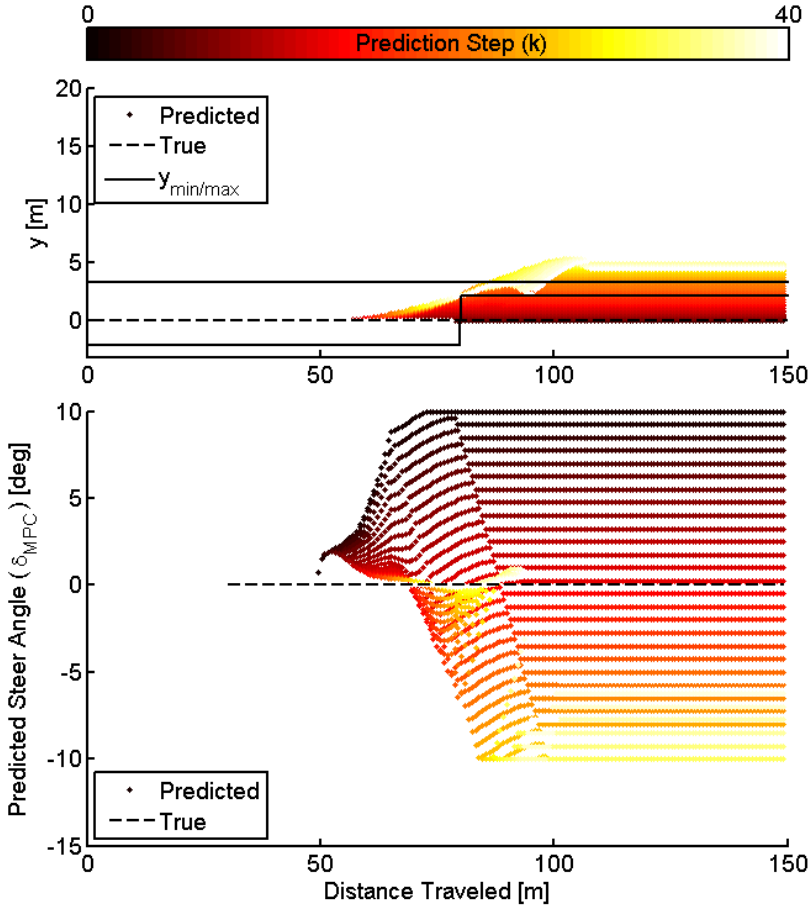

Figure 3.9: Predicted vehicle trajectories and attendant steering inputs for a lane change maneuver, *p*=40, *n*=40

Notice that as soon as the maneuver can no longer satisfy position constraints, the controller saturates both δ and $\Delta\delta$ in a vain attempt to guide the vehicle back onto the navigable road surface. As soon as these constraints activate, the predicted threat saturates.

The above results show that the MPC-based threat assessment provided by the proposed framework gives a similar, albeit more situation- and plant-aware threat assessment to that based on a constant radius turn. When calculated from the maximum

MPC-predicted lateral acceleration (∞-norm), these predictions provide slightly earlier warning which explicitly accounts for more complex hazard geometry and more realistic actuator limits.

3.4.2 Threat Assessment with Autonomous Control

As mentioned in 3.3, assessing threat based on a controller-achievable maneuver requires some measure of how well the predicted threat/state represents what the vehicle would actually experience under autonomous control. This relationship between predicted threat and the controller's ability to maintain true threat at or below this level plays an important role in the semi-autonomous control implementation discussed in Chapter 4. Below, threat assessments using various controller and prediction parameters are compared to the true vehicle state and shown to provide a reliable estimate of the vehicle's true states under autonomous control.

I) Single Hazard Avoidance

Figure 3.10 shows how predicted front wheel sideslip (Φ_α) as assessed by various prediction norms compares to true front wheel sideslip (α).

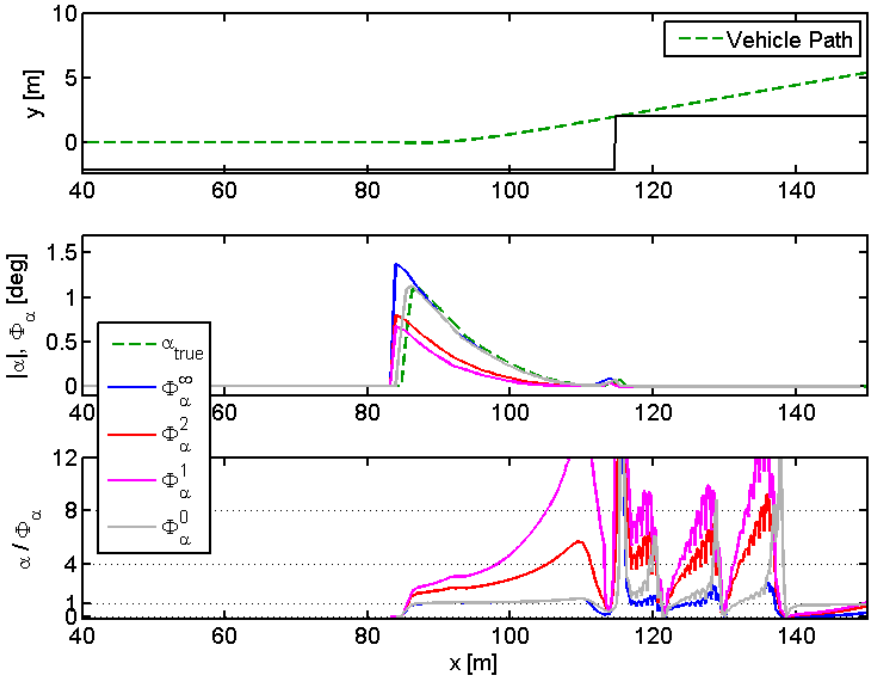

Figure 3.10: Threat assessment using the front wheel slip metric

As Figure 3.10 illustrates, threat assessment based on the next available sample of front wheel slip (Φ^0_α) most closely estimated the true threat at that location. This is not surprising as the "0" norm samples the vehicle's next predicted state (5 ms forward in time) from the vehicle's current state. Notice in the third subplot that the ratio of predicted-to-true slip from this norm is nearly unity leading up to the hazard. This close correlation between prediction and reality also implies that for the low sideslip and yaw angles experienced in this maneuver, the linear controller model closely approximates the plant.

Figure 3.10 also shows that the ∞-norm closely approximates the true vehicle state from almost the moment the hazard is "seen" at x≈85 m to the point at which the host vehicle successfully clears the hazard corner (x≈114 m). This close correlation is also apparent in the third subplot where the ∞-norm result is nearly overlayed with the "0"-norm result at $\alpha_{true}/\alpha_{\text{pred}} = 1$. The only significant difference between the ∞- and the "0" norms here is that the former anticipates the hazard slightly earlier and adjusts its threat assessment accordingly. This anticipation, together with the ∞-norm's accurate prediction of true front wheel slip (or the slip to be expected if the controller is given full control authority) make it an especially useful norm for governing semi-autonomous control. The ∞-norm is thus used exclusively in the simulations and experiments presented in Chapter 4.

Figure 3.11 shows how threat assessment based on lateral acceleration performs in an autonomous control context.

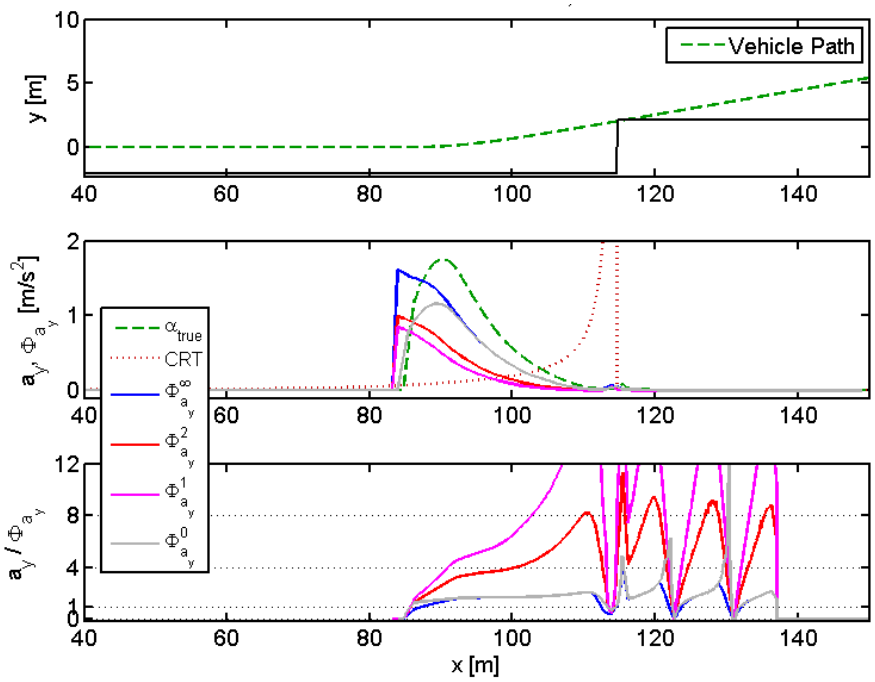

Figure 3.11: Threat assessment using the lateral acceleration metric

Notice that while threat assessments based on the Φ_{a_y} metric lead true lateral acceleration (similar to those predicted by Φ_α), they fail to accurately capture the magnitude of this state as evidenced in the third subplot. Where for Φ_α-based threat assessment, this ratio of true-to-predicted state was nearly unity for the ∞- and "0"-norms, the Φ_{a_y}-based assessment exhibits ratios closer to 1.7. This may evidence greater sensitivity in this metric to model mismatch, further warranting the use of Φ_α- or Φ_J-based metrics for threat assessment and semi-autonomous control.

Figure 3.12 shows how modified objective function cost (with α weighted in the objective function) performs as a threat metric.

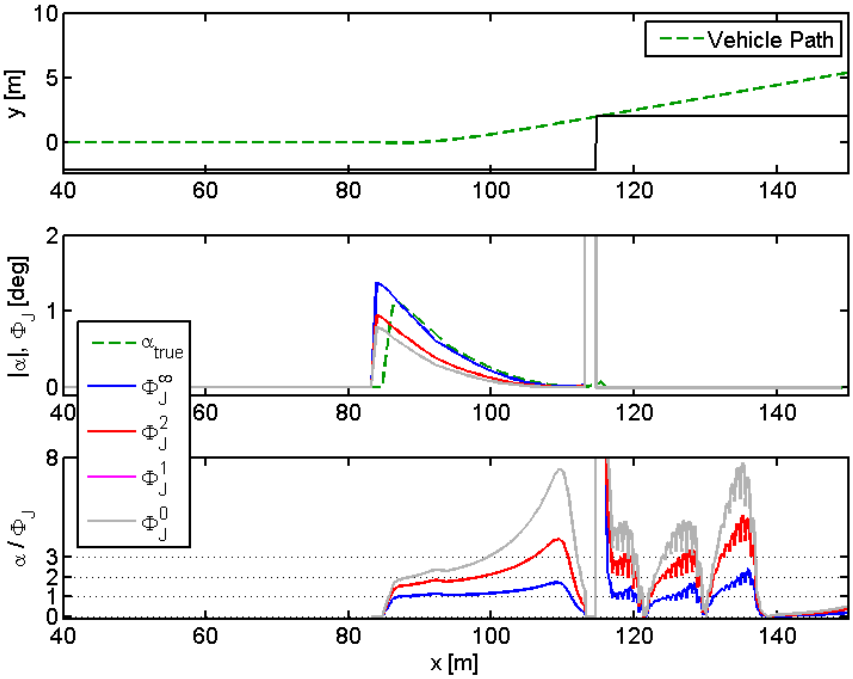

Figure 3.12: Threat assessment using the objective function cost metric

Similar to Φ_α, Φ_J accurately predicts front wheel sideslip when used in conjunction with both the ∞- and "0"-norms. The only significant difference between these two metrics occurs at x≈113 m. At this location, the predicted vehicle trajectory slightly violates the corner of the y_{min} constraint, causing a spike in J_{SI} and a corresponding spike in Φ_J. This slight constraint violation, while not unexpected when position constraints are softened, may be accounted for by providing a "buffer region" around hazards when defining constraint positions.

Figure 3.13 shows the effect of prediction horizon on threat assessments Φ_α and Φ_J. Notice that as prediction horizon increases, the autonomous MPC controller effectively smoothes the avoidance maneuver in order to reduce both steering inputs and front wheel sideslip (which are both penalized in the objective function). This control input smoothing affects both predicted and actual threat in a similar fashion, leading to nearly identical $\alpha/\Phi_{\tilde{x}}$ ratios for each metric. From a robustness standpoint, this is desirable as it suggests that the autonomous MPC controller configured as described in Chapter 2 can be used to plan, predict, and track optimal (i.e. threat-minimizing) trajectories through a constrained corridor. This ability is key to the semi-autonomous control method described in the next chapter.

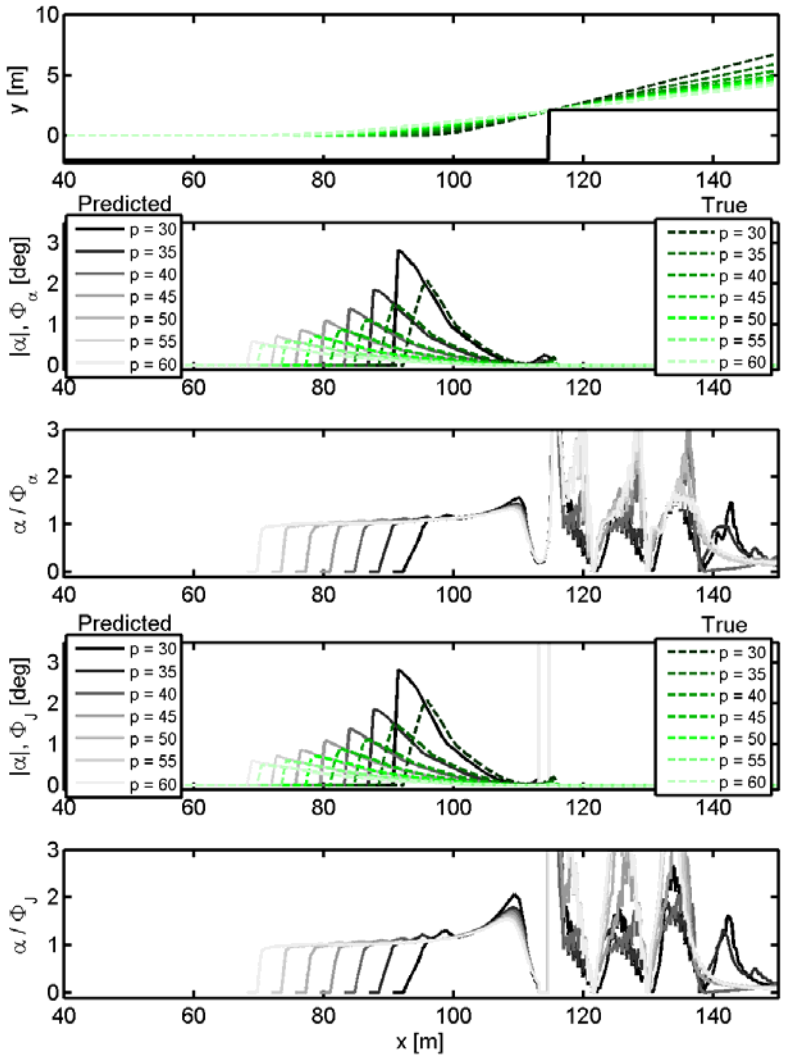

Figure 3.13: Threat assessment using Φ_α and Φ_J for varying prediction horizons

II) Lane Change

Figure 3.14 shows the result of threat assessment using the ∞ norm of the Φ_α and Φ_J metrics in a lane change maneuver.

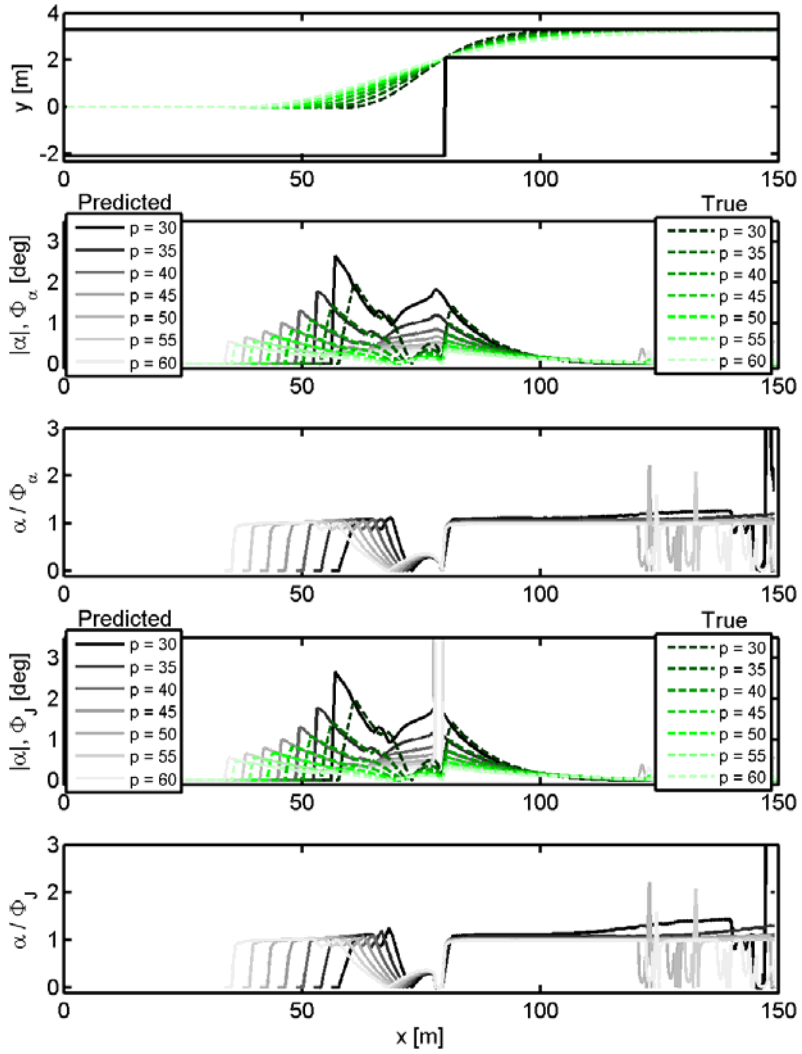

Figure 3.14: Threat assessment using Φ_α and Φ_J for varying prediction horizons in a lane change maneuver

Notice that between $x\approx60$ and $x\approx70$, the true front sideslip decreases sharply as the vehicle clockwise right to remain within the narrow corridor. Meanwhile, the threat prediction increases in anticipation of the corrective maneuver required to remain within the corridor. This leads to a temporary reduction in $\alpha/\Phi_{\bar{x}}$. As the vehicle passes the corner of the first hazard at $x \approx 85$m, true slip once again matches predicted slip. These

results suggest that the MPC controller may be configured to accurately plan, assess, and track aggressive maneuvers using Φ^{∞}_{α} and Φ^{∞}_{J} metrics.

3.5 Summary and Conclusions

This chapter has developed a method for assessing the threat posed by a given scenario from the trajectory plan of a constrained MPC controller. This method has been compared to others that assume a constant radius turn (CRT) avoidance maneuver. When hazard geometry is simple, this method's prediction closely mirrors and slightly preempts the CRT-based assessment. For more complex hazard avoidance scenarios, such as those requiring a lane change maneuver, this method is shown to account for the increased threat, thus providing a significant improvement over simple CRT-based assessments.

The principal contribution of this chapter was the demonstration of this method's ability to accuracy predict an MPC-controlled vehicle's performance as it tracks the MPC-predicted trajectory plan through a constrained corridor. Two metrics are shown to provide a nearly one-to-one mapping of predicted threat to true threat, suggesting that, if provided full control of a vehicle, this MPC controller can reasonably be expected to maintain critical vehicle states/threat at or below their predicted values. Chapter 4 explains why this is important to the design of the overall semi-autonomous system.

Note that in this chapter, only results from MPC controllers penalizing front wheel slip in the objective function ($R_{\alpha\alpha}>0$) were shown. For a comparison of predictions obtained using this objective function setup to an objective function that penalizes lateral acceleration rather than front wheel slip ($R_{a_y a_y}>0$), see Appendix B.

4

CHAPTER 4: SEMI-AUTONOMOUS CONTROL

4.1 Introduction

This chapter describes the final component of the semi-autonomous framework: a shared control scheme for active hazard avoidance. The controller described here builds on the methods for path planning and threat assessment described in Chapters 2 and 3. The resulting control framework provides a powerful means of semi-autonomously avoiding road hazards.

4.1.1 Intervention Law

Given a best case vehicle path through the environment (Chapter 2) and a corresponding threat assessment (Chapter 3), a semi-autonomous intervention law determines how much control authority to allocate to the driver and how much to allocate to the MPC controller. This allocation is based on the scalar threat assessment Φ. Generally speaking, low predicted threat causes more of the driver's input and less of the controller's input to be applied to the vehicle while high threat allows controller input to dominate that of the driver. An intervention function is defined to allow for a smooth blending of driver and controller inputs.

Denoting the current driver input by u_{dr} and the current controller input by u_{MPC}, the blended input seen by the vehicle, u_v, is defined as

$$u_v = K(\Phi)u_{MPC} + (1 - K(\Phi))u_{dr} \tag{4.1}$$

The intervention function $K(\Phi)$ translates predicted vehicle threat Φ into a scalar blending gain $K \in [0 \quad 1]$, defined as

$$K = \begin{cases} 0 & 0 \le \Phi \le \Phi_{eng} \\ f(\Phi) & \Phi_{eng} < \Phi < \Phi_{aut} \\ 1 & \Phi_{aut} \le \Phi \end{cases}. \qquad (\mathbf{4.2})$$

As shown in (4.2), the shape of K is described by the threat level at which the MPC controller engages (Φ_{eng}) and the level at which the MPC control system assumes full authority and effectively acts as an autonomous controller (Φ_{aut}). When the predicted threat Φ is less than the low-threat threshold Φ_{eng}, K is set to zero, effectively passing all of the driver's control input (and none of the controller's) to the vehicle. Above the high-threat threshold Φ_{aut}, K is set to one. This allows the MPC controller full control authority to autonomously track the high-threat path. Once the predicted threat is reduced to a safe(r) level (i.e. below Φ_{aut}), the driver's control authority is increased.

In this chapter, linear and piecewise linear intervention functions are employed, though nonlinear formulations – including some with dependence on controller/plant/environmental parameter dynamics – have also been tested. In the results below, linear and piecewise linear intervention functions were parameterized by Φ_{eng} and Φ_{aut} as in (4.3). Figure 4.1 illustrates gain (K) as a function of threat (Φ) for various forms of $f(\Phi)$.

$$f(\Phi) = \frac{\Phi_{aut} - \Phi}{\Phi_{aut} - \Phi_{eng}} \qquad (\mathbf{4.3})$$

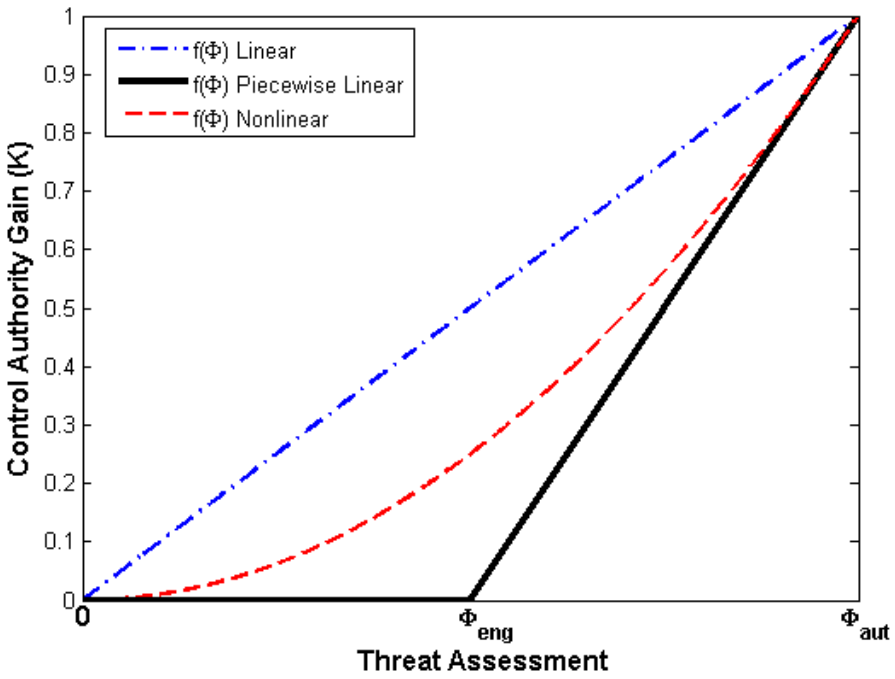

Figure 4.1: Intervention laws used to translate threat assessments into controller blending gains

The intervention threshold Φ_{eng} may be chosen based on driver preference. Increasing Φ_{eng} widens the "low threat" band in which the driver's inputs are unaffected by the controller. While this provides greater driver freedom for low-threat situations, this freedom comes at the cost of increasing the rate of controller intervention when Φ_{eng} is exceeded. This increased rate of intervention may adversely affect driver experience, as discussed in the results below.

Increasing the value of Φ_{aut}, on the other hand, delays complete controller intervention until more severe maneuvers are predicted. This threshold can be set to ensure the controlled maneuvers remain feasible. When physically-limited states, such as front wheel sideslip α or modified objective function cost J_{SI}, are used for threat assessment, Φ_{aut} may be set at known stability limits of these states. In the case of front wheel sideslip, the friction-limited bounds on the linear region of the tire force curve (2.11) suggest $\Phi_{aut} \leq 5^{\circ}$ on surfaces with a friction coefficient $\mu = 1$. Setting $\Phi_{aut} \leq 5^{\circ}$ thus places an effective limit on the amount of front wheel sideslip allowed in semi-autonomous operation. By the time the predicted hazard avoidance maneuver reaches this

level of severity, the controller has full control authority and can – unless unforeseen constraints dictate otherwise – guide the vehicle to safety.

When controller intervention is based on Φ_J (rather than Φ_α), control authority gains become coupled with the "optimal" MPC solution. With an appropriate cost function formulation and choice of ρ_{SI}, this guarantees that 1) the threat metric regulating controller intervention is minimized in the path planning process (and associated control calculation) and 2) the controller maintains complete control authority when constraints are binding. Note that due to the additive presence of other objective function terms such as constraints and input costs, intervention based on $\vec{J}_{SI}$ may cause Φ_J to reach threshold values Φ_{eng} and Φ_{aut} before the predictive state α reaches a critical level. This behavior is by design, since constraint violation is seen as an added threat warranting additional control intervention. For this reason, similar thresholds are used below to govern slip-based (Φ_α) and cost-based (Φ_J) intervention.

4.1.2 Driver Input Consideration

In some scenarios, driver inputs may differ significantly from controller inputs. Such cases can lead to abrupt adjustments in the overall steering input (u_v) as K increases. These abrupt changes may saturate steering rate constraints (which are limited by the available steering actuators) and may be uncomfortable and/or unnerving to the human driver. To account for differences between driver and controller input, K may be augmented by an additional term to increase controller intervention in proportion to the driver's deviation from the best case input. This augmentation can be described by

$$K_{aug}\left(\Phi, u_{MPC}, u_{dr}\right) = f\left(\Phi\right) + \left(1 - f\left(\Phi\right)\right)\left(1 - e^{\frac{-\left|u_{MPC} - u_{dr}\right|}{\Delta u_{\max}}}\right) \tag{4.4}$$

where $f(\Phi)$ is defined as in (4.2) and $\Delta u_{\max}$ represents the maximum difference between driver and controller inputs $\left(\Delta u_{\max} = u_{\max} - u_{\min}\right)$. Figure 4.2 shows the effect of this modification on piecewise linear intervention laws.

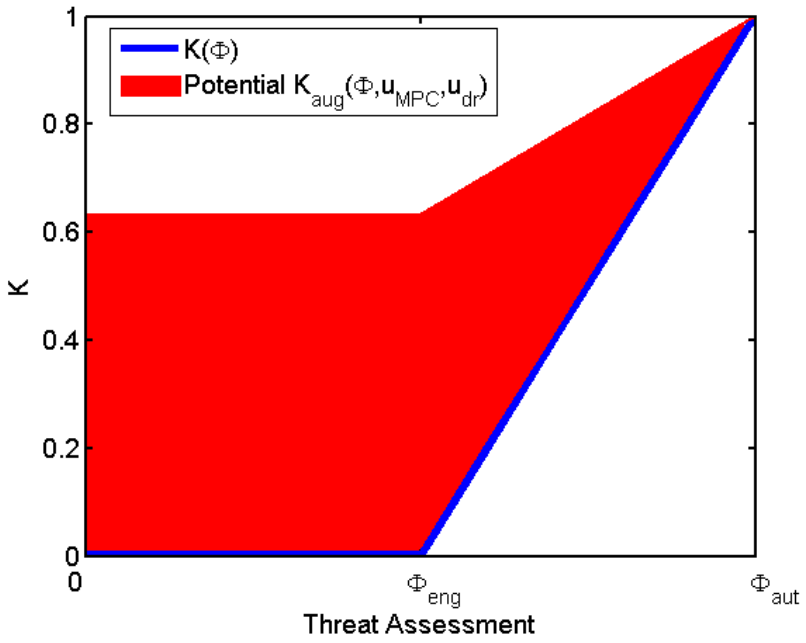

Figure 4.2: Intervention law showing the effect of augmenting *K* according to driver-controller input deviation

4.2 Simulation Studies

Semi-autonomous hazard avoidance was tested for various threat metrics (Φ_α and Φ_J), intervention thresholds (Φ_{eng} and Φ_{aut}), and intervention laws (K and K_{aug}) for several avoidance maneuvers and diverse driver inputs. Simulation setup and results are presented below.

4.2.1 Simulation Setup

Controller performance was simulated using Plant B (described in 2.3.1). The vehicle model described by (2.26) – (2.29), with the parameters given in Table 2.1 was used in the receding horizon controller. Controller parameters were set as specified in Table 2.2. Both front-wheel-slip- and cost-based threat assessment were tested as inputs to the intervention law, with intervention thresholds Φ_{eng} and Φ_{aut} varied from 0 to 2 and 2.5 to 5 degrees respectively. Blending gains K and K_{aug} were both tested to assess the effect of each on semi-autonomous system performance.

I) Driver Input

Open-loop and closed-loop driver inputs were tested. Open-loop inputs were simulated by pre-specifying a sequence of driver inputs and implementing this sequence independent of the resulting vehicle trajectory. The trajectory independence of these inputs was chosen to emulate an inattentive driver. For the tests below, the driver's steer angle was held constant at $\delta_{dr} = 0^{o}$ as though s/he did not see the impending hazard.

Closed-loop inputs were used to emulate an attentive driver who actively attempts to track a desired trajectory. Here, a pure pursuit driver model similar to the one described in [82] was used. This model implements proportional feedback on the path tracking error, with the main tuning parameter being the lookahead distance L (illustrated in Figure 4.3).

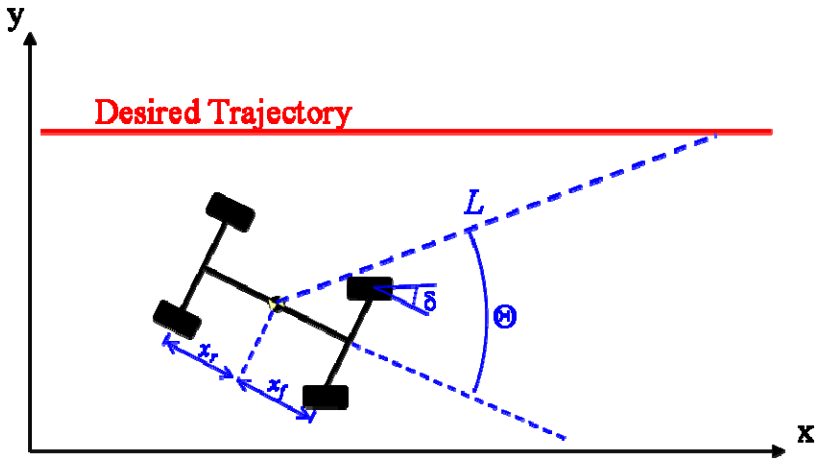

Figure 4.3: Illustration of pure pursuit driver model parameters

In simulation, the lookahead distance L was reduced (or "de-tuned") to simulate a poor driver input and increased (or tuned) to simulate an experienced driver. Together with the wheelbase length, this distance forms a gain on path error as shown in the steering calculation:

$$\delta = \tilde{y}\frac{2(x_f + x_r)}{L^2}\sin(\Theta). \qquad (4.5)$$

where $\tilde{y} = y_{des}(t) - y(t)$.

Figure 4.4 shows a block diagram of the semi-autonomous controller with the pure pursuit driver in the loop.

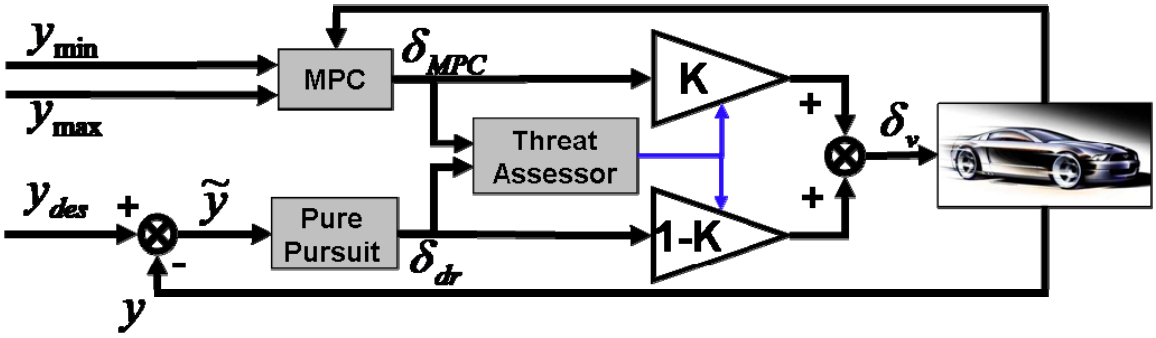

Figure 4.4: Block diagram of "pure pursuit" driver in the loop with MPC controller

II) Maneuvers

Lane-keeping, hazard avoidance, and multiple hazard avoidance maneuvers similar to those described in 2.3.1 IV) were used to test the semi-autonomous controller's ability to share control with a human driver while keeping the vehicle within the safe corridor. With the exception of lane-keeping maneuvers – for which closed-loop driver inputs are difficult to credibly simulate – both open- and closed-loop driver inputs were tested with each maneuver. Simulations with moving hazards similar to those described in 2.3.1 V) were also tested.

4.2.2 Simulation Results

The semi-autonomous controller maintained the vehicle within the navigable corridor for each of the threat metrics, intervention thresholds, intervention laws, maneuvers, and driver inputs tested. Results from these simulations are shown below.

I) Threat Metrics and Intervention Thresholds

Control systems that intervened semi-autonomously according to the threat posed by front wheel sideslip (α) and objective function cost (J) were shown to successfully satisfy safety constraints while allowing significant driver control. In the rest of this chapter's figures, Φ_α indicates simulations conducted using front wheel slip to assess threat and regulate controller intervention, while Φ_J indicates simulations that used modified objective function cost. Such tests are also referred to as Φ_α-regulated and Φ_J-

regulated maneuvers. Figures 4.5—4.8 show the results of semi-autonomous double lane change (or "multiple hazard avoidance") simulations with driver steer input δ_{dr}=0. Figure 4.5 compares the results of one such scenario when each metric is used to estimate threat and regulate controller intervention. For both maneuvers, $\Phi_{eng} = 0$ and $\Phi_{aut} = 3$.

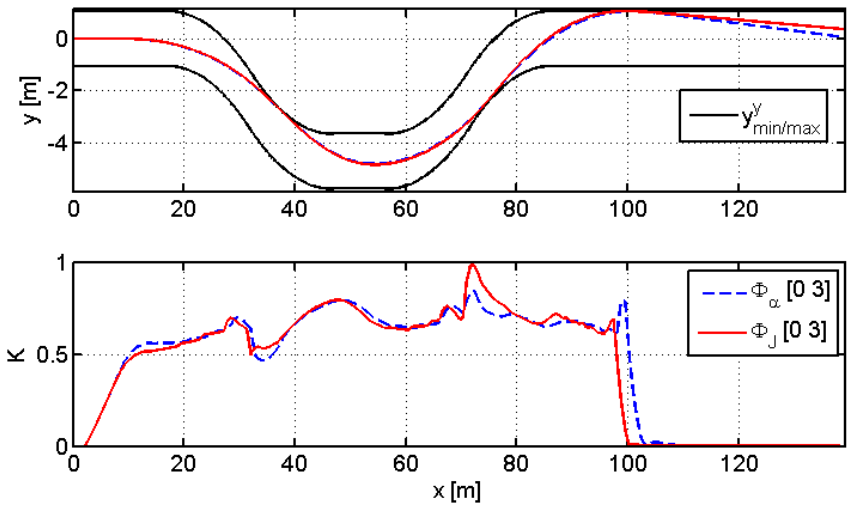

Figure 4.5: Comparison of controller intervention based on threat metrics Φ_α and Φ_J when driver steer $\delta_{dr} = 0$

Notice in Figure 4.5 that Φ_α- and Φ_J-regulated controllers perform similarly when the vehicle trajectory operates far away from constraints. Near constraints, the two diverge, as the additional cost terms in Φ_J $(0.5\ R_\delta\ \delta^2 + 0.5\ R_{\Delta\delta}\ \Delta\delta^2 + 0.5\ \rho_{SI}\ \varepsilon^2)$ cause higher peaks in $K = f(\Phi_J)$ than those seen for $K = f(\Phi_\alpha)$.

Intervention laws with varying threat thresholds for controller engagement (Φ_{eng}) and full autonomy (Φ_{aut}) were also shown to satisfy lane constraints while honoring driver inputs whenever possible. Sideslip thresholds Φ_{eng} and Φ_{aut} (in units of degrees) are denoted in figure legends as [Φ_{eng} Φ_{aut}].

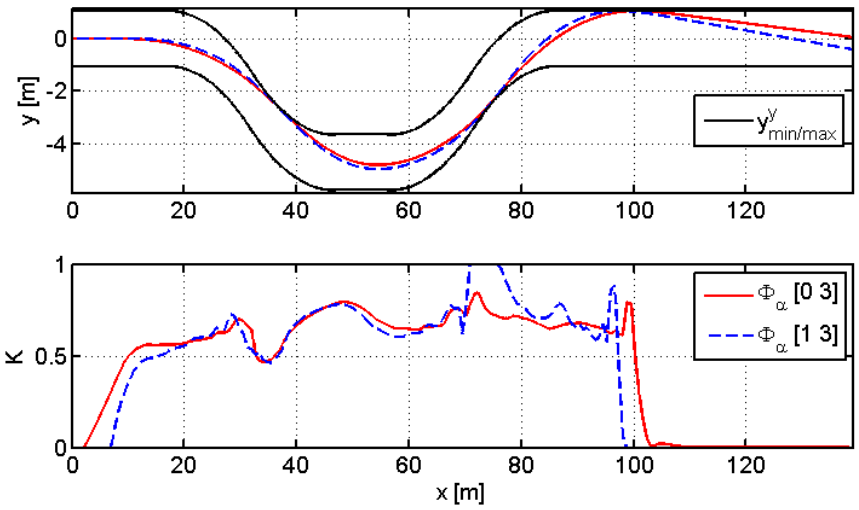

(a)

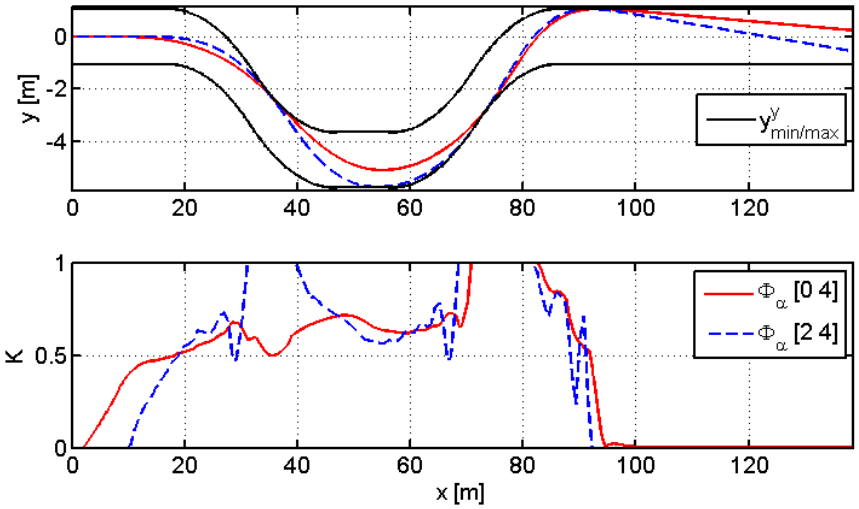

(b)

Figure 4.6: Effect of intervention thresholds [Φ_{eng} Φ_{aut}] on Φ_{α}-regulated double lane change maneuvers with $\delta_{dr} = 0$

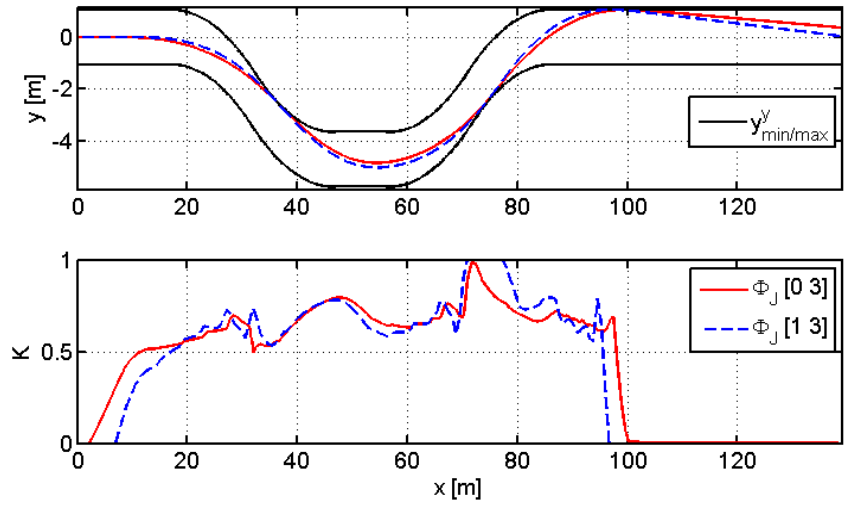

(a)

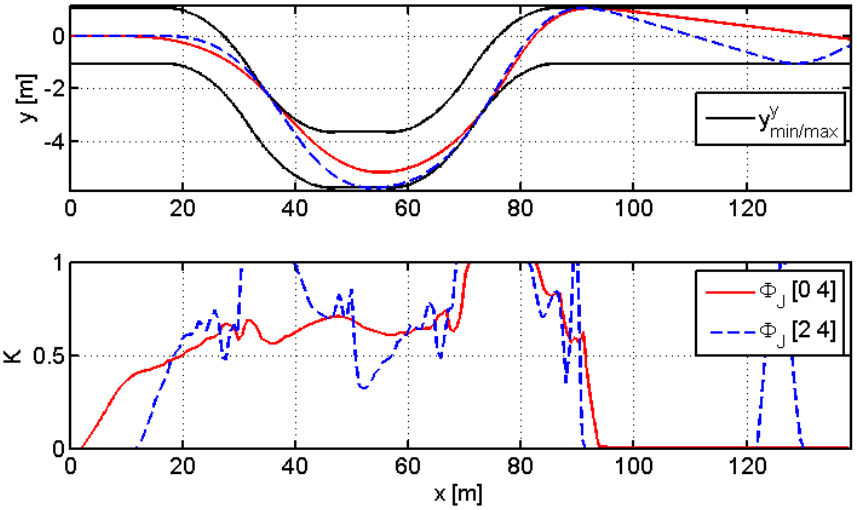

(b)

Figure 4.7: Effect of intervention thresholds [Φ_{eng} Φ_{aut}] on Φ_J-regulated double lane change maneuvers with $\delta_{dr} = 0$

As Figures 4.6 and 4.7 illustrate, increasing Φ_{eng} delays controller intervention K at the cost of more rapid increases and more frequent saturation of the control authority allotment. This late intervention, while allowing the human driver greater autonomy far from constraints/hazards, may ultimately require more control authority to regain control of the vehicle if the driver does not make the correction on his/her own. For example, increasing Φ_{eng} from 0 to 2 deg as shown in Figures 4.6 and 4.7 ultimately increases the average intervention metric K over the entire maneuver by 0.9 % for Φ_α-regulated intervention and 7.0 % for Φ_J-regulated intervention. This tradeoff between early, small,

and persistent intervention (low Φ_{eng}) and late, large, and periodic intervention (high Φ_{eng}) and their effect on average K over the entire maneuver is plotted in Figure 4.8.

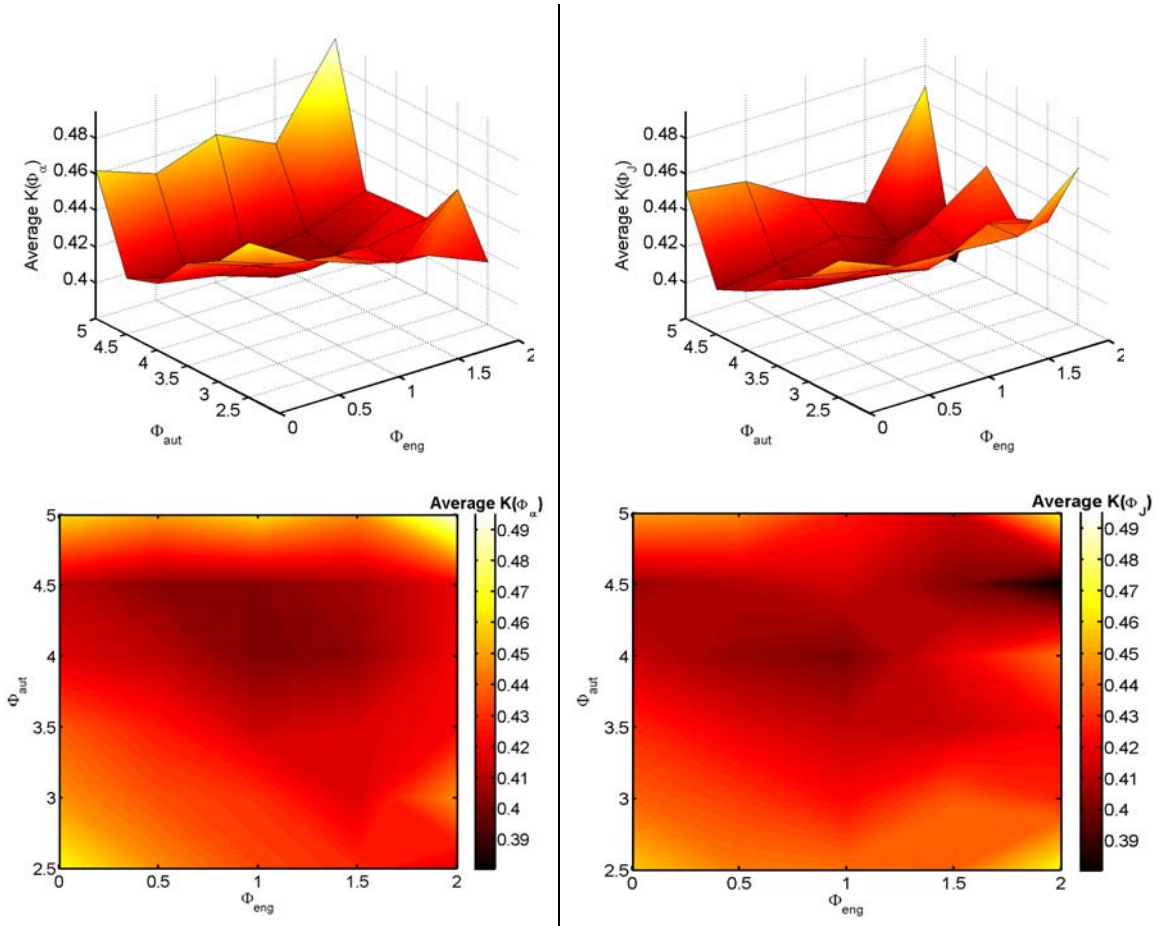

Figure 4.8: Effect of intervention thresholds [Φ_{eng} Φ_{aut}] on average intervention *K* for double lane change maneuvers regulated by Φ_{α} (column a) and Φ_J (column b)

As Figure 4.8 (a) and (b) show, average controller intervention generally decreases with increasing Φ_{aut} until $\Phi_{aut} \approx 4.5^{\circ}$. When the controller waits until threat Φ_{α} > 4.5 deg to take full control of the vehicle, the intervention required to keep the vehicle inside the navigable corridor increases rapidly. This comes as a result of the rapid increase in front wheel slip near the boundary of the linear tire force curve (2.11) and establishes a natural upper limit on Φ_{aut}.

Also notice that, for this scenario, the engagement threshold (Φ_{eng}) may be tuned according to driver preference without significantly affecting average overall

intervention. Taken together, these results suggest that for some maneuvers and driver inputs, this framework tends to "average out" controller intervention for various Φ_{eng} and Φ_{aut} settings, allowing for considerable driver preference tuning without dramatically changing the average K. In this scenario, for example, the maximum change in $K(\Phi_\alpha)$ across the entire range of Φ_{eng} and Φ_{aut} was 0.09.

These results also suggest that similar bounds on Φ_{eng} and Φ_{aut} may be applied when modified objective function cost (J_{SI}) is used to assess threat and regulate controller intervention. As shown in Figure 4.8 (b), basing controller intervention K on Φ_J changes average K over the entire maneuver by only 0.8 percent when compared to the Φ_α-regulated configuration (from $\overline{K}(\Phi_\alpha) = 0.430$ to $\overline{K}(\Phi_J) = 0.427$). This result follows from the abovementioned performance similarities between the Φ_J- and Φ_α- regulated configurations. Far from constraints, the two configurations perform similarly. Near the constraints, the spikes in $K(\Phi_J)$ tend to correct the vehicle trajectory, ultimately reducing the need for further intervention.

II) Threat Assessment

Semi-autonomous control changes the degree to which the MPC-based "best case" threat assessment matches true vehicle states. That is, when the MPC controller is not given full control authority, the vehicle trajectory it predicts based on those inputs does not necessarily match the trajectory actually followed by the vehicle. While this does not affect the accuracy of the controller's "best case" or "autonomously-achievable" threat assessment, it does illustrate one key effect of input scaling on prediction accuracy as discussed below.

For the autonomous case (i.e. when K = 1), the ratio of true-to-predicted front wheel sideslip was shown in 3.4.2 to be close to unity for both Φ_α- and Φ_J-based threat assessment. In the semi-autonomous case, with Φ_{eng} = 0º and Φ_{aut} = 3º, this ratio decreases from unity in inverse proportion to the level of control authority K given to the MPC input calculation. Figure 4.9 shows the results of a hazard avoidance maneuver with $\delta_{dr} = 0$ and using a) $K = f(\Phi_\alpha)$ and b) $K = f(\Phi_J)$.

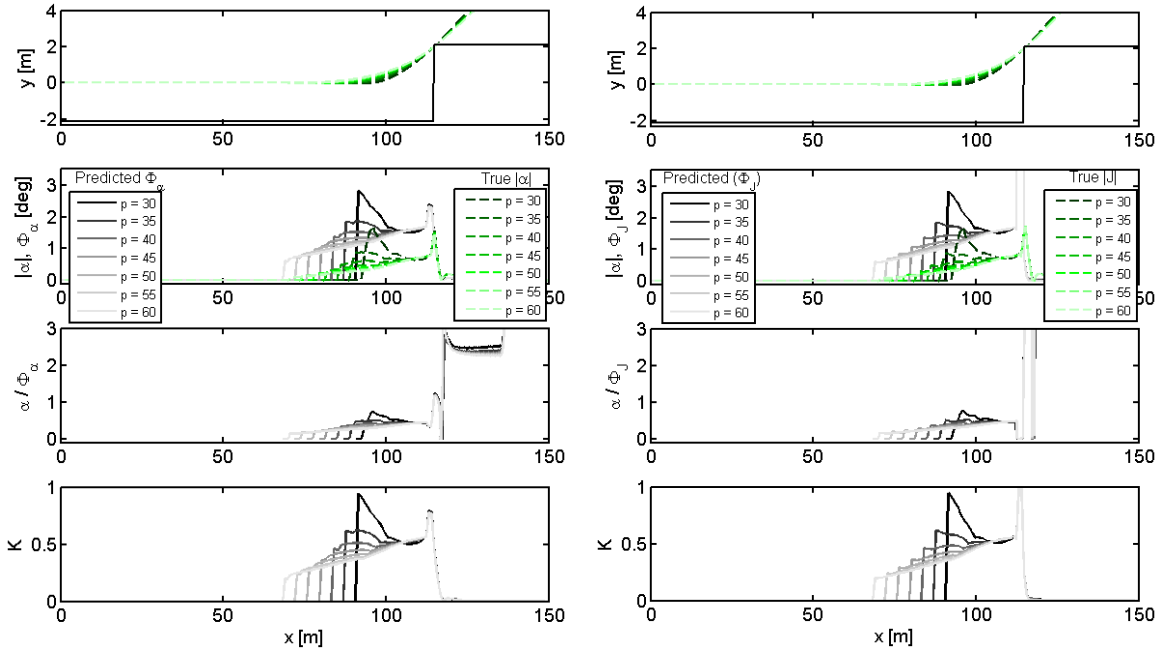

(a) **(b)**

Figure 4.9: Hazard avoidance simulations showing the effect of intervention gains *K* on threat assessment accuracy

Notice that, in contrast to the results obtained using K=0 (i.e. no active countermeasures) and K=1 (i.e. autonomous control) shown in 3.4.1 and 3.4.2 respectively, the ratio of true-to-predicted threat for these semi-autonomous simulations increases with increasing K values. This differs from the uncontrolled and autonomously-controlled tests for which this ratio remained near unity for all of the prediction horizons tested. The difference in the semi-autonomous case is a result of input scaling; multiplying the MPC input by $K < 1$ changes (and in the case of $\delta_{dr} < \delta_{MPC}$ decreases) the steering input seen by the vehicle. This difference in incremental steering input $\Delta\mathbf{u}$ accumulates as a difference in $\mathbf{u}$, causing the true vehicle trajectory to more closely follow the path implied by the driver's inputs. As a result, the vehicle experiences less front wheel sideslip than the optimal trajectory predicts. When K approaches 1, as seen in the simulations with short prediction horizons, the predicted threat level converges to the true threat level.

Figure 4.9 also shows that trajectory-planning and threat assessment in the semi-autonomous framework is more influenced by prediction horizon than similar autonomously-controlled (K=1) scenarios. When K=1, the MPC input closely tracks the

predicted trajectory (and its corresponding threat states) as long as the linearized controller model closely matches the plant. For this range of prediction horizons $\left(p = \{30 \cdots 60\}\right)$ and this hazard avoidance scenario, the controller model closely matches the plant. As a consequence, the predicted threat level closely matches the true threat level. For semi-autonomous simulations on the other hand, K is threat-dependent. Since predicted threat decreases with increasing prediction horizons (which provide a longer effective lookahead distance over which to smooth the avoidance maneuver), K also decreases with increasing prediction horizon. As mentioned above, the further K gets from 1, the more the predicted threat level may overestimate (for $\delta_{dr} < \delta_{MPC}$) or underestimate (for $\delta_{dr} > \delta_{MPC}$) true threat level, depending on the maneuver.

To summarize, the MPC-predicted trajectory/threat closely matches the true MPC-controlled vehicle trajectory for maneuvers in which the controller model closely matches the plant. When MPC inputs are blended with driver inputs in proportion to predicted threat, the true vehicle trajectory begins to diverge from the "best case" prediction. This does not diminish the utility of using the MPC prediction for threat assessment; the best case maneuver at any instant remains the best case maneuver whether the human driver follows it or not. What it does show – albeit empirically – is that for high-threat maneuvers that require K=1, the MPC controller is able to closely track the optimal avoidance trajectory. This guarantees that as long as Φ_{eng} and Φ_{aut} are set to appropriately low values (i.e. within the range for which the MPC model closely approximates the plant), and the prediction horizon is long enough that the controller has sufficient time to plan avoidance trajectories around hazards, the semi-autonomous controller can prevent departure from the navigable road corridor and guide the vehicle to safety.

III) Intervention Laws – *K* and K_{aug}

Semi-autonomous simulations based on the augmented intervention law K_{aug} (4.4) were also shown to satisfy safety and stability requirements for various maneuvers and driver steering inputs. Figure 4.10 compares a semi-autonomous simulation that does not consider the driver-controller steering difference (K) to one that does (K_{aug}). Note that the large peak values of K_{aug} combined with small input differences (recall that $\delta_{driver} = 0$ for

both simulations) leads to only slight differences in controller intervention for this maneuver. In these particular simulations, $\Phi = \Phi_\alpha$ and $[\Phi_{eng} \ \ \Phi_{aut}] = [0\ 3]$ deg.

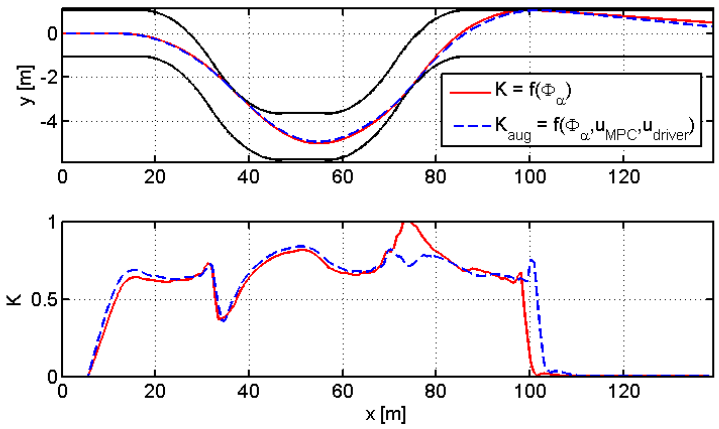

Figure 4.10: Comparison of semi-autonomous multiple hazard avoidance simulations based on intervention laws *K* and K_{aug}

Figure 4.10 shows that for certain maneuvers, driver inputs, and intervention thresholds Φ_{eng} and Φ_{aut}, augmenting *K* does not necessarily increase the average controller intervention. In these particular simulations, the opposite is observed. This is due to the slightly increased intervention early in the maneuver by the augmented controller, which reduced its subsequent intervention at $x \approx 75$m. Figure 4.11 shows how augmenting *K* according to variation between driver and controller steer affects average overall intervention for this maneuver.

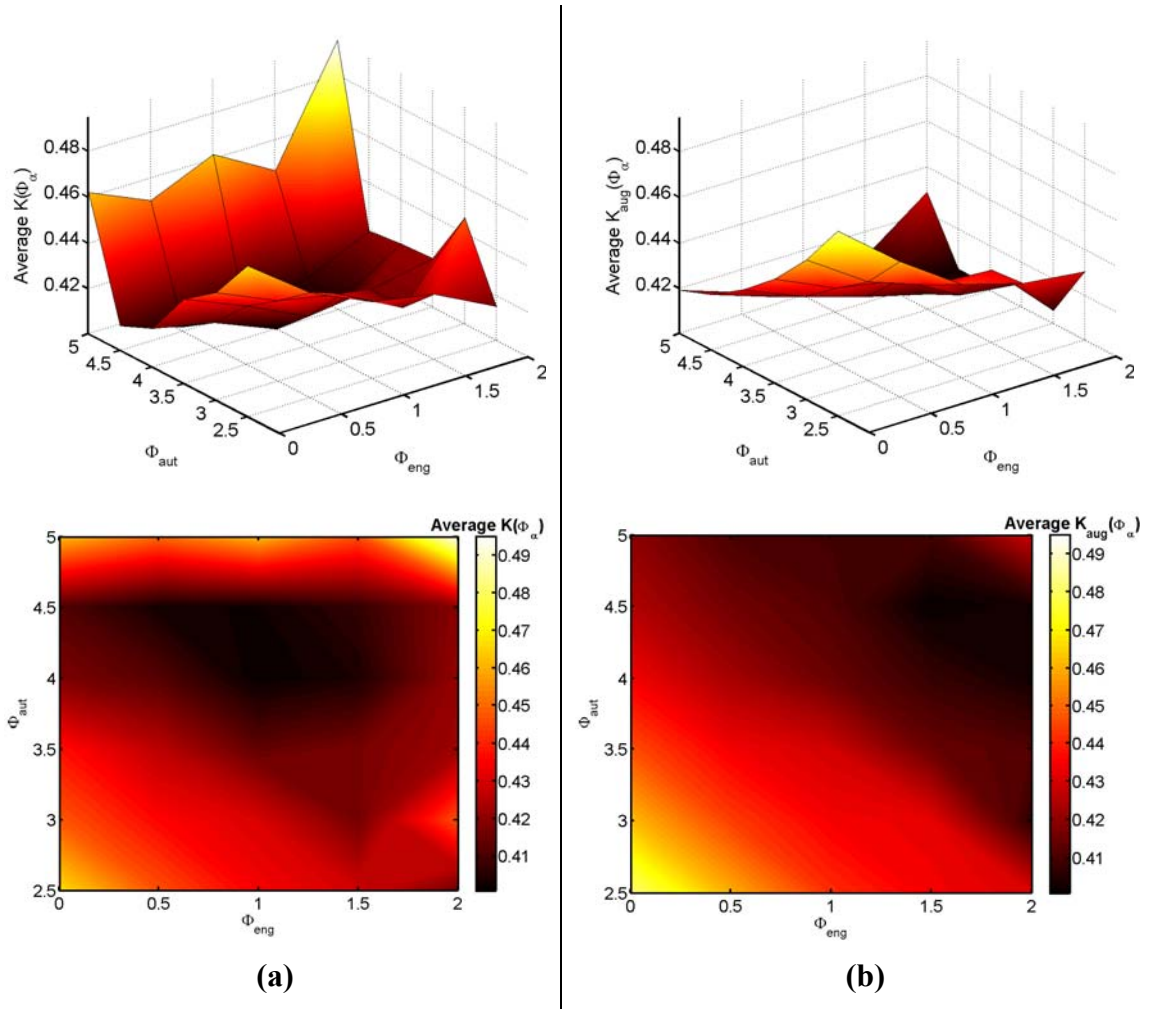

Figure 4.11: Effect of varying intervention thresholds [Φ_{eng} Φ_{aut}] on average intervention K (column a) and K_{aug} (column b) for double lane change

As Figure 4.11 shows, the driver-input-aware intervention law K_{aug} often leads to a similar average intervention as that calculated by the driver-input-unaware K. Also notice that for this maneuver, intervention governed by K_{aug} is less affected by changes in Φ_{aut} than K due to the extra term $\left(1-f\left(\Phi\right)\right)\left(1-e^{\frac{-\left|u_{MPC}-u_{dr}\right|}{\Delta u_{\max}}}\right)$. Notice that even for large values of Φ_{aut} – which for the unaugmented configuration led to delayed intervention and precipitous increases in K – the augmented controller was able to maintain relatively low average intervention over the entire maneuver.

To summarize, augmenting the intervention law via (4.4) maintains similar average controller intervention to the unaugmented controller while allowing for higher

Φ_{aut} settings. As noted in 4.2.2 I) above (pg. 80), the ability of these threat metrics (Φ_α and Φ_J) and intervention laws (K and K_{aug}) to allow for a wide range of thresholds and intervention characteristics without significantly changing average controller intervention or maneuver feasibility allows for considerable driver-preference-based tuning. This provides a significant advantage in a consumer market which strongly emphasizes configurability and personalization.

IV) Closed-Loop Drivers and Trajectory Stabilization

In addition to ensuring that the vehicle remains within a navigable road corridor, the semi-autonomous control framework presented in this thesis also exhibits performance advantages similar to those of yaw and roll stability controllers. That is, not only does the controller intervene to arrest corridor departure, but it also maintains stability-critical states (such as front wheel sideslip) below a given threshold while doing so. Appropriate threshold settings place an effective limit on the sideslip allowed before the controller takes full control of the vehicle and attempts to stabilize the vehicle. This soft limit ensures that as soon as the vehicle trajectory required to remain within the safe corridor becomes sever enough to require high levels of slip, the controller has been given full control authority and may – barring the unanticipated effects of unmodeled disturbances – safely stabilize the vehicle.

In the presence of a closed-loop "pure-pursuit" driver control, the moderating effect of semi-autonomous intervention on both the vehicle trajectory and driver input becomes apparent. Figure 4.12 shows one such simulation in which the semi-autonomous controller improved the driver's ability to track a desired path. In this simulation, the pure pursuit driver model was designed with a short lookahead (L = 10 m). At V_{host}=20 m/s, this corresponds to an effective lookahead horizon of 0.5 seconds, which for the pure pursuit controller lead to large steering gains and consequent difficulty in tracking the desired trajectory without loosing control of the vehicle.

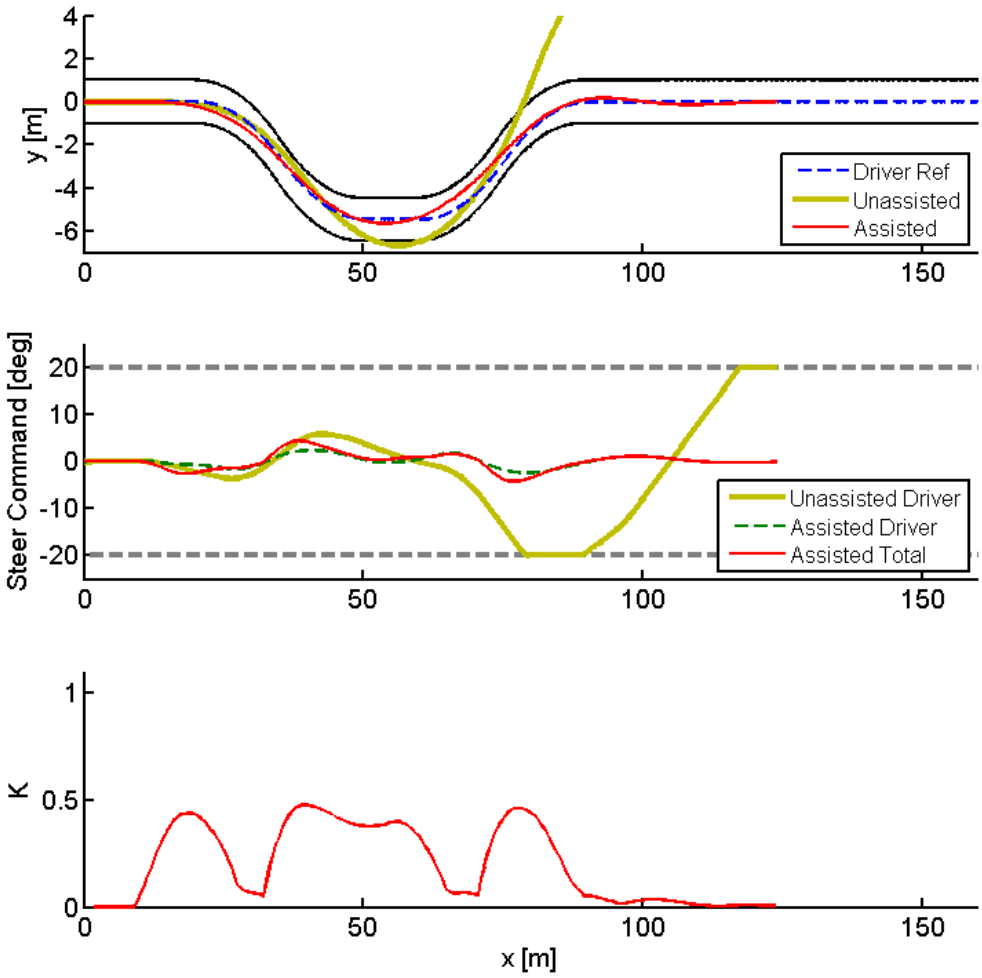

Figure 4.12: Effect of semi-autonomous intervention on a closed-loop "pure-pursuit" driver and vehicle trajectory

In this scenario, including the semi-autonomous controller in the control loop reduces the magnitude of the driver's inputs. Whereas a short lookahead distance and its attendant high steering gains (4.5) caused the unassisted driver to oversteer and loose control of the vehicle, the assisted driver was more moderate in its steer commands and thus maintained control of the vehicle. Moreover, allocating less than 50% of the available control authority to the MPC controller was sufficient to keep the vehicle inside the corridor and within 0.4 meters of the desired trajectory. The combined effect of both inputs (driver and controller) is a vehicle trajectory that more closely tracks the driver's desired trajectory than either the pure pursuit controller or corridor-based MPC controller would have done on its own. Figure 4.13 compares the evolution of stability-critical

states including sideslip (β), yaw rate ($\dot{\psi}$), roll angle (φ), and lateral acceleration ($\ddot{y}$) resulting from driver-only (a) and semi-autonomous (b) control. Notice that under driver-only control, the vehicle spins around completely at x≈100 m.

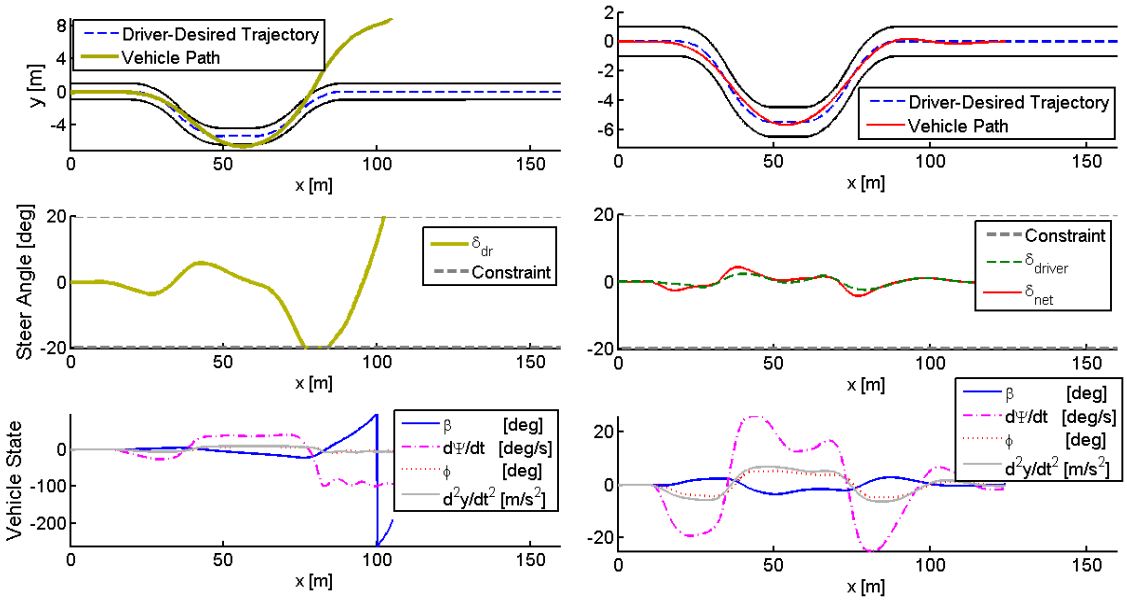

(a) **(b)**

Figure 4.13: Comparison of vehicle paths, steering inputs, and state evolution for assisted (b) and unassisted (a) closed-loop drivers

It is important to note that improved path tracking is not entirely the result of the MPC controller's actions; the controller seeks only to keep the vehicle within a navigable corridor, while the intervention law only allows it the required control authority in proportion to stability-related threat. Were the MPC controller to navigate the vehicle autonomously, the resulting trajectory would look similar to those shown in Figure 2.11 (which minimize front wheel sideslip). The "assisted" (i.e. semi-autonomous) trajectory shown in Figure 4.12 tracks the desired trajectory specifically due to a control authority allocation that allows the driver significant freedom to track a desired path while allowing the MPC controller just enough control authority to stabilize and keep the vehicle within a navigable corridor.

Finally, Figure 4.14 shows how predicted threat Φ_α compares to true front wheel sideslip in the semi-autonomous maneuver shown above (Figure 4.13 b). As discussed in 4.2.2 II) above, this threat assessment temporarily leads and slightly overestimates true front wheel slip.

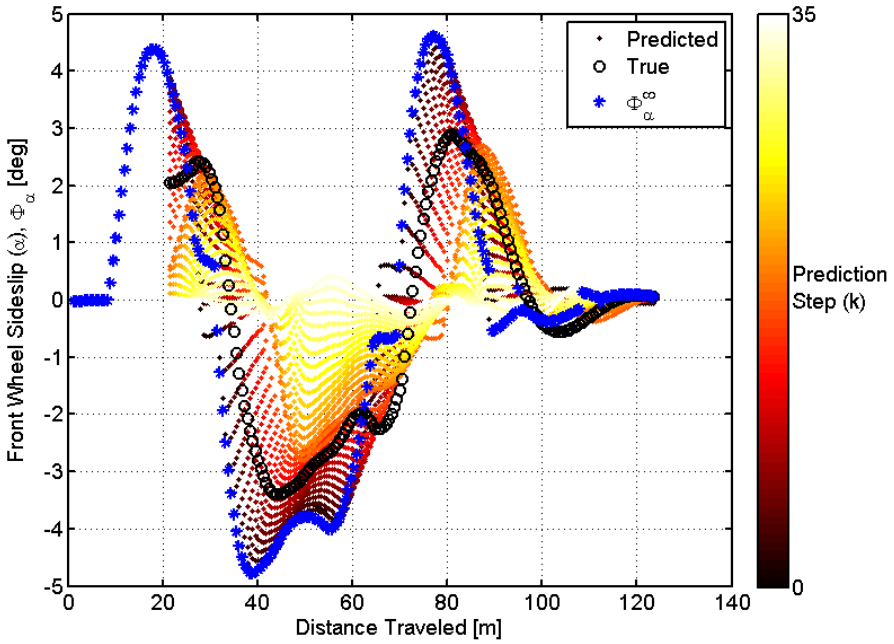

Figure 4.14: Predicted vs. true threat for a semi-autonomous simulation with a pure pursuit driver model in the loop

Similar favorable results were obtained for various scenarios with a pure-pursuit driver in the loop. Figure 4.15 shows the effect of semi-autonomous control on a driver attempting to track a step in reference trajectory. This maneuver attempts to emulate the behavior of a driver who, upon noticing a hazard, performs a sudden (panicked) lane-change maneuver to avoid it.

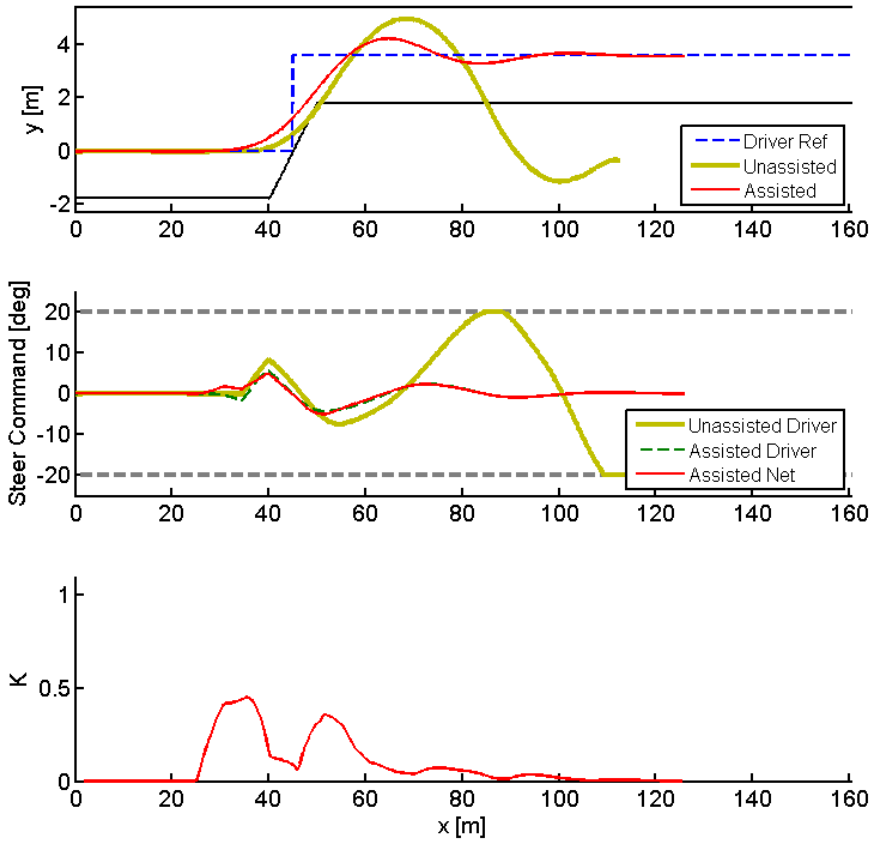

Figure 4.15: Effect of semi-autonomous intervention on the inputs of a "startled" closed-loop driver

Notice again that even in the presence of steering rate constraints (seen active in the linear segments of the steer command), the semi-autonomous controller successfully stabilizes the vehicle, allowing the emulated driver to closely track the intended path without leaving the navigable roadway.

Figure 4.16 demonstrates similar advantages when the driver attempts to swerve within a lane.

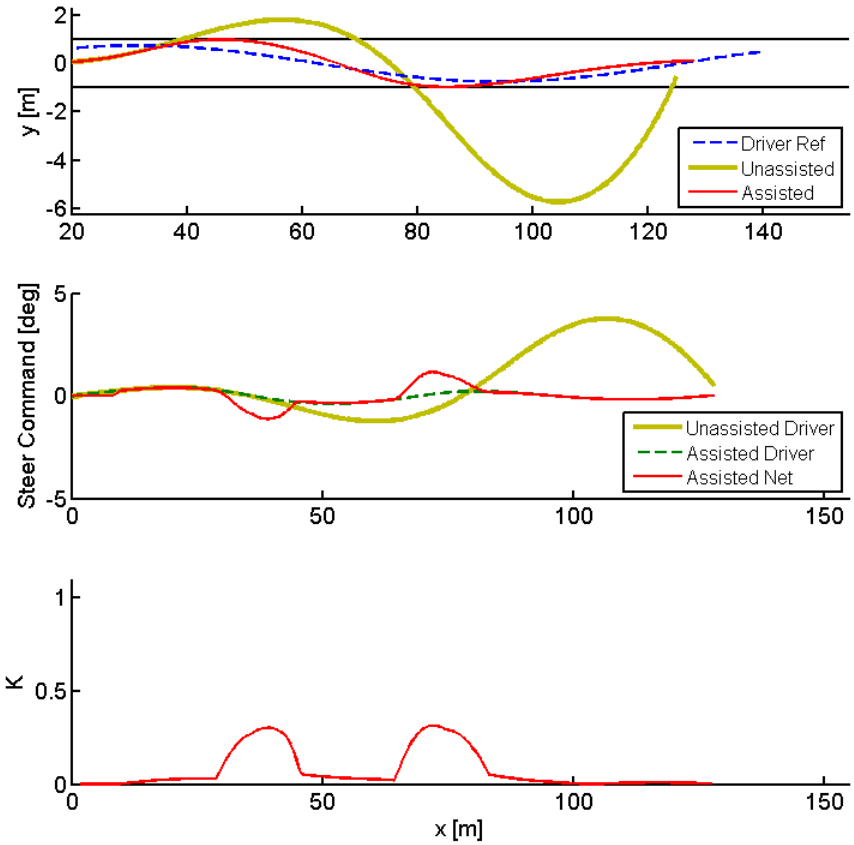

Figure 4.16: Effect of semi-autonomous intervention on the inputs of a driver swerving in a lane

As in other scenarios, this simulation shows that the controller is able to effectively assist the driver while taking less than 35% of the available control authority. Similar lane-keeping results were obtained the experiments presented in section 4.3.2.

V) Moving Hazards

In simulation studies, the semi-autonomous controller proved capable of avoiding moving hazards. One scenario is shown in Figure 4.17 below. Note that in the plots, the vehicle's center of gravity lies at the leftmost edge of the predicted trajectory. The trajectory prediction is color-coded according to predicted front wheel sideslip and marked a sequence of bullets, with the exception of the step with the highest predicted sideslip – which is marked by a circle.

T1 = 1.05 sec

T2 = 4.25 sec

T3 = 5.95 sec

T4 = 6.15 sec

T5 = 7.80 sec

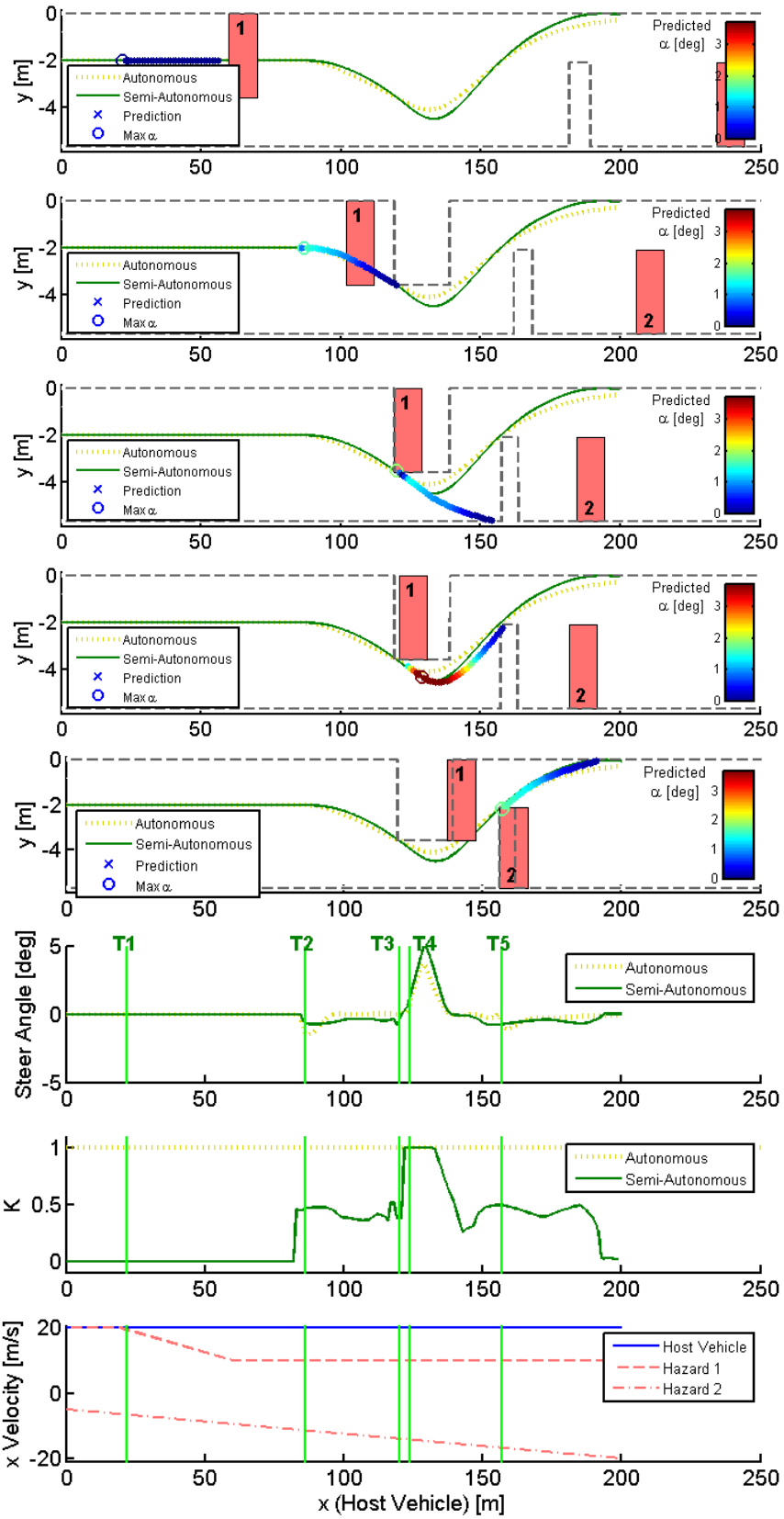

Figure 4.17: Semi-autonomous control with moving hazards

In this scenario, the host vehicle initially trails obstacle 1 while both travel at 20 m/s. At T1, obstacle 1 begins to decelerate, prompting the host vehicle to begin a passing maneuver at T2. At T3, the host clears the first obstacle and "sees" an accelerating obstacle 2 in the oncoming lane at T4. Adjusting quickly in response to the heightened threat, the semi-autonomous controller takes complete control of the vehicle and successfully guides it safely past the hazard. Note that by using the first-order-hold obstacle state estimation approach described by (2.35) and (2.37), the predicted collision time and location does not explicitly account for the acceleration of each hazard. Instead, it adjusts its estimate at each sampling instant according to the current velocity of each hazard. This adjustment is apparent in Figure 4.17 as a shift in the corridor boundaries as the hazards accelerate.

4.3 Experimental Studies

Experimental testing* was performed using a human-driver-operated test vehicle at Ford's Dearborn Development Center on dry asphalt ($\mu \approx 1$) as described in Section 2.4.1. An inertial and GPS navigation system was used to measure vehicle position, sideslip, yaw angle, and yaw rate while a 1 GHz dSPACE processor ran controller code and interfaced with steering actuators. As in simulations, lane data was assumed to have been derived from forward-looking sensors and therefore predefined virtually.

Finally, while this setup's AFS mechanism transmits a slight (and undesirable) torque feedthrough from the controller to the driver, exceptional results were obtained in semi-autonomous tests. Future implementations, however, may benefit from the use of active steering mechanisms that reduce this torque feedthrough such as Electronic Power Assist Steering (EPAS) or pure steer-by-wire.

4.3.1 Experimental Setup

Three common scenarios were used to analyze system performance. In each scenario, obstacles, hazards, and driver targets were represented to the driver by cones

* Experimental studies were carried out in collaboration with Steven Peters

and lane markings and to the controller by a constrained corridor (with onboard sensing and constraint mapping assumed to have been performed previously by "virtual sensors" and high-level planners, respectively). Lane-keeping tests required a swerving driver to navigate a straight lane of constant width. Single hazard avoidance tests required that the vehicle avoid a roadway-restricting hazard on a straight roadway. Finally, multiple hazard avoidance tests required that the vehicle navigate around two hazards with a double lane change maneuver. These scenarios are described below.

I) Scenarios

Lane keeping experiments tested the threat assessment and intervention characteristics of the controller when the driver maneuvered inside and outside of a given lane. Six pairs of cones were set up along ~200 meters of a 3.35-meter-wide lane to guide the driver's intended path and thus improve experimental repeatability. As shown in Figure 4.18 (not to scale), the second- and third sets of cones required the driver to steer the vehicle to the edge of the navigable lane while the final two targets required that he attempt to depart the lane. Lane boundaries illustrated below by dashed lines were enforced via lateral position constraints $y^{y}_{min/max}$ in the controller.

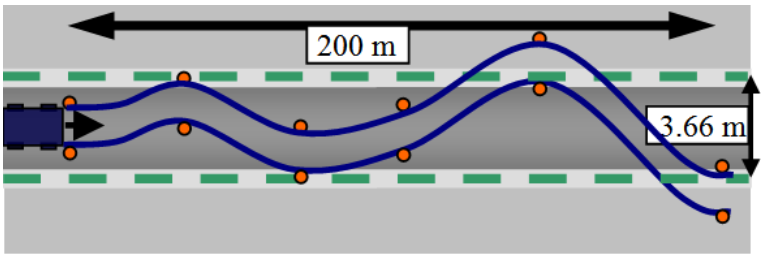

Figure 4.18: Lane keeping test setup showing circles where cones were placed to guide the human driver's inputs. Lane boundaries delineated by dashed lines were represented as constraints y^{y}_{min} and y^{y}_{max} to the semi-autonomous controller

In each of these tests, the driver attempted to maneuver through the cones. For maneuvers that remained inside the lane, little controller intervention was desirable. When the driver's path came close to departing the lane, the controller intervened to keep the vehicle inside it. Of interest in this scenario were the inherent tradeoffs between tracking the human driver's desired trajectory and remaining within the lane.

The setup for hazard avoidance and multiple hazard avoidance experiments was similar to that described in Section 2.4.1. Hazard avoidance tests required that the vehicle avoid an obstacle in the current lane of travel. In these tests, the vehicle was driven at a constant velocity in the center of a lane with the driver holding the steering wheel at $\delta = 0$, as if asleep or inattentive. A row of cones blocked the vehicle's lane of travel, requiring the controller to: 1) plan a safe lane change maneuver around them, 2) assess the threat posed by that maneuver, and 3) intervene as necessary to avoid the hazard. Figure 4.19 illustrates this test setup.

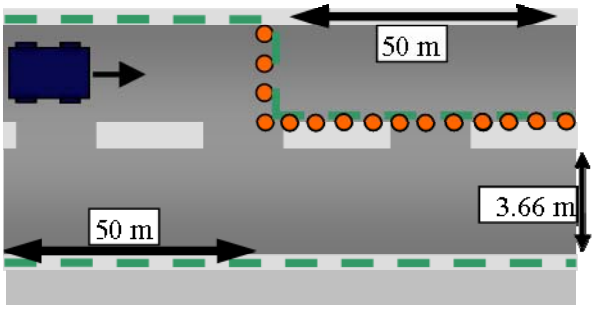

Figure 4.19: Hazard avoidance test setup showing hazard cone placement (large circles) and lane boundaries (dashed) enforced by the controller

Multiple hazard avoidance experiments tested the controller's ability to navigate more complex road/hazard setups that required maneuvers with appreciable load transfer. In these tests (illustrated in Figure 4.20), both lanes of travel were blocked at different locations, forcing the vehicle to change lanes to avoid the first hazard, then change lanes again to avoid the second, as in a double lane change maneuver.

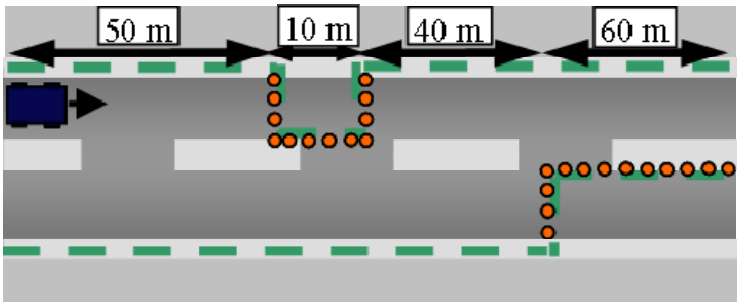

Figure 4.20: Multiple hazard avoidance test setup showing hazard cone placement (circles) and lane boundaries (dashed)

These tests were conducted using two different types of driver inputs. Drowsy or otherwise inattentive drivers were emulated by a constant driver steer input of zero

degrees. In these tests, the unassisted driver's path formed a straight line that intersected with the obstacle(s). To represent an alert driver's steering inputs, drivers were asked in separate tests to steer around stationary obstacles. The urgency of these driver steer events was varied – sometimes avoiding the obstacle(s) with a smooth input, others steering at the last minute, and still others, turning the wrong way into an obstacle. Of particular interest in such interactions were the controller's intervention characteristics and the interaction between the controller and the driver. Experiments were conducted at vehicle velocities of 5, 10, and 14 meters per second.

II) Controller Configuration

The best-case path calculated by the MPC controller is influenced by the MPC objective function, constraint setup, and prediction and control horizons. Vehicle and controller parameters used in experiments were the same as those used in simulation (shown in (2.26) – (2.29) and Table 2.2, respectively). Various threat metrics (Φ_α and Φ_J), intervention thresholds (Φ_{eng} and Φ_{aut}), and intervention laws ($K(\Phi)$ and $K_{aug}(\Phi)$) were tested in order to understand their effects on controller performance. Because prediction (p) and control (n) horizons strongly affect path planning, threat assessment, and controller intervention, these were also varied to assess their impact on overall system performance. In general, longer prediction horizons led to smoother optimal vehicle trajectory predictions and, consequently, lower threat assessments. Real time computation limits constrained the feasible prediction and control horizons used in field tests to 40- and 20- sampling periods, respectively, when 50 ms sampling periods were used. For consistency, only experiments using $p = 40$ and $n = 20$ are shown below.

III) Intervention Law Configuration

Front wheel sideslip α and modified objective function cost J_{SI} were each used to assess threat. Threat metrics based on both of these predictors (Φ_α and Φ_J) were calculated using the motion plan generated by the MPC algorithm as described by Table 3.1 and (3.3). Various threat thresholds (Φ_{eng} and Φ_{aut}) and both intervention laws ($K(\Phi)$ and $K_{aug}(\Phi)$) were also tested to understand their effect on vehicle performance and driver experience.

4.3.2 Experimental Results

The semi-autonomous framework proved capable of keeping the vehicle within the safe region of travel for each of the scenarios tested, with three different human drivers, and using multiple combinations of threat metrics, intervention thresholds, and intervention laws. Unless otherwise noted, the driver steer input was zero for each of the experiments (with the exception of lane-keeping experiments) shown below.

I) Threat Metrics and Intervention Thresholds

Figure 4.21 shows the results of three Φ_α-regulated lane-keeping tests with varying intervention thresholds [Φ_{eng} Φ_{aut}]. Recall that in these tests, the driver was instructed to attempt to track the path traced here by a black dashed line.

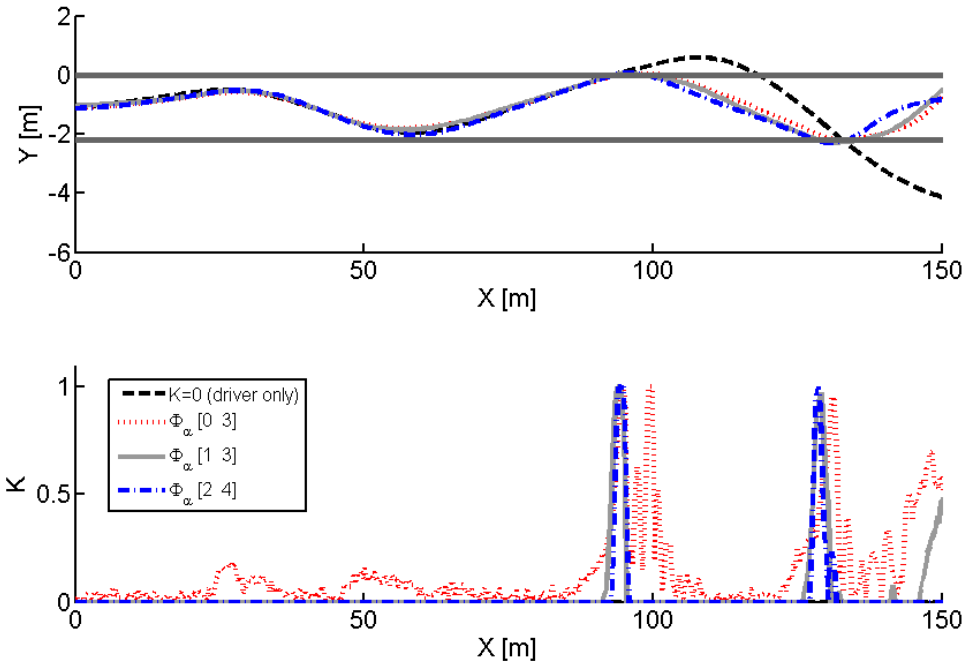

Figure 4.21: Results of lane keeping tests with no controller action (dashed), and semi-autonomous controller intervention (dotted, solid, and dash-dot)

The dashed black line in Figure 4.21 represents the vehicle trajectory under complete driver control ($K = 0$), and is shown here and in subsequent plots as a reference for the trajectory the driver would have followed had the semi-autonomous controller not engaged. For various intervention thresholds, the semi-autonomous controller successfully kept the driver within the safe corridor while allowing him significant

control authority while inside this corridor (x≈-20m to x≈70m). Only when the vehicle was about to depart from the corridor did the controller intervene to prevent departure. Note that at x≈10m and x≈50m, the threat assessment increased slightly due to the increased level of sideslip required to remain within the lane. This led to a corresponding increase in K for the configuration with $\Phi_{eng} = 0°$. When the driver corrected the vehicle heading, K returned to approximately zero. By increasing Φ_{eng} as in ([1° 3°] and [2° 4°]), much of this low-threat intervention was eliminated.

Good experimental results were obtained using both front wheel slip Φ_α and objective function cost Φ_J as threat metrics. Figure 4.22 compares two such experiments, both of which use $\Phi_{eng} = 0°$ and $\Phi_{aut} = 3°$, to tests with zero intervention (dashed) and autonomous control (solid).

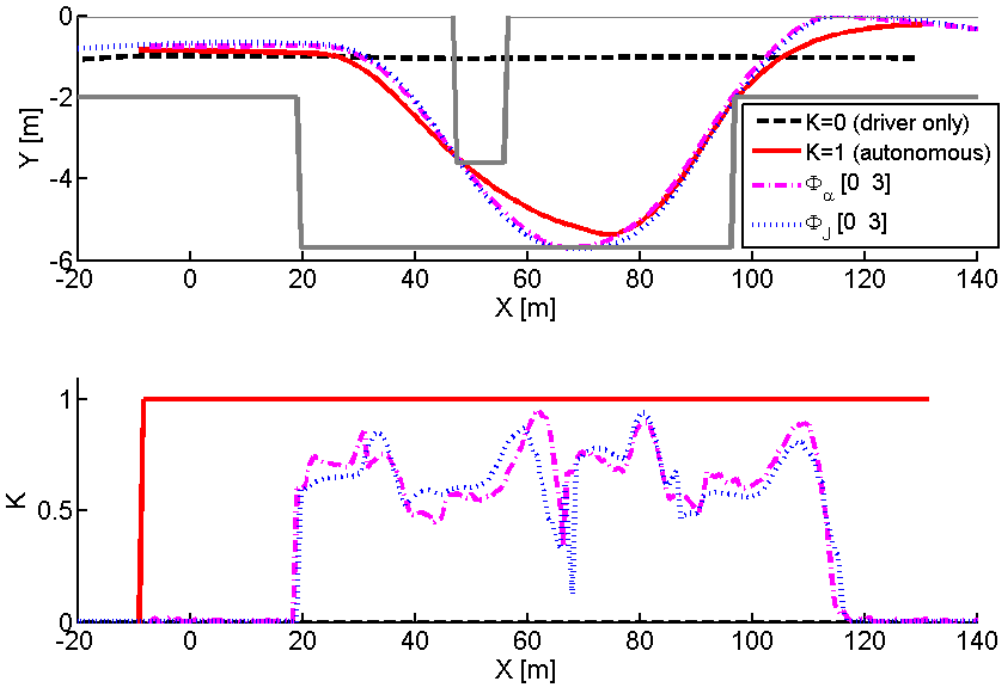

Figure 4.22: Results of multiple hazard avoidance tests comparing intervention based on Φ_α and Φ_J to autonomous control

Figure 4.23 compares controller performance in a hazard avoidance scenario when Φ_α and Φ_J are used to regulate controller intervention.

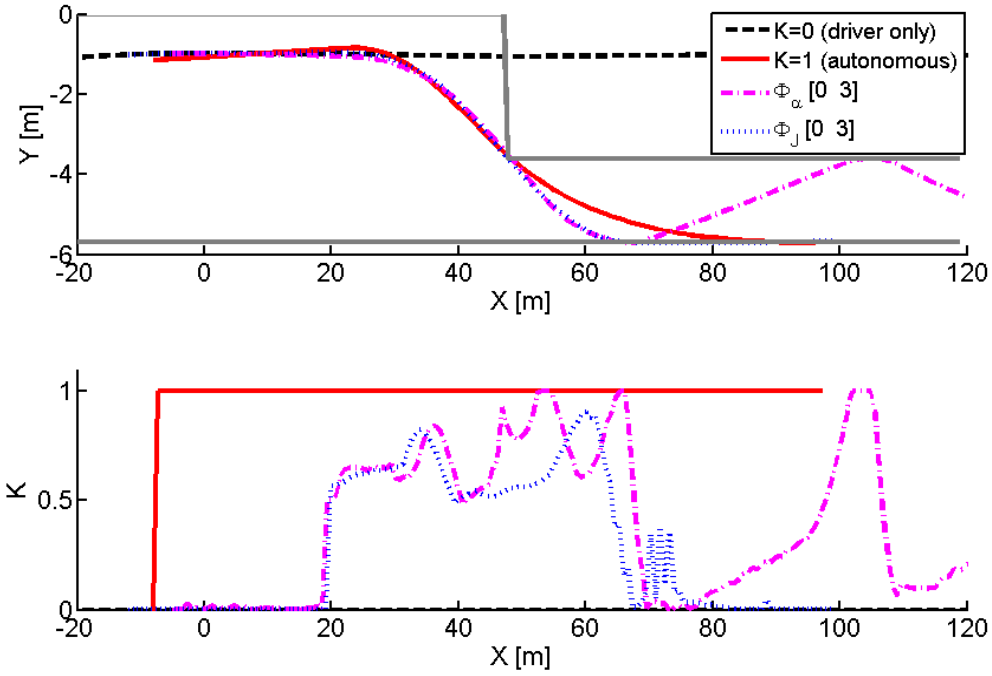

Figure 4.23: Results of hazard avoidance tests with no controller action (dashed), autonomous control (solid), Φ_α-regulated intervention (dash-dot), and Φ_J-regulated intervention (dotted)

Similar to the multiple hazard avoidance experiments, controller intervention in hazard avoidance experiments allowed the driver significant freedom to follow a desired trajectory while that trajectory remained both stable and safely within the navigable road corridor. When the controller intervened near the corridor boundary, it allocated enough control authority to the controller to avert departure or loss of control. Note that the trajectory oscillation observed in the Φ_α-regulated experiment was a result of an overcorrection on the part of the controller at x≈65m. The vehicle trajectory proceeded to rebound from $y^y_{\max}$ because the driver's input remained at zero. Were the driver more attentive as a result of the first intervention incident, the low levels of K directly following the initial rebound would have allowed him significant control authority to correct and straighten out the vehicle.

Figure 4.23 also shows the results of an autonomous experiment in which the controller was given full control authority (K=1). Notice that for the given driver input (δ_{driver} = 0), the vehicle path under semi-autonomous control closely resembles the "best case" (i.e. autonomously-achieved) path while exerting an average intervention gain (K)

of only 0.40 and 0.28 for Φ_α- and Φ_J - regulated intervention, respectively. This is significant as it shows that for similar (small) driver inputs, the controller effectively follows a near-optimal trajectory while conceding significant control authority to the human driver.

Finally, notice that the noise exhibited at x ≈ 70 m in Figure 4.23 is a result of the vehicle's skirting closely along $y^y_{\min}$. Because controller inputs are very small in this region, the driver felt little of this noise. However, and as noted above, such noise may be reduced by increasing Φ_{eng} as shown in Figure 4.24.

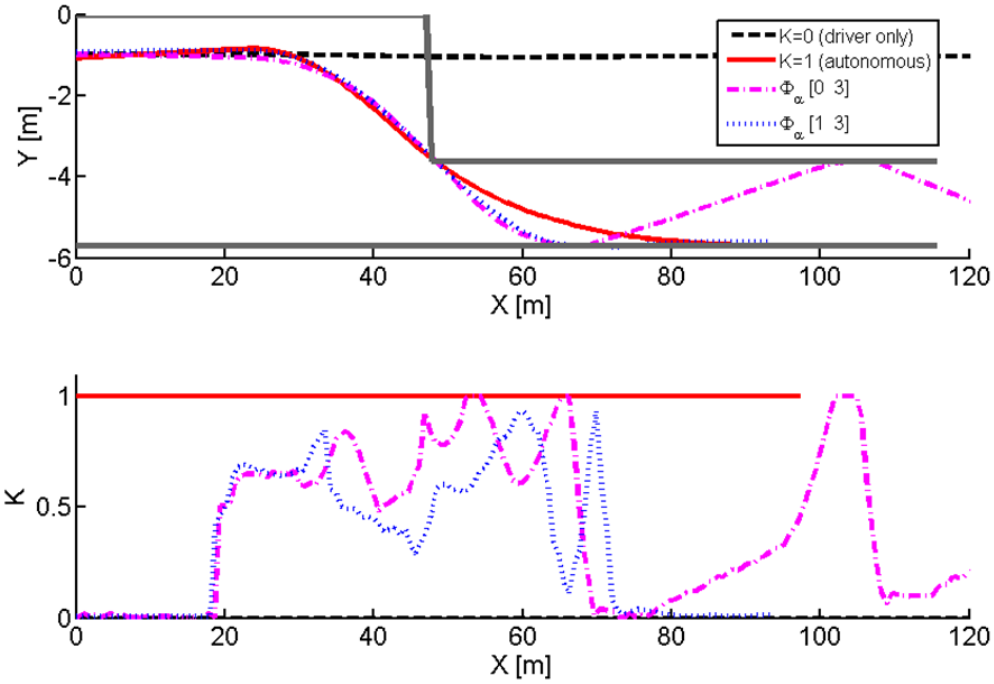

Figure 4.24: Results of hazard avoidance tests showing the effect of setting $\Phi_{eng} > 0$

As Figure 4.21 shows, both semi-autonomous trajectories closely resemble the objective-function-optimal path taken by the autonomous controller. Notice that using threshold settings Φ_α = [1 3]º, the semi-autonomous controller delays intervention slightly compared to the experiment without a low-threat intervention deadband (Φ_α = [0 3]º). While both controllers experience a spike in the intervention level at x≈70m, the [1 3]º threshold settings delay the intervention spike until the MPC-calculated inputs have subsided. This avoids the slight oversteer experienced in the [0 3]º test. Overall, however, both sets of intervention thresholds proved effective in semi-autonomous control.

II) Intervention Laws – K and K_{aug}

Intervention laws considering driver input via (4.4) were also shown to effectively allocate control authority based on both the predicted maneuver threat and the current driver input. Figure 4.25 shows how augmenting intervention gains $K(\Phi_\alpha)$ and $K(\Phi_J)$ according to (4.4) affected the performance of the semi-autonomous controller.

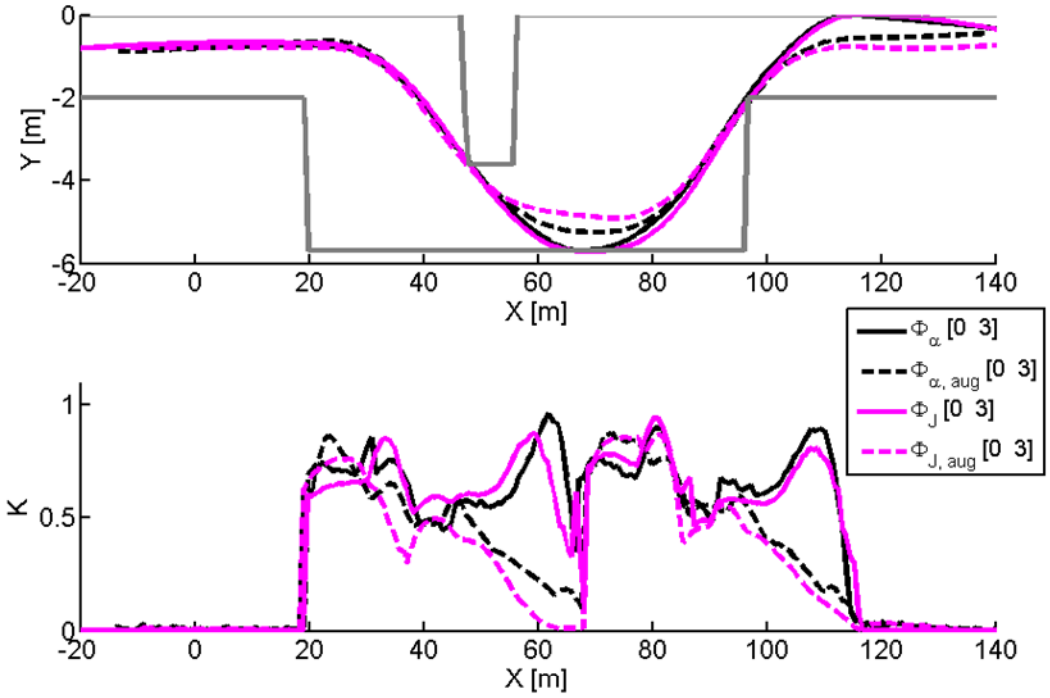

Figure 4.25: Multiple hazard avoidance maneuver showing the effect of augmenting Φ_α and Φ_J to account for differences between driver and controller steer

Note from Figure 4.25 that in this particular scenario, the effect of controller augmentation on controller intervention and vehicle performance appears more pronounced than the effect of using different threat assessments (Φ_α vs. Φ_J). This is consistent with the observation that for less demanding maneuvers (i.e. those which can be accomplished without violating lane constraints), the objective function cost is almost exclusively a function of front wheel slip and performs similarly to the front-slip-modulated configuration. When these configurations are augmented via (4.4), initial intervention increases, allowing a subsequently smoother trajectory which ultimately requires less controller intervention (average K) altogether. Generally, augmenting K in

proportion to driver-controller input discrepancy resulted in smoother controller intervention that was more acceptable to the human driver. That is, controller intervention based on the augmented threat metric $\Phi_{\alpha,\text{aug}}$ or $\Phi_{J,\text{aug}}$ was generally more gradual and less startling to the driver.

III) Closed-Loop Drivers

The results above (Figures 4.21—4.25) show scenarios in which the driver input remained at zero. Experiments were also conducted in which the driver swerved at the last minute to avoid hazards. Two such scenarios are shown in Figure 4.26.

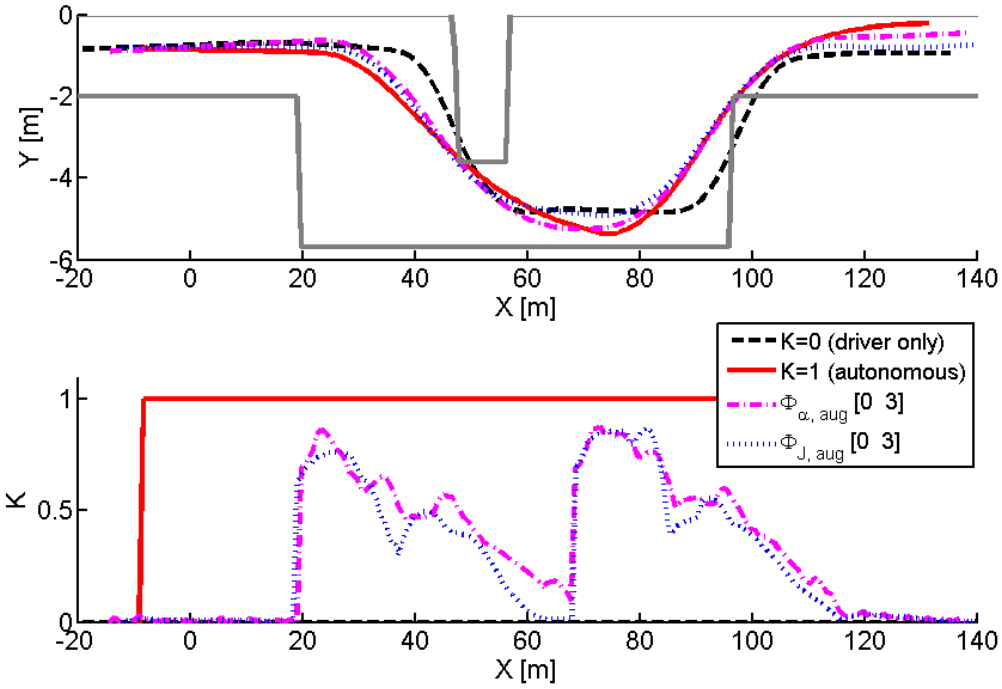

Figure 4.26: Multiple hazard avoidance maneuvers showing the controller's moderating effect on the inputs of the human driver

Notice that in both semi-autonomous cases, controller intervention slightly preceded a late driver reaction. The combined effect of both inputs was sufficient to avoid both road hazards. Once again, this intervention appears similar to the optimal trajectory followed by the autonomous controller.

It should be noted that in each of the experimental results presented in this chapter and in all of the other simulated and experimental results conducted to date, the semi-autonomous controller behaves as a stable closed-loop system. A rigorous stability proof, however, is a topic of current investigation and is therefore not presented here.

IV) Driver Experience

While all three human drivers were generally satisfied with the controller's performance, their feedback on each of this study's approximately 180 experiments provided some insight into desirable intervention configurations and how these may vary from driver to driver. A very preliminary assessment of how different threat metrics and intervention laws interacted with the human driver is presented here. This is not, however, intended as a general treatment of human factors involved in semi-autonomous vehicle control; such a treatment is the subject of future work.

Following each experiment, the driver was asked how comfortable he felt with the (semi-autonomously-controlled) vehicle's response to his inputs. This qualitative feedback was recorded and correlated with the data from each maneuver. Though this correlation did not turn up a single dominant performance metric, it did show that in general, test drivers generally felt more comfortable during maneuvers with relatively-low average and peak controller intervention (K) and very low average and peak lateral acceleration ($\ddot{y}$). When controller intervention remained low, the drivers felt a greater sense of control. At low levels of lateral acceleration, they tended to mention better ride comfort.

Figure 4.27 averages the maximum and mean values of K and $\ddot{y}$ over all maneuvers and drivers in order to compare threat metrics Φ_α and Φ_J to the autonomous controller. As seen in various simulation and experimental results presented in this chapter, semi-autonomous control based on either of these threat metrics tends to result in similar K and $\ddot{y}$ values. The aggregate statistics shown in Figure 4.27 also suggest that the semi-autonomous controller achieves similar vehicle stability and ride comfort (both of which are closely tied to $\ddot{y}$) to the optimal (i.e. autonomous) trajectory while taking on average less than 30% of the available control from the driver. This result confirms what was suggested by simulation results in Section 4.2.2: the proposed framework robustly

allows for significant changes in its intervention law while maintaining many of the performance advantages offered by an optimal autonomous controller.

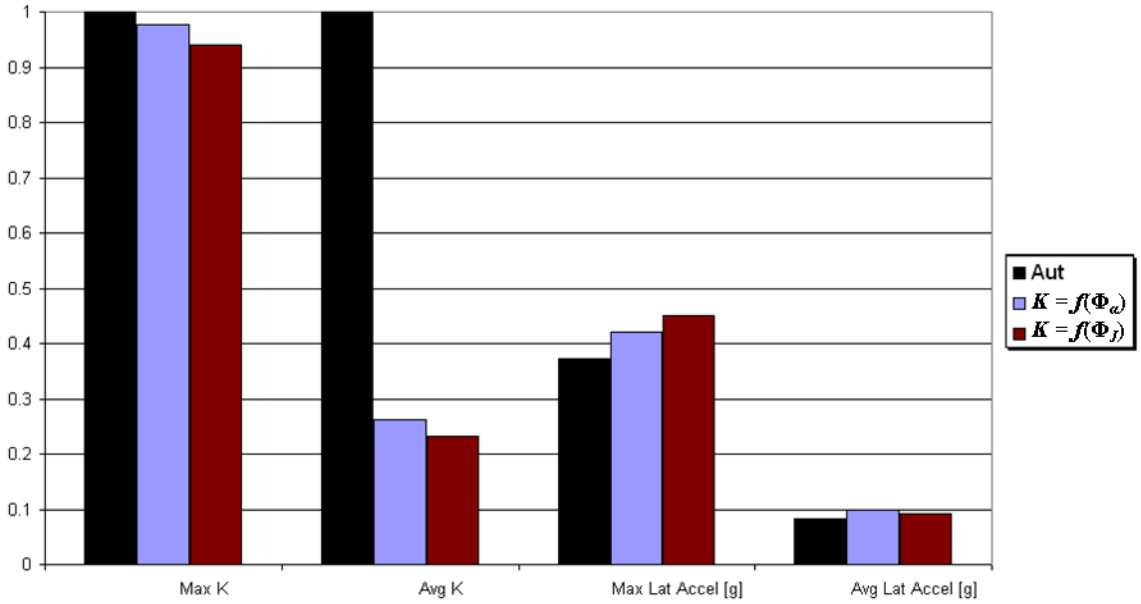

Figure 4.27: Performance metrics averaged across all experiments and drivers

Figure 4.28 shows how threat metrics Φ_α and Φ_J and intervention laws K and K_{aug} affect performance metrics over the maneuver. Notice here that while these intervention laws and threat metrics are of similar magnitude, they do exhibit one definite trend; augmenting controller intervention according to the difference between driver and controller steer (K_{aug}) generally leads (in an averaged sense) to higher average K and subsequently lower peak lateral accelerations. This was also inferred from the scenario-specific results shown in this chapter and justifies the utility of this augmented intervention law as a means of improving vehicle performance and ride comfort.

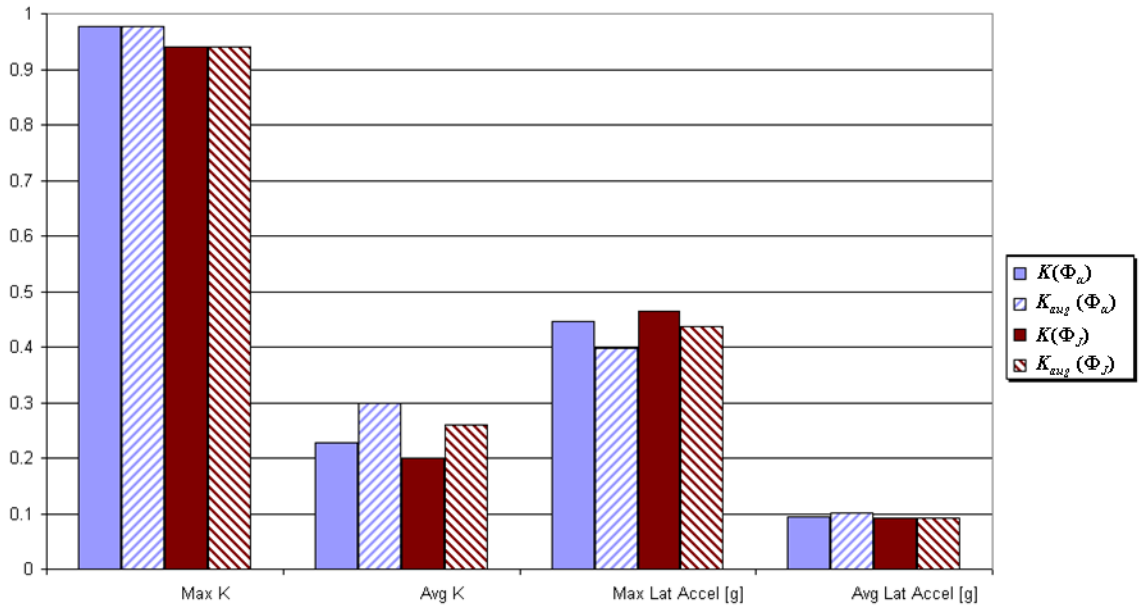

Figure 4.28: Effect of threat metrics and intervention laws on the average performance of all three drivers

The trends explained above also roughly hold for each driver individually. That is, while each driver's performance and consequent controller activity differed slightly, the relative merits of each controller configuration discussed above tended on average to affect all three drivers similarly (i.e. lower maximum lateral acceleration using the augmented controller, etc). Appendix C breaks down performance metrics as a function of threat metrics and intervention laws for each driver.

4.4 Summary and Conclusions

This chapter has described the integration of MPC-based path planning, threat assessment, and semi-autonomous control into a unified framework for hazard avoidance and stability control. This framework provides an elegant and effective means of semi-autonomously avoiding road hazards while conceding significant control authority to a human driver. Simulation and experimental results have shown this controller's performance to be robust to (driver-preference-based) changes in its intervention law and thresholds. They have also demonstrated its utility as a stability controller capable of satisfying position, input, and plant dynamic constraints in the presence of system-inherent time delays. Additionally, this framework has been shown to successfully

circumnavigate both static and dynamic road hazards given multiple scenarios, various driver inputs, and diverse threat metrics and intervention laws.

Finally, while human factors have not been studied in depth here, it is expected that with additional investigation, a best case, or average driver-preferred intervention law may be described and intervention settings tuned accordingly.

REFERENCES

[1] National Highway Traffic Safety Administration (NHTSA), *2007 Traffic Safety Annual Assessment - Highlights*, NHTSA National Center for Statistics and Analysis, 2008.

[2] J.R. McBride, J.C. Ivan, D.S. Rhode, J.D. Rupp, M.Y. Rupp, J.D. Higgins, D.D. Turner, and R.M. Eustice, "A perspective on emerging automotive safety applications, derived from lessons learned through participation in the DARPA Grand Challenges," *Journal of Field Robotics*, vol. 25, 2008, pp. 808-840.

[3] P. Falcone, M. Tufo, F. Borrelli, J. Asgarit, and H. Tseng, "A linear time varying model predictive control approach to the integrated vehicle dynamics control problem in autonomous systems," *46th IEEE Conference on Decision and Control 2007, CDC, Dec 12-14 2007*, Piscataway, NJ 08855-1331, United States: Institute of Electrical and Electronics Engineers Inc., 2008, pp. 2980-2985.

[4] J. Pohl, W. Birk, and L. Westervall, "A driver-distraction-based lane-keeping assistance system," *Proceedings of the Institution of Mechanical Engineers. Part I: Journal of Systems and Control Engineering*, vol. 221, 2007, pp. 541-552.

[5] M. Weilkes, L. Burkle, T. Rentschler, and M. Scherl, "Future vehicle guidance assistance - combined longitudinal and lateral control," *Automatisierungstechnik*, vol. 42, Jan. 2005, pp. 4-10.

[6] J. Liu, J. Wu, and Y. Su, "Development of an interactive lane keeping control system for vehicle," *VPPC 2007 - 2007 IEEE Vehicle Power and Propulsion Conference, Sep 9-12 2007*, Piscataway, NJ 08855-1331, United States: Institute of Electrical and Electronics Engineers Computer Society, 2007, pp. 702-706.

[7] J. Leonard, J. How, S. Teller, M. Berger, S. Campbell, G. Fiore, L. Fletcher, E. Frazzoli, A. Huang, S. Karaman, O. Koch, Y. Kuwata, D. Moore, E. Olson, S. Peters, J. Teo, R. Truax, M. Walter, D. Barrett, A. Epstein, K. Maheloni, K. Moyer, T. Jones, R. Buckley, M. Antone, R. Galejs, S. Krishnamurthy, and J. Williams, "A perception-driven autonomous urban vehicle," *Journal of Field Robotics*, vol. 25, 2008, pp. 727-774.

[8] L. Guo, J. Wang, and K. Li, "Lane keeping system based on THASV-II platform," *IEEE International Conference on Vehicular Electronics and Safety, ICVES 2006, Dec 13-15 2006*, Piscataway, NJ 08855-1331, United States: Institute of Electrical and Electronics Engineers Computer Society, 2006, pp. 305-308.

[9] J. Fritsch, T. Michalke, A. Gepperth, S. Bone, F. Waibel, M. Kleinehagenbrock, J. Gayko, and C. Goerick, "Towards a human-like vision system for Driver Assistance," *Intelligent Vehicles Symposium, 2008 IEEE*, 2008, pp. 275-282.

[10] P.C. Calhoun and E.M. Queen, "Entry Vehicle Control System Design for the Mars Smart Lander.," *presented at the AIAA Atmospheric Flight Mech. Conf.*, Monterey, CA: 2002.

[11] Wei-Min Lu and D. Bayard, "Guidance and control for Mars atmospheric entry: adaptivity and robustness," *Proceedings of 14th World Congress of IFAC 99, 5-9 July 1999*, Kidlington, UK: Elsevier Sci, 1999, pp. 383-8.

[12] L.B. Cremean, T.B. Foote, J.H. Gillula, G.H. Hines, D. Kogan, K.L. Kriechbaum, J.C. Lamb, J. Leibs, L. Lindzey, C.E. Rasmussen, A.D. Stewart, J.W. Burdick, and R.M. Murray, "Alice: An information-rich autonomous vehicle for high-speed desert navigation," *Journal of Field Robotics*, vol. 23, 2006, pp. 777-810.

[13] R.S. Smith, K.D. Mease, D.S. Bayard, and D.L. Farless, "Aeromaneuvering in the martian atmosphere: simulation-based analyses," *Journal of Spacecraft and Rockets*, vol. 37, 2000, pp. 139-142.

[14] T. Besselmann and M. Morari, "Hybrid Parameter-Varying Model Predictive Control for Autonomous Vehicle Steering," *European Journal of Control*, vol. 14, May. 2008, pp. 418-431.

[15] F. Borrelli, P. Falcone, T. Keviczky, J. Asgari, and D. Hrovat, "MPC-based approach to active steering for autonomous vehicle systems," *International Journal of Vehicle Autonomous Systems*, vol. 3, 2005, pp. 265-291.

[16] P. Falcone, F. Borrelli, H.E. Tseng, J. Asgari, and D. Hrovat, "Integrated Braking and Steering Model Predictive Control Approach in Autonomous Vehicles," *5th IFAC Symposium on Advances in Automotive Control*, Berkeley, CA: 2007.

[17] T. Keviczky, P. Falcone, F. Borrelli, J. Asgari, and D. Hrovat, "Predictive control approach to autonomous vehicle steering," *2006 American Control Conference, Jun 14-16 2006*, Piscataway, NJ 08855-1331, United States: Institute of Electrical and Electronics Engineers Inc., 2006, pp. 4670-4675.

[18] P. Falcone, F. Borrelli, H. Tseng, J. Asgari, and D. Hrovat, "Linear time-varying model predictive control and its application to active steering systems: Stability analysis and experimental validation," *International Journal of Robust and Nonlinear Control*, vol. 18, 2008, pp. 862-875.

[19] S. Suh and A.B. Bishop, "Tube concept and its application to the obstacle-avoiding minimum-time trajectory planning problem," *Proceedings of the 1987 IEEE International Conference on Systems, Man and Cybernetics.*, New York, NY, USA: IEEE, 1987, pp. 14-20.

[20] S. Thrun, M. Montemerlo, H. Dahlkamp, D. Stavens, A. Aron, J. Diebel, P. Fong, J. Gale, M. Halpenny, G. Hoffmann, K. Lau, C. Oakley, M. Palatucci, V. Pratt, P. Stang, S. Strohband, C. Dupont, L. Jendrossek, C. Koelen, C. Markey, C. Rummel, J. van Niekerk, E. Jensen, P. Alessandrini, G. Bradski, B. Davies, S. Ettinger, A. Kaehler, A. Nefian, and P. Mahoney, "Stanley: The robot that won the DARPA Grand Challenge," *Journal of Field Robotics*, vol. 23, 2006, pp. 661-692.

[21] B. Kim, D. Necsulescu, and J. Sasiadek, "Model predictive control of an autonomous vehicle," *2001 IEEE/ASME International Conference on Advanced Intelligent Mechatronics Proceedings, Jul 8-12 2001*, 2001, pp. 1279-1284.

[22] P. Falcone, H. Eric Tseng, F. Borrelli, J. Asgari, and D. Hrovat, "MPC-based yaw and lateral stabilisation via active front steering and braking," *Vehicle System Dynamics*, vol. 46, 2008, pp. 611-628.

[23] R. Mobus and Z. Zomotor, "Constrained optimal control for lateral vehicle guidance," *Proceedings of the 2005 IEEE Intelligent Vehicles Symposium, 6-8 June 2005*, Piscataway, NJ, USA: IEEE, 2005, pp. 429-34.

[24] P. Falcone, F. Borrelli, H. Tseng, J. Asgari, and D. Hrovat, "A hierarchical model predictive control framework for autonomous ground vehicles," *Proceedings of the 2008 American Control Conference, ACC, Jun 11-13 2008*, Piscataway, NJ 08855-1331, United States: Institute of Electrical and Electronics Engineers Inc., 2008, pp. 3719-3724.

[25] S. Vitabile, S. Bono, and F. Sorbello, "An embedded real-time automatic lane-keeping system," *Knowledge-Based Intelligent Information and Engineering Systems: KES 2007-WIRN 2007. 11th International Conference, KES 2007. XVII Italian Workshop on Neural Networks., 12-14 Sept. 2007*, Berlin, Germany: Springer-Verlag, 2007, pp. 647-54.

[26] T. Sattel and T. Brandt, "From robotics to automotive: Lane-keeping and collision avoidance based on elastic bands ," *Vehicle System Dynamics*, vol. 46, Jul. 2008, pp. 597-619.

[27] J. Jansson, "Collision avoidance theory with application to automotive collision mitigation," Doctoral Dissertation, Linkoping University, 2005.

[28] J. Ackermann, "Robust decoupling of car steering dynamics with arbitrary mass distribution," *Proceedings of the 1994 American Control Conference. Part 2 (of 3), Jun 29-Jul 1 1994*, Green Valley, AZ, USA: American Automatic Control Council, 1994, pp. 1964-1968.

[29] A. Alleyne, "Comparison of alternative intervention strategies for Unintended Roadway Departure (URD) control," *Vehicle System Dynamics*, vol. 27, 1997, pp. 157-186.

[30] P. Falcone, F. Borrelli, J. Asgari, H.E. Tseng, and D. Hrovat, "Predictive active steering control for autonomous vehicle systems," *IEEE Transactions on Control Systems Technology*, vol. 15, 2007, pp. 566-580.

[31] A. Alleyne, "A comparison of alternative obstacle avoidance strategies for vehicle control," *Vehicle System Dynamics*, vol. 27, Jun. 1997, pp. 371-92.

[32] T. Pilutti, G. Ulsoy, and D. Hrovat, "Vehicle steering intervention through differential braking," *Proceedings of the 1995 American Control Conference, Jun 21-23 1995*, 1995, pp. 1667-1671.

[33] A. Bemporad, M. Morari, V. Dua, and E. Pistikopoulos, "The explicit linear quadratic regulator for constrained systems," *Automatica*, vol. 38, 2002, pp. 3-20.

[34] T. Tsukagoshi and H. Wakaumi, "Highly-reliable semi-autonomous vehicle control on lattice lane," *Proceedings. IROS '90. IEEE International Workshop on Intelligent*

Robots and Systems '90. Towards a New Frontier of Applications, 3-6 July 1990, New York, NY, USA: IEEE, 1990, pp. 731-8.

[35] Nan-Ning Zheng, Shuming Tang, Hong Cheng, Qing Li, G. Lai, and F. Wang, "Toward intelligent driver-assistance and safety warning system," *IEEE Intelligent Systems*, vol. 19, Mar. 2004, pp. 8-11.

[36] T. Brandt, T. Sattel, and M. Bohm, "Combining haptic human-machine interaction with predictive path planning for lane-keeping and collision avoidance systems," *2007 IEEE Intelligent Vehicles Symposium, IV 2007, Jun 13-15 2007*, Piscataway, NJ 08855-1331, United States: Institute of Electrical and Electronics Engineers Inc., 2007, pp. 582-587.

[37] T. Pilutti and A.G. Ulsoy, "Identification of driver state for lane-keeping tasks," *IEEE Transactions on Systems, Man, and Cybernetics Part A:Systems and Humans.*, vol. 29, 1999, pp. 786-502.

[38] M. Netto, J. Blosseville, B. Lusetti, and S. Mammar, "A new robust control system with optimized use of the lane detection data for vehicle full lateral control under strong curvatures," *ITSC 2006: 2006 IEEE Intelligent Transportation Systems Conference, Sep 17-20 2006*, Piscataway, NJ 08855-1331, United States: Institute of Electrical and Electronics Engineers Inc., 2006, pp. 1382-1387.

[39] Peng Cheng, Zuojun Shen, and S. Lavalle, "RRT-based trajectory design for autonomous automobiles and spacecraft," *7th National Conference on Robotics, Sept. 2001*, Poland: Silesian Univ. of Technol, 2001, pp. 167-94.

[40] C. Tan, R. Sutton, and J. Chudley, "An integrated collision avoidance system for autonomous underwater vehicles," *International Journal of Control*, vol. 80, Jul. 2007, pp. 1027-49.

[41] R. Vaidyanathan, C. Hocaoglu, T.S. Prince, and R.D. Quinn, "Evolutionary path planning for autonomous air vehicles using multiresolution path representation," *2001 IEEE/RSJ International Conference on Intelligent Robots and Systems, Oct 29-Nov 3 2001*, Institute of Electrical and Electronics Engineers Inc., 2001, pp. 69-76.

[42] B. Capozzi and J. Vagners, "Evolving (semi)-autonomous vehicles," *AIAA Guidance, Navigation, and Control Conference and Exhibit*, 2001.

[43] N. Tsourveloudis, K. Valavanis, and T. Hebert, "Autonomous vehicle navigation utilizing electrostatic potential fields and fuzzy logic," *IEEE Transactions on Robotics and Automation*, vol. 17, 2001, pp. 490-7.

[44] E.J. Rossetter and J. Christian Gardes, "Lyapunov based performance guarantees for the potential field lane-keeping assistance system," *Journal of Dynamic Systems, Measurement and Control, Transactions of the ASME*, vol. 128, 2006, pp. 510-522.

[45] K. Kyriakopoulos, P. Kakambouras, and N. Krikelis, "Navigation of nonholonomic vehicles in complex environments with potential fields and tracking," *Proceedings of IEEE International Conference on Robotics and Automation, 22-28 April 1996*, New York, NY, USA: IEEE, 1996, pp. 3389-94.

[46] G. Engelman, J. Ekmark, L. Tellis, M.N. Tarabishy, G.M. Joh, R.A. Trombley, and R.E. Williams, "Threat level identification and quantifying system," U.S. Patent US 7034668 B2, April 25, 2006.

[47] A. van der Horst, "A time-based analysis of road user behavior in normal and critical encounters," Ph.D. Thesis, Delft University, Delft, The Netherlands, 1990.

[48] R. Kiefer, J. Salinger, and J. Ference, *The Status of NHTSA's Rear-End Crash Prevention Research Program*, Washington, DC: NHTSA, 2005.

[49] R. Kiefer, D. LeBlanc, M. Palmer, J. Salinger, R. Deering, and M. Shulman, *Development and validation of functional definitions and evaluation procedures for collision warning/avoidance system*, Washington, DC: Crash Avoidance Metrics Partnership (CAMP), 1999.

[50] S. Brunson, E. Kyle, N. Phamdo, and G. Preziotti, *Alert Algorithm Development Program NHTSA Rear-End Collision Alert Algorithm*, Washington, DC: The Johns Hopkins University Applied Physics Laboratory, 2002.

[51] A. Polychronopoulos, M. Tsogas, A. Amditis, U. Scheunert, L. Andreone, and F. Tango, "Dynamic situation and threat assessment for collision warning systems: The EUCLIDE approach," *2004 IEEE Intelligent Vehicles Symposium, June 14,2004 - June 17,2004*, Parma, Italy: Institute of Electrical and Electronics Engineers Inc., 2004, pp. 636-641.

[52] H. Yu, M. Spenko, and S. Dubowsky, "An adaptive shared control system for an intelligent mobility aid for the elderly," *Autonomous Robots*, vol. 15, 2003, pp. 53-66.

[53] J.J. Gibson and L.E. Crooks, "A Theoretical Field-Analysis of Automobile-Driving," *The American Journal of Psychology*, vol. 51, Jul. 1938, pp. 453-471.

[54] G. Prokop, "Modeling human vehicle driving by model predictive online optimization," *Vehicle System Dynamics*, vol. 35, Jan. 2001, pp. 19-53.

[55] F. Biral, M. Da Lio, and E. Bertolazzi, "Combining safety margins and user preferences into a driving criterion for optimal control-based computation of reference maneuvers for an ADAS of the next generation," *2005 IEEE Intelligent Vehicles Symposium Proceedings, 6-8 June 2005*, Piscataway, NJ, USA: IEEE, 2005, pp. 36-41.

[56] E. Bertolazzi, F. Biral, and M. Da Lio, "Future advanced driver assistance systems based on Optimal Control: the influence of "risk functions" on overall system behavior and on prediction of dangerous situations," *2004 IEEE Intelligent Vehicles Symposium, 14-17 June 2004*, Piscataway, NJ, USA: IEEE, 2004, pp. 386-91.

[57] C. Garcia, D. Prett, and M. Morari, "Model predictive control: theory and practice-a survey," *Automatica*, vol. 25, May. 1989, pp. 335-48.

[58] E.F. Camacho and C. Bordons, *Model Predictive Control*, New York, NY, USA: Springer, 2004.

[59] M. Lelic and M. Zarrop, "Generalized pole-placement self-tuning controller: Part 1. Basic algorithm," *International Journal of Control*, vol. 46, 1987, pp. 547-568.

[60] M. Lelic and P. Wellstead, "Generalized pole-placement self-tuning controller: Part 2. Application to robot manipulator control," *International Journal of Control*, vol. 46, 1987, pp. 569-601.

[61] L.D. Baskar, B. De Schutter, and H. Hellendoorn, "Model predictive control for intelligent speed adaptation in intelligent vehicle highway systems," *Proceedings of the 17th IEEE International Conference on Control Applications, CCA, Sep 3-5 2008*, New York, NY 10016-5997, United States: Institute of Electrical and Electronics Engineers Inc., 2008, pp. 468-473.

[62] P. Doganis, E. Aggelogiannaki, and H. Sarimveis, "A combined model predictive control and time series forecasting framework for production-inventory systems," *International Journal of Production Research*, vol. 46, 2008, pp. 6841-6853.

[63] M. Mahfouf and D. Linkens, "Non-linear generalized predictive control (NLGPC) applied to muscle relaxant anaesthesia," *International Journal of Control*, vol. 71, 1998, pp. 239-257.

[64] D. Clarke and R. Scattolini, "Constrained receding-horizon predictive control," *IEE Proceedings D: Control Theory and Applications*, vol. 138, 1991, pp. 347-354.

[65] E. Mosca and J. Zhang, "Stable redesign of predictive control," *Automatica*, vol. 28, 1992, pp. 1229-1233.

[66] J. Gossner, B. Kouvaritakis, and J. Rossiter, "Stable generalized predictive control with constraints and bounded disturbances," *Automatica*, vol. 33, 1997, pp. 551-568.

[67] J. Rossiter, B. Kouvaritakis, and J. Gossner, "Feasibility and stability results for constrained stable generalized predictive control," *Automatica*, vol. 31, 1995, pp. 863-877.

[68] P. Scokaert and D. Mayne, "Min-max feedback model predictive control for constrained linear systems," *IEEE Transactions on Automatic Control*, vol. 43, 1998, pp. 1136-1142.

[69] B. Kouvaritakis, J. Rossiter, and A. Chang, "Stable generalised predictive control. An algorithm with guaranteed stability," *IEE Proceedings D: Control Theory and Applications*, vol. 139, 1992, pp. 349-363.

[70] A. Richards and J.P. How, "Robust variable horizon model predictive control for vehicle maneuvering," *International Journal of Robust and Nonlinear Control*, vol. 16, 2006, pp. 333-351.

[71] J.H. Lemelson and R.D. Pedersen, "GPS vehicle collision avoidance warning and control system and method," U.S. Patent 5983161, November 9, 1999.

[72] Z. Zomotor and U. Franke, "Sensor fusion for improved vision based lane recognition and object tracking with range-finders," *Proceedings of the 1997 IEEE Conference on Intelligent Transportation Systems, ITSC, Nov 9-12 1997*, Piscataway, NJ, USA: IEEE, 1997, pp. 595-600.

[73] H. Fritz, A. Gern, H. Schiemenz, and C. Bonnet, "CHAUFFEUR Assistant - A driver assistance system for commercial vehicles based on fusion of advanced ACC

and lane keeping," *Proceedings of the 2004 IEEE Intelligent Vehicles Symposium, Jun 14-17 2004*, Piscataway, NJ 08855-1331, United States: Institute of Electrical and Electronics Engineers Inc., 2004, pp. 495-500.

[74] W. Langson, I. Chryssochoos, W. Rakovic, and D. Mayne, "Robust model predictive control using tubes," *Automatica*, vol. 40, 2004, pp. 125-133.

[75] R. Scattolini and S. Bittanti, "On the choice of the horizon in long-range predictive control--some simple criteria," *Automatica*, vol. 26, Sep. 1990, pp. 915-917.

[76] D. Clarke, C. Mohtadi, and P. Tuffs, "Generalized Predictive Control - Part II. Extensions and Interpretations," *Automatica*, vol. 23, 1987, pp. 149-160.

[77] P. Falcone, F. Borrelli, J. Asgariy, H.E. Tsengy, and D. Hrovat, "A model predictive control approach for combined braking and steering in autonomous vehicles," *Proceedings of the 2007 Mediterranean Conference on Control and Automation, MED, Jul 27-29 2007*, Piscataway, NJ 08855-1331, United States: Institute of Electrical and Electronics Engineers Computer Society, 2007.

[78] H. Lee and M. Tomizuka, "Coordinated longitudinal and lateral motion control of vehicles for IVHS," *Transactions of the ASME. Journal of Dynamic Systems, Measurement and Control*, vol. 123, Sep. 2001, pp. 535-43.

[79] Y. Wei, H. Meng, H. Zhang, and X. Wang, "Vehicle Frontal collision warning system based on improved target tracking and threat assessment," *Proceedings of the 10th International IEEE Conference on Intelligent Transportation Systems, ITSC 2007, September 30,2007 - October 03,2007*, Seattle, WA, United states: Institute of Electrical and Electronics Engineers Inc., 2007, pp. 167-172.

[80] C. Kurutas, K. Elsacer, D. Schramm, and M. Hiller, "Modeling and simulation of the effect of reversible belt pretensioners," *Proceedings of the 2006 IEEE International Conference on Mechatronics, ICM, July 03,2006 - July 05,2006*, Budapest, Hungary: Inst. of Elec. and Elec. Eng. Computer Society, 2006, pp. 119-124.

[81] R. Fuller, "Determinants of time headway adopted by truck drivers," *Ergonomics*, vol. 24, 1981, pp. 463-474.

[82] A. Ollero and G. Heredia, "Stability analysis of mobile robot path tracking," *Proceedings of the 1995 IEEE/RSJ International Conference on Intelligent Robots and Systems. Part 3 (of 3), Aug 5-9 1995*, Piscataway, NJ, USA: IEEE, 1995, pp. 461-466.

A

APPENDIX A: ADAMS PLANT PARAMETERS

Figure A.1 shows the ADAMS Car® model used to represent the vehicle plant in simulation. This model represents a generic high-centered light truck with a double wishbone suspension, and rack and pinion steering.

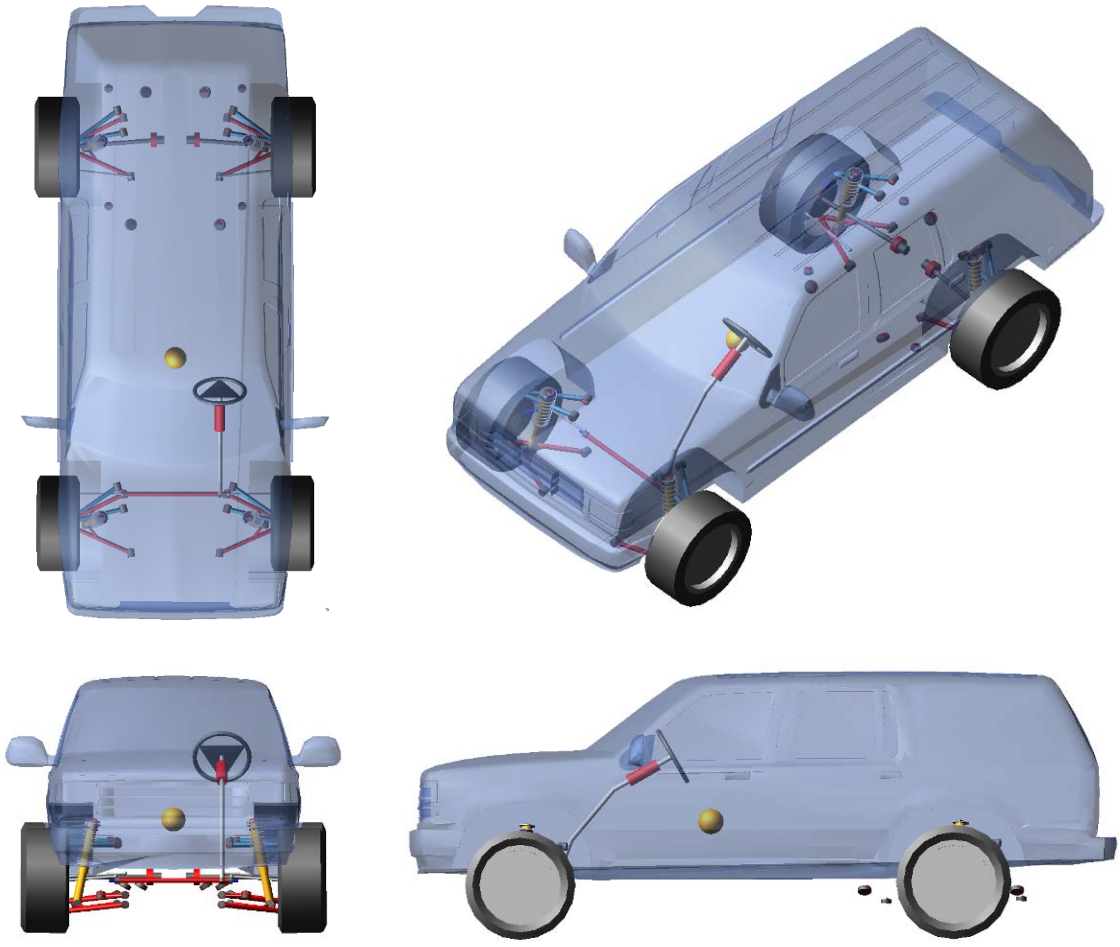

Figure A.1: ADAMS Car® plant model used in simulation

Table A.1 describes the parameters of the ADAMS plant.

Table A.1: Plant model parameters for ADAMS vehicle model

Parameter	Value [units]
Total mass	**2450 [kg]**
Body mass	2210 [kg]
Unsprung mass	240 [kg]
Wheel mass	60 [kg]
Body roll inertia	1240 [kg·m^2]
Body gyroscopic inertia	0 [kg·m^2]
Wheel gyroscopic inertia	0.2 [kg·m^2]
Measurements	
Wheelbase	2.85 [m]
Track width	1.62 [m]
C.G. height	0.76 [m]
C.G. longitudinal distance from front wheels	1.07 [m]
Wheel diameter	0.79 [m]
Tire full width	0.24 [m]
Suspension and tire stiffness	
Suspension spring stiffness	40,000 [N/m]
Suspension roll stiffness	3700 [N·m/deg]
Suspension damping	5,300 [N·s/m]
Tire vertical stiffness	250,000 N/m
Tire cornering stiffness	1200 N/deg (F_z = 6000 N)
Steering wheel ratio	**35 deg/deg**

B

APPENDIX B: THREAT ASSESSMENT COMPARISON

In Chapter 2, threat assessment accuracy was defined as the degree to which predicted threat at a given location matches the true threat at that location when the vehicle is controlled autonomously by the MPC controller. The results presented in Chapter 2 were obtained using an objective function of the form

$$\left(J_{\alpha}\right)_k = \sum_{i=k+1}^{k+p} \frac{1}{2} \bar{\alpha}^{\mathrm{T}} R_{\alpha\alpha} \bar{\alpha} + \sum_{i=k}^{k+p-1} \frac{1}{2} u_i{}^{\mathrm{T}} \mathbf{R}_u u_i + \sum_{i=k}^{k+p-1} \frac{1}{2} \Delta u_i{}^{\mathrm{T}} \mathbf{R}_{\Delta u} \Delta u_i \tag{B.1}$$

This objective function setup penalizes front wheel sideslip (rather than lateral acceleration), leaving some question as to whether such a weighting actually minimizes lateral vehicle acceleration or whether minimizing lateral acceleration requires that $\bar{\alpha}$ and $R_{\alpha\alpha}$ in (B.1) be replaced by $\ddot{\bar{y}}$ and $R_{\ddot{y}\ddot{y}}$ to form

$$\left(J_{\ddot{y}}\right)_k = \sum_{i=k+1}^{k+p} \frac{1}{2} \ddot{\bar{y}}^{\mathrm{T}} R_{\ddot{y}\ddot{y}} \ddot{\bar{y}} + \sum_{i=k}^{k+p-1} \frac{1}{2} u_i{}^{\mathrm{T}} \mathbf{R}_u u_i + \sum_{i=k}^{k+p-1} \frac{1}{2} \Delta u_i{}^{\mathrm{T}} \mathbf{R}_{\Delta u} \Delta u_i \tag{B.2}$$

The results discussed in Section 2.3.2 (see Figures 2.9—2.11) suggest that in the context of MPC-based corridor navigation, various vehicle states may be penalized in the objective function with relatively similar corridor tracking performance. Extending this result to threat assessment suggests that either lateral acceleration or front wheel sideslip may be penalized in the MPC objective function without significantly affecting the threat assessed by various metrics (Φ_{α}, Φ_J, or $\Phi_{\ddot{y}}$) and/or threat calculations (∞-, 2-, or "0"-norms defined in Table 3.1). The columns of Table B.1 compare the accuracy of $\Phi_{\ddot{y}}$-based threat assessments (their nearness to true values of lateral vehicle acceleration) when lateral acceleration "a_y" is penalized in the objective function ("$\boldsymbol{J}_{\ddot{y}}$") to the same assessment when front wheel sideslip "α" is penalized ("$\boldsymbol{J}_{\alpha}$").

Table B.1: Comparison of threat assessments for autonomous controllers penalizing lateral acceleration and front wheel slip

	$J_{\ddot{y}}$	J_{α}
∞-norm	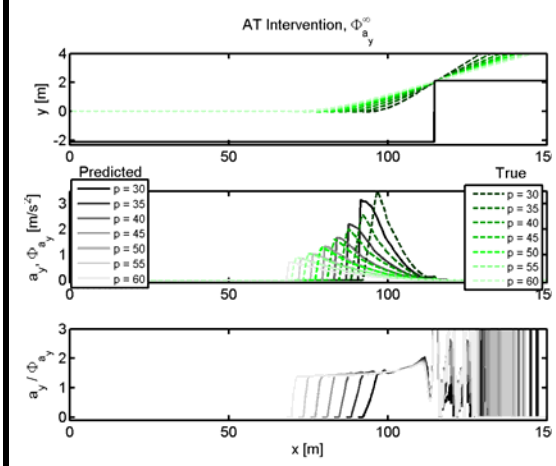	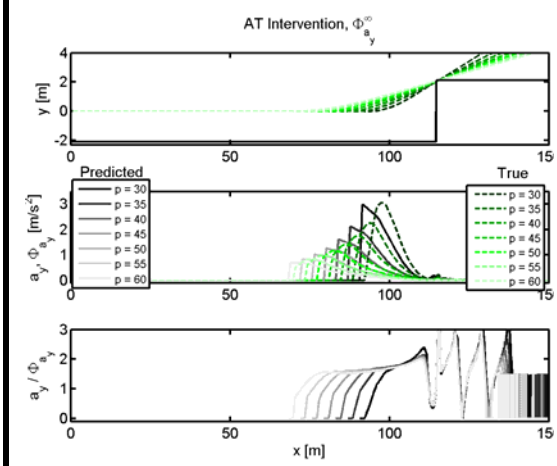
"0"-norm	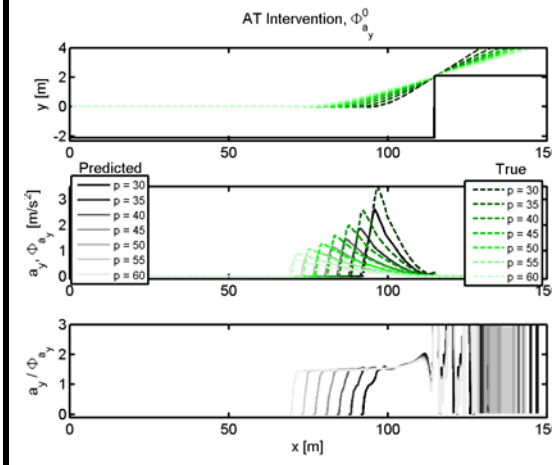	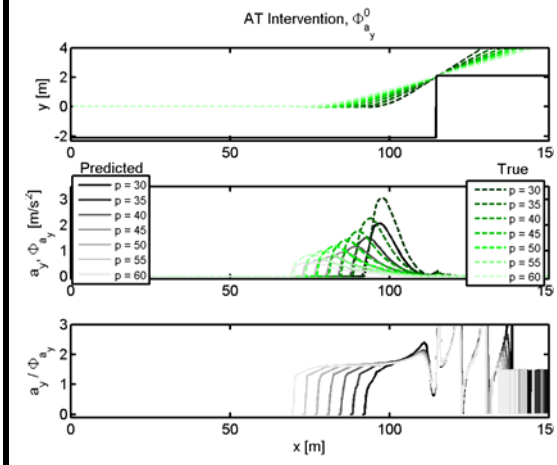
2-norm	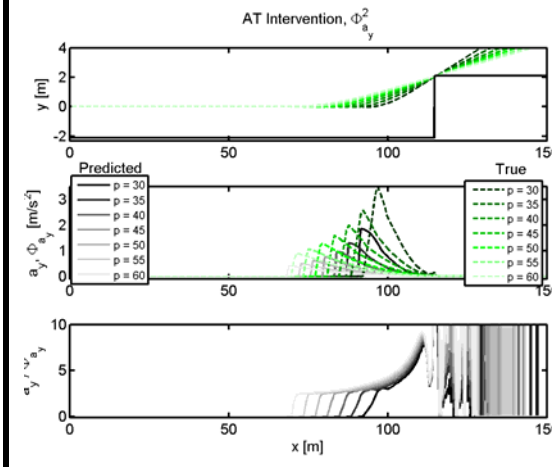	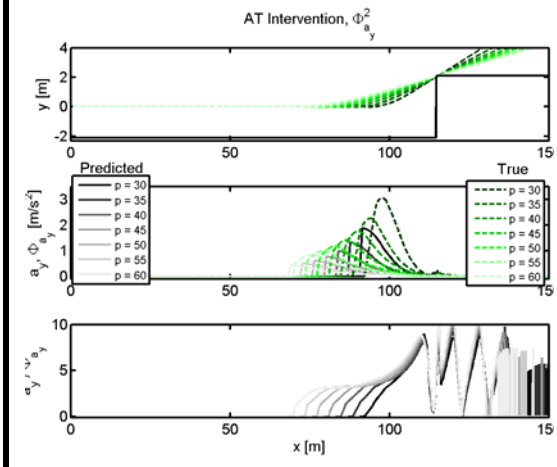

Table B.1 confirms the assumption that weighting either of the dynamically-coupled states a_y or α in the MPC objective function leads to similar vehicle trajectories and threat assessments. Notice, however, that while these trajectories and corresponding threat assessments are similar and lead to a consistent predicted/true threat ratio, this ratio is slightly different for each and in both cases is greater than unity. This discrepancy is caused by model mismatch between the controller (using Model B) and the plant (using Plant B). This model mismatch arises due to some uncertainty in true plant parameters such as mass, inertia, and tire cornering stiffness. As model parameters more closely approximate true plant parameters, this ratio of true-to-predicted threat in autonomous controller operation grows closer to unity.

Comparing the columns of Table B.1 also shows that in this maneuver, penalizing front wheel sideslip in the objective function actually leads to lower lateral acceleration than penalizing lateral acceleration itself. This likely follows from the dependence of front wheel sideslip on yaw rate and steering input (as minimizing front slip minimizes a combination of yaw rate and steering input, both of which are dynamically related to lateral acceleration). The result of this analysis suggests that penalizing front wheel sideslip in the objective function leads to a similar threat assessment and slightly lower lateral vehicle acceleration in autonomous avoidance maneuvers.

Table B.2 compares threat assessments based on lateral acceleration ($\Phi_{\ddot{y}}$), front wheel sideslip (Φ_α), and objective function cost (Φ_J) when the controller uses cost functions (B.1) and (B.2). Comparing each metric's assessment to true values of lateral acceleration, front wheel sideslip, or objective function cost shows that using the objective function weighting (B.2) while assessing threat based on Φ_α^∞ or Φ_J^∞ leads to generally lower (more stable) states and better (closer to unity) threat assessments than using (B.1) or $\Phi_{\ddot{y}}^\infty$. This results support the choice of these threat metrics (Φ_α and Φ_J), the ∞-norm, and the J_α objective function weighting used in this thesis's simulations and experiments.

Table B.2: Comparison of objective function weighting variables and threat metrics

	$J_{\ddot{y}}$	J_{α}
$\Phi_{\ddot{y}}$	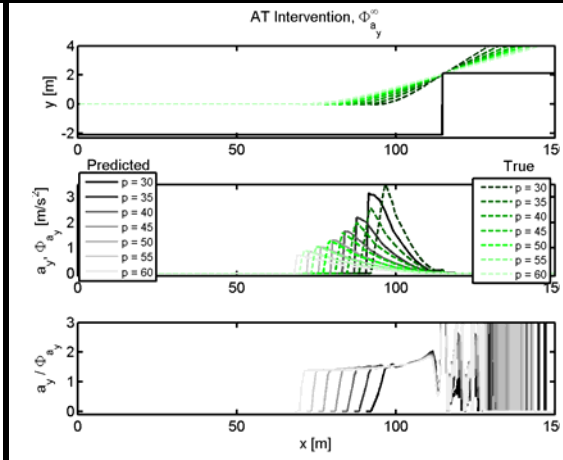	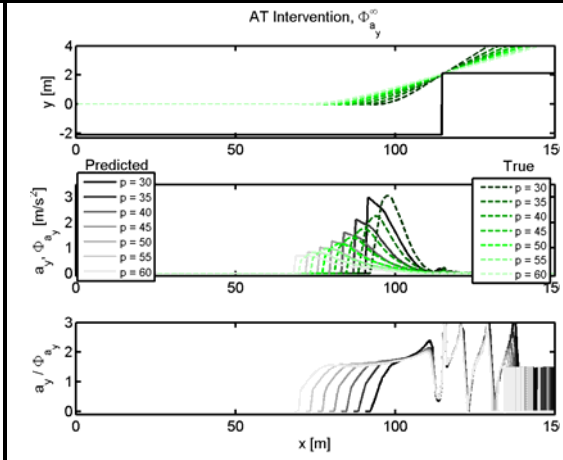
Φ_{α}	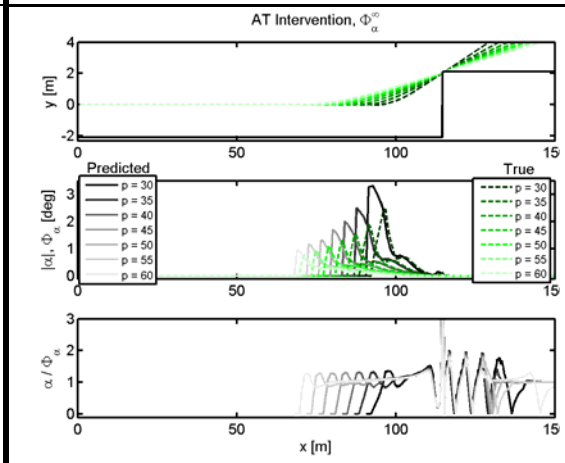	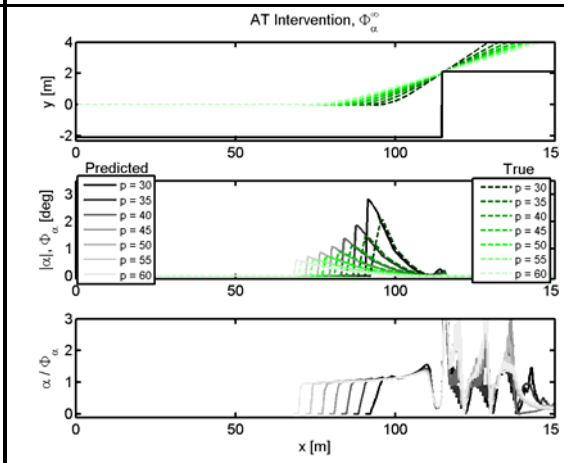
Φ_{J}	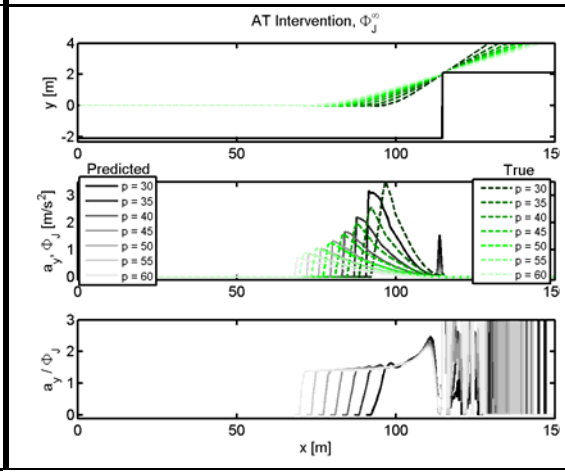	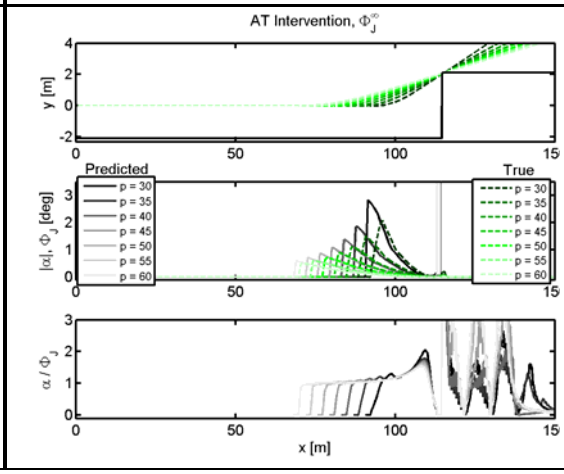

C

APPENDIX C: DRIVER-SPECIFIC PERFORMANCE METRICS

Figures C.1—C.3 show how different intervention laws affected individual test drivers. This data is presented to support the overall (averaged over all drivers) results presented 4.3.2 IV) and substantiates the observation that the four principal intervention laws studied in these experiments $\left(K(\Phi_\alpha), K_{aug}(\Phi_\alpha), K(\Phi_J), \text{and } K_{aug}(\Phi_J)\right)$ similarly affect key performance metrics of multiple drivers. For example, nearly all of these semi-autonomous controller setups successfully assisted the human driver to avoid hazards (in a combination of lane-keeping, hazard avoidance, and multiple hazard avoidance experiments) while using less than 50% of the available control authority. These driver-specific results also corroborate the conclusion that augmenting controller intervention according to the difference between driver and controller steer (K_{aug}) generally leads to higher average K and subsequently lower peak lateral accelerations.

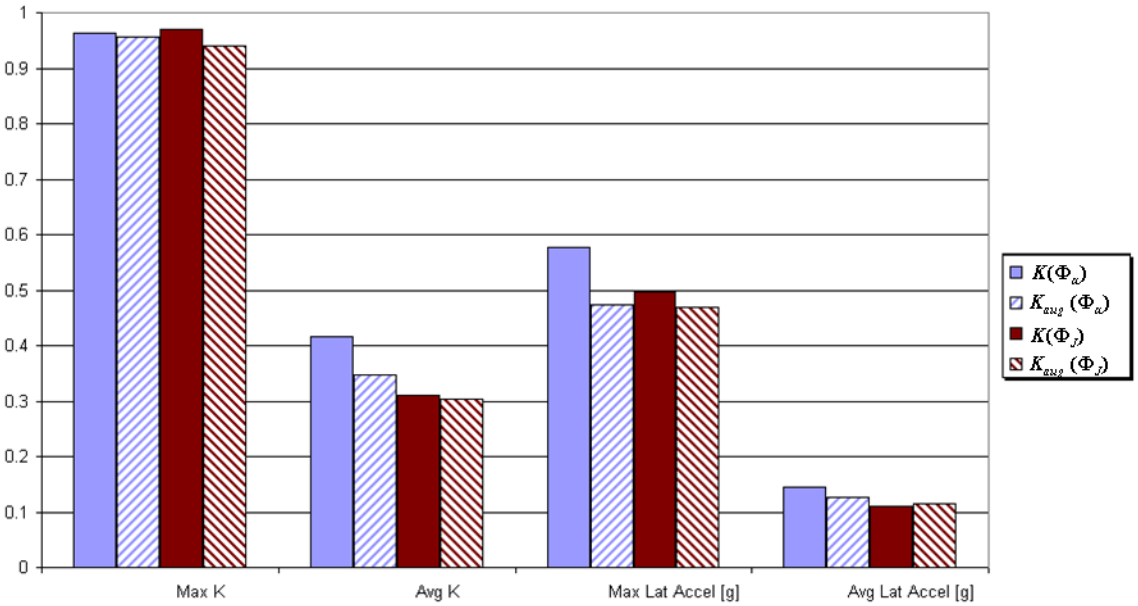

Figure C.1: Driver 1 threat metric and intervention law interactions

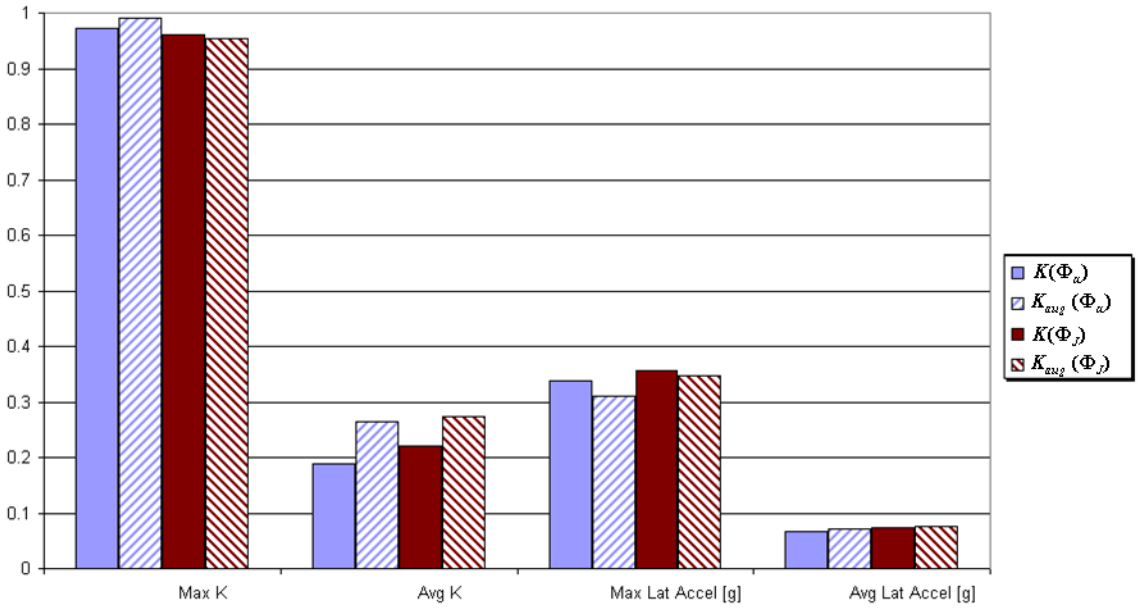

Figure C.2: Driver 2 threat metric and intervention law interactions

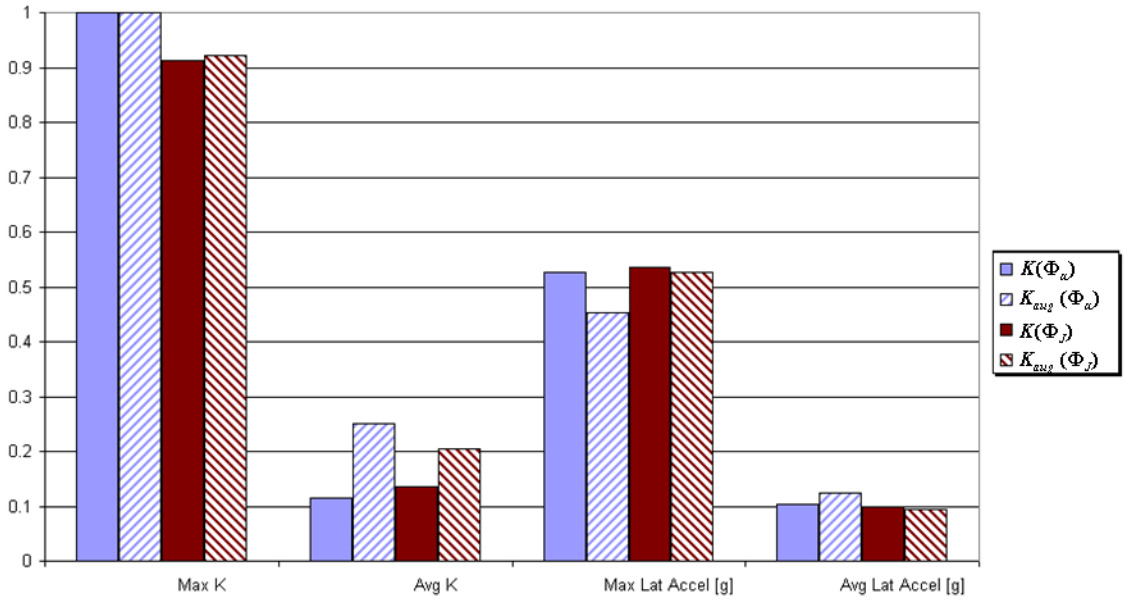

Figure C.3: Driver 3 threat metric and intervention law interactions